

PHOTODYNAMIC THERAPY WITH UPCONVERSION NANOPARTICLES

by

Burcu Güteryüz

B.Sc., Physics, Middle East Technical University, 2010

M.Sc., Department of Metallurgical and Materials Engineering, Middle East
Technical University, 2014

Submitted to the Institute of Biomedical Engineering

in partial fulfillment of the requirements

for the degree of

Doctor

of

Philosophy

Boğaziçi University

2022

ACKNOWLEDGMENTS

I would like to state that this study cannot be accomplished without the precious support of many people. Initially, I want to express my intimate thanks to Prof. Dr. Murat Gülsoy for guiding me throughout this study. His wisdom and advices were enlightened my pathway when I especially faced complications. I would also like to extend my deepest gratitude to Assistant Prof. Dr. Uğur Ünal for giving an opportunity to study in his lab at Koç University and helping me to understand nanoparticles synthesis.

I must also introduce my gratefulness to Prof. Dr. Can Yücesoy and Prof. Dr. Bora Garipcan for sharing their knowledge and evaluations regarding this work. Besides, I am greatly thankful to Dr. Selçuk Birdoğan, Dr. Bilge Gedik Uluocak, and Dr. Barış Yağcı for their assistance in material characterizations.

I would like to thank my colleagues; Dr. Mustafa Kemal Ruhi, Melike Güney, Ayşe Işık, Heba Agha, Begüm Balkan, Hayriye Öztatlı, and Sabra Rostami from Biomedical Engineering in BOUN, and Dr. Hande Āavuş Arslan from Haliç University, for their suggestions and wonderful friendships.

Throughout this thesis study, Prof. Dr. Oya Oğuz and Prof. Dr. Ömer Oğuz were exceedingly supported me in Haliç University. Their understanding and patience were extremely important for me to fulfill this research so I want to express my gratitude to them.

Lastly, I am always loved and emotionally supported by my dear family entire of my life. I want deeply to present my endless gratitude, and respect to my dad Atilla Güleryüz, my mom Nurten Güleryüz, and my brother Barış Güleryüz. I would never have been the person I am today without them.

Cancer is a dreadful disease today and I lost my family members because of it. I would like to dedicate this study to my beloved uncle "Necdet Güteryüz", aunt "Nur Aydemir", and nephew's husband "Hasan Sarı".

ACADEMIC ETHICS AND INTEGRITY STATEMENT

I, Burcu Güteryüz, hereby certify that I am aware of the Academic Ethics and Integrity Policy issued by the Council of Higher Education (YÖK) and I fully acknowledge all the consequences due to its violation by plagiarism or any other way.

Name :

Signature:

Date:

ABSTRACT

PHOTODYNAMIC THERAPY WITH UPCONVERSION NANOPARTICLES

Photodynamic therapy (PDT) is an alternative approach to conventional methods (i.e. chemotherapy and radiotherapy) that can be utilized to treat various cancers with less side effects. However, PDT has some restrictions such as photosensitizers delivery and light penetration depth. It was realized that these problems can be overcome with the improvements in nanotechnology; and today, many researchers have been initiated to study on PDT with various combinations of photosensitizers-nanoparticles.

Recently, upconversion nanoparticles (UCNP) have revealed promising results with different surface designs. UCNP's unique anti-Stokes conversion capabilities enable the transmission of near-infrared (NIR) to visible light, providing a solution to the light penetration depth problem of traditional PDT. Since they have organic structure, UCNP do not show high biotoxicity and additional surface modifications allow photosensitizers delivery to the desired region of a body.

In this study, Yb/Er doped UCNP was synthesized and coated with porous silica to merge MC540 and ZnPc photosensitizers. In order to prevent photosensitizers leakage over time and optically strengthen the nanoparticles for PDT activity, silica surface was conjugated with APTES-gold nanoparticles. Experiments on prostate cancer cells with this novel design revealed two notable results: (I) nanoplatforms exerted high biocompatibility that even 2 mg/ml concentration could be employed, and (II) the viability of cells was successfully reduced up to 35%. Furthermore, PDT effect of 3-4 nm sized gold nanoparticles on cells was detected for the first time.

Keywords: Photodynamic Therapy, Upconversion Nanoparticles, Mesoporous Silica, Gold Nanoparticles, MC540 and ZnPc Photosensitizers, Prostate Cancer.

ÖZET

UPCONVERSION NANOPARÇACIKLAR İLE FOTODİNAMİK TERAPİ

Fotodinamik terapi (FDT), çeşitli kanserleri daha az yan etki ile tedavi etmek için kullanılabilen geleneksel yöntemlere (kemoterapi ve radyoterapi gibi) alternatif bir yaklaşımdır. Bununla birlikte, PDT'nin, ışığa duyarlılaştırıcıların dağıtımı ve ışık penetrasyon derinliği gibi bazı kısıtlamaları vardır. Nanoteknolojideki gelişmelerle bu sorunların aşılabileceği anlaşılmış; ve bugün, birçok araştırmacı, çeşitli ışığa duyarlılaştırıcı-nanopartikül kombinasyonları ile PDT üzerinde çalışmaya başlamıştır.

Son zamanlarda, upconversion nanoparçacıklar (UCNP), farklı yüzey tasarımları ile umut verici sonuçlar ortaya koymuştur. UCNP'nin benzersiz anti-Stokes yeteneği, yakın kızılötesi ışığı (NIR) görünür dalga boyuna dönüştürmesini sağlayarak geleneksel FDT'nin ışık penetrasyon derinliği sorununa çözüm sunar. UCNP, organik yapıya sahip olduğu için yüksek biyotoksisite göstermez ve ek yüzey modifikasyonları, fotosensitizanların vücudun istenilen bölgesine iletilmesine izin verir.

Bu çalışmada, MC540 ve ZnPc ışığa duyarlılaştırıcıların birleştirmek için Yb/Er katkılı UCNP sentezlendi ve gözenekli silika ile kaplandı. Zamanla fotosensitizanların sızıntısını önlemek ve nanoparçacıkları optiksel olarak güçlendirmek için silika yüzeyi APTES-altın nanoparçacıkları ile kaplandı. Bu yeni tasarımla prostat kanseri hücreleri üzerinde yapılan deneyler, iki değerli sonuç ortaya çıkardı: (I) nanoplatformlar, 2 mg/ml konsantrasyonun bile kullanılabilmesiyle yüksek biyoyumluluk sergiledi ve (II) hücrelerin canlılığı başarıyla %35'e kadar düşürüldü. Ayrıca, 3-4 nm boyutlu altın nanoparçacıkların hücreler üzerindeki PDT etkisi ilk kez tespit edildi.

Anahtar Sözcükler: Fotodinamik Terapi, Upconversion Nanoparçacıklar, Gözenekli Silika, Altın Nanoparçacıklar, MC540 ve ZnPc Fotosensitizanlar, Prostat Kanseri.

TABLE OF CONTENTS

ACKNOWLEDGMENTS	iii
ACADEMIC ETHICS AND INTEGRITY STATEMENT	v
ABSTRACT	vi
ÖZET	vii
LIST OF FIGURES	xi
LIST OF TABLES	xiv
LIST OF SYMBOLS	xv
LIST OF ABBREVIATIONS	xvi
1. INTRODUCTION	1
1.1 Motivation	1
1.2 Objectives	2
1.3 Outline	3
2. BACKGROUND	4
2.1 Photodynamic Therapy	4
2.1.1 Mechanisms in PDT	5
2.1.1.1 Light Absorption	6
2.1.1.2 Excited-State Processes of Electrons	6
2.1.2 Novel Methodologies in PDT	7
2.2 Upconversion Nanoparticles	10
2.2.1 Energy Mechanisms of UCNP	11
2.2.2 Designing Upconversion Nanoparticles for Enhanced Luminescence	13
2.3 Surface Modification of UCNP for Biological Applications	14
2.3.1 Ligand Engineering	15
2.3.2 Ligand Attraction	17
2.3.3 Surface Silanization	18
2.3.4 UCNP-Metal Connections	19
3. MATERIALS AND METHODS	22
3.1 Upconversion Nanoparticles Synthesis	22
3.1.1 Materials and Instrumentation	22

3.1.2	UCNP Preparation	22
3.2	Mesoporous Silica Coating on UCNP Surface	24
3.2.1	Materials and Instrumentation	25
3.2.2	UCNP@mSiO ₂ Synthesis	25
3.3	Decorating UCNP with Au Nanoparticles	27
3.3.1	Materials and Instrumentation	28
3.3.2	UCNP@Au Production	28
3.4	Loading Photosensitizers into Porous Silica	29
3.4.1	Materials and Instrumentation	30
3.4.2	MC540 and ZnPc loading into UCNP@Au	30
3.5	Temperature Measurements	32
3.5.1	Materials and Instrumentation	32
3.5.2	Analyzing Temperature Change	32
3.6	Reactive Oxygen Measurements	33
3.6.1	Materials and Instrumentation	33
3.6.2	ROS Detection	34
3.7	<i>In Vitro</i> Experiments	34
3.7.1	Materials and Instrumentation	34
3.7.2	Cell Culturing	35
3.7.3	Cellular Uptake of Nanoplatforms	35
3.7.4	Dark Toxicity Measurements	37
3.7.5	Investigating Photodynamic Therapy	38
3.8	Statistical Analysis	39
4.	RESULTS OF MATERIAL CHARACTERIZATION	40
4.1	Dynamic Light Scattering (DLS)	41
4.2	Scanning and Transmission Electron Microscope (SEM and TEM)	44
4.3	Optical Properties of Materials	46
4.4	Loading Photosensitizers and Leakage	48
4.5	Fourier Transform Infrared Spectroscopy (FTIR)	50
4.6	Energy Dispersive Spectroscopy (EDS)	52
5.	RESULTS OF APPLICATIONS	53
5.1	Thermal Change	53

5.2	Reactive Oxygen Species Measurement	55
5.3	Light - Tissue Interaction: Simulation	57
5.4	Imaging Cells	58
5.5	Photodynamic Therapy Results	60
5.5.1	Cytotoxicity of Photosensitizers	60
5.5.2	Only 980 nm Laser Application	62
5.5.3	Base Nanoplatform: UCNP@Au	63
5.5.4	MC540 & ZnPc Loaded UCNP@Au	64
6.	DISCUSSION	67
7.	CONCLUSION	75
7.1	List of publications produced from the thesis	76
	REFERENCES	77

LIST OF FIGURES

Figure 2.1	Schematic illustration of photodynamic therapy action.	5
Figure 2.2	Designed Jablonski Diagram for photosensitizers upon light application.	7
Figure 2.3	Presentation of the mechanisms for the lanthanide doped upconversion nanoparticles: (a) ESA, (b) ETU, (c) CSU, (d) CR, and (e) PA.	12
Figure 2.4	The design of upconversion nanoparticles.	14
Figure 2.5	Ligand surface engineering for UCNP.	16
Figure 2.6	Ligand attraction procedure for UCNP.	17
Figure 2.7	Surface silanization of UCNP.	20
Figure 3.1	Digital photographs at various steps of reactions during Yb/Er doped UCNP synthesis	25
Figure 3.2	(a) During oleate capped UCNP phase transfer to CTAB with heat increase white bubbles formation (inset) and followed by their disappearance, (b) Silica coating protocol completed nanoparticles (UCNP@mSiO ₂).	27
Figure 3.3	(a) The prepared gold seeds, and (b) UCNP@Au formation.	29
Figure 3.4	The digital photographs of (a) only MC540 loading, and (b) only ZnPc Loading, and (c) both MC540 - ZnPc loading.	31
Figure 3.5	Schematic illustration of <i>in vitro</i> experiments.	38
Figure 4.1	Synthesis steps of nanoplateforms.	40
Figure 4.2	DLS measurements for UCNP.	42
Figure 4.3	DLS measurements for UCNP@mSiO ₂ .	42
Figure 4.4	DLS measurements of gold (Au) seeds.	43
Figure 4.5	SEM and TEM images of (a) Yb/Er doped UCNP in 200 nm scale, (b) mesoporous silica coated UCNP in 200 nm scale, (c) amine conjugated UCNP@mSiO ₂ in 1 μm scale, and gold nanoparticle coated UCNP@APTES (d) 200 nm scale, and (e) 50 nm scale.	44

Figure 4.6	Visualization of (a) UCNP@mSiO ₂ (inset image: d-spacing of UCNP in 2 nm scale), and (b) UCNP@Au with TEM measurements (20 nm scale)	45
Figure 4.7	(a) Fluorescence of UCNP under 980 nm wavelength, and (b) the Jablonski diagram for this process.	46
Figure 4.8	UCNP@mSiO ₂ behaviour with 980 nm light irradiance.	47
Figure 4.9	Emissions of UCNP and the matching absorption peaks of (a) photosensitizers, and (b) Au nanoparticles.	47
Figure 4.10	Absorptions of (a)MC540, and (b) ZnPc in different concentrations.	48
Figure 4.11	Photosensitizers' leakages from (a) UCNP@APTES, and (b) UCNP@Au.	49
Figure 4.12	FTIR spectra of UCNP, UCNP@mSiO ₂ , UCNP@APTES, and UCNP@Au.	51
Figure 4.13	FTIR spectra of ZnPc, MC540, and both PS loaded UCNP@Au.	51
Figure 4.14	Elemental map analysing of UCNP@Au.	52
Figure 5.1	Thermal differentiation of MC540 & ZnPc loaded UCNP@APTES.	54
Figure 5.2	Thermal differentiation of ZnPc & MC540 loaded UCNP@Au.	55
Figure 5.3	Photobleaching of DPBF under 980 nm laser irradiation (1W/cm ²) in the presence of UCNP@Au nanoplatforms (a) with PS and (b) without PS.	56
Figure 5.4	(a) Optical parameters of biological tissue (dermis) and (b) Relative fluence rate of penetrated light into dermis tissue for different wavelengths.	58
Figure 5.5	Images of PC-3 cells with optical microscope: (a-c) control group, (d-f) 0.1 mg/mL loaded nanoplatforms group, and (g-i) 0.5 mg/mL loaded nanoplatforms group.	59
Figure 5.6	Dark toxicity results for MC540 and ZnPc photosensitizers on PC-3 cells. P values: *P<0.05, and **P<0.01.	61
Figure 5.7	PDT for various concentrations of ZnPc via 660 nm laser (400 mW/cm ² , 5 minutes). P values: *P<0.05, and **P<0.01.	61
Figure 5.8	PC-3 cells viability upon 980 nm light exposure with different powers and duration; (a) 5 minutes, and (b) 10 minutes. P value: *P<0.05.	63

- Figure 5.9 UCNP@Au (without PS loading) dark toxicity and PDT property under 980 nm laser (1 W/cm², 5 minutes). P value: *P<0.05. 64
- Figure 5.10 Dark toxicity and PDT (980 nm laser with 1 W/cm² and 5 minutes application) measurements for various concentrations of ZnPc and MC540 loaded UCNP@Au. P values: *P<0.05, and **P<0.01. 65

LIST OF TABLES

Table 4.1	Sizes of nanoparticles with DLS and SEM-TEM measurements.	45
Table 4.2	Loading amount of photosensitizers.	49
Table 5.1	Corresponding concentrations of photosensitizers inside UCNP@Au.	66

LIST OF SYMBOLS

c	Velocity of Light
λ	Wavelength of Light
ν	Frequency of Light
S_0	Ground State
S_1	Excited State
h	Planck's constant
μ_a	Absorption Coefficient of Tissue
μ_s	Reduced Scattering Coefficient of Tissue
g	Anisotropy Factor
n	Refractive Index

LIST OF ABBREVIATIONS

APTES	3-Aminopropyltriethoxysilane
Au np	Gold Nanoparticles
CR	Cross Relaxation
CSU	Cooperative Sensitization Upconversion
CTAB	Hexadecyl-trimethyl-ammonium bromide
CW	Continuous Wave
DLS	Dyanamic Light Scattering
DMSO	Dimethyl Sulfoxide
EDS	Energy Dispersive Spectroscopy
ETU	Energy Transfer Upconversion
FTIR	Fourier Transform Infrared Spectroscopy
IC	Internal Crossing
ISC	Intersystem Crossing
MC540	Merocyanine 540
NIR	Near Infrared
OA	Oleic Acid
PA	Photon Avalanche
PCI	Photochemical Internalization
PDT	Photodynamic Therapy
PS	Photosensitizers
PTT	Photothermal Therapy
ROS	Reactive Oxygen Species
SEM	Scanning Electron Microscopy
SPR	Surface Plasmon Resonance
TEM	Transmission Electron Microscopy
TEOS	Tetraethyl Orthosilicate
UCNP	Upconversion Nanoparticles
UCNP@Au	Gold Nanoparticles Assambled UCNP@APTES

UCNP@APTES	APTES Coated UCNP@mSiO ₂
UCNP@mSiO ₂	Mesoporous Silica Coated UCNP
VIS	Visible
ZnPc	Zinc Phtalocyanine

1. INTRODUCTION

1.1 Motivation

According to the global statistics in 2020, the leading reason of death is cancer in the world [1]. In fact, it is a kind of disease that causes severe pain and ultimate death due to the uncontrollable growth of damaged cells and metastasis to the surrounding tissue. There are two main reasons that traditional methods have unsuccessful results: (i) late stage tumors metastasis too fast, and (ii) cancer cells develop resistance to the treatments in time. Besides, patients' quality of life reduce during treatments, i.e. chemotherapy, radiotherapy, or surgical dissection. The primary motivation behind this study is to improve cancer treatment using a non-invasive approach. Photodynamic therapy (PDT), among other methodologies, has a potential future for treating cancers with minimized side effects.

Photodynamic effect of light - photosensitive materials (e.g. photosensitizers (PS)) combination were realized almost one centuries ago and it is still not considered as a conventional treatment [2]. When the researches and clinical practices on PDT is examined, it can be seen that the penetration-depth of light performed to activate the photosensitizers is the major problem. As a matter of fact, light energy increases as their wavelength decreases and commercially available photosensitizers require mostly visible (VIS) range to be activated. Unluckily, VIS range cannot penetrate more than a few millimeters [3]. However, advances in nanotechnology have changed the fate of PDT in terms of treatment depth. In 2007, transducer-nanomaterials called photon upconverting nanoparticles were used to convert near-infrared light (974 nm) to VIS light (540 nm), so that PDT was activated with such a low-energy light for the first time [4]. Afterwards, many studies were concentrated on upconversion nanoparticles (UCNP) due to their extraordinary optical behavior can be used to deal with major problem of PDT, penetration depth. The second motivation of this research is to provide a solution for this serious limitation of PDT by using UCNP.

One of the important components of PDT is photosensitizers, and many researchers working in this field have developed different types of PS using various chemical combinations [5]. An ideal photosensitizer should present high quantum yield, good biocompatibility, and excitability with longer wavelengths. However, there is still no PS that provides all the ideal features. For instance, most high efficient PS are not biocompatible. In order to eliminate less biocompatibility issue of PS, nano-transfer systems have been developing [6]. Since conveying PS to the desired biological site is crucial, this work is also directed to design an efficient delivery system for both UCNP and PS.

It is necessary to observe the produced novel system on biological applications to understand its efficiency. Possible limitations (i.e. thermal, less reactive species generation, high dark toxicity) should be considered. Then, they can be used on a leading cancers such as breast, colon, prostate, or stomach. Experimentally using a newly produced nano-system on biology and determining the real activity is the last motivation of this work.

1.2 Objectives

The main propose of this study is to design and synthesize a new nano-delivery system to improve photodynamic therapy on prostate cancer. This approach is aimed to include upconversion nanoparticles (UCNP) synthesis to convert NIR light into multiple VIS wavelengths, porous silica coating to upload dual photosensitizers (MC540 and ZnPc), and gold functionalization to enhance UCNP emissions. Material characterizations, optical properties of materials, and encapsulated PS amounts will be decided with proper equipment. As the preliminary biological applications, the preferred PDT elements (i.e. 980 nm laser and PS-nanoplatform system) will be evaluated in a manner of thermal change, reactive oxygen species generation, and penetration depth. Lastly, *in vitro* analysis will be carried on prostate carcinoma cell lines (PC-3) via cellular internalization and dark toxicity of PS / nanoplatforms, only light toxicity, and PDT efficiency experiments.

1.3 Outline

The upcoming chapters of thesis comprise shortly the followings:

- **Chapter 2:** The overall background of photodynamic therapy, upconversion nanoparticles, and surface arrangements for biological applications were presented with respect to the researches on this field.
- **Chapter 3:** In this division, the used materials and methodologies were explained for both synthesise of nanoplatforms - photosensitizers combination, and experiments on temperature differentiation, reactive species production, and prostate cancer cells.
- **Chapter 4:** Nanoplatforms' material characterization procedures, and results were given in this part.
- **Chapter 5:** The outcomes of applications were supplied with the necessary explanations.
- **Chapter 6:** The results were discussed in detail for the whole study.
- **Chapter 7:** In this section, this research was concluded and possible future studies were proposed.

2. BACKGROUND

2.1 Photodynamic Therapy

Photodynamic Therapy (PDT) is a potential approach to treat the lesions like tumors by merging light and drugs/dyes recognized as photosensitizers (PS) in the existence of oxygen. Although light has been using as a therapeutic method since ancient civilizations, both light and acridine dye combination lethal effect on *infusoria*, as a first PDT application, was discovered by Tappeiners' group in 1900s [2]. Since the PDT phenomenon first emerged, significant advances have been made with improvements in photosensitizers and light sources.

Photosensitizers are one of the main elements for PDT applications. Some of the drawbacks of PS have been observed since Photophrin 2, the purified version of Hematoporphyrin derivative, was used in the first clinical trials as PDT drug [7]. Thus, many studies focused on to develop the ideal PS. The properties of PS should include the followings; (I) efficient ROS generation, (II) higher absorption feature at the longer wavelengths, (III) high biocompatible characteristics [2]. However, the produced photosensitizers so far have not been able to show all the necessary virtues at the same time.

The used light sources to activate PS, on the other hand, can be natural sunlight, arc lamps, slide projectors, or lasers [8]. In fact, the mostly preferred sources are laser systems to initiate PDT. They can produce coherent light and the generated light can be applied outer or inner parts of body via optical fibers [8]. Regardfully, the wavelength of the laser requires matching with the absorption spectra of the used PS.

After stimulating PS with light, reactive oxygen species (ROS) such as singlet oxygen (1O_2), hydrogen peroxide (H_2O_2), hydroxyl radical ($\cdot OH$), and superoxide anion (O_2^-) generation can be triggered [9]. It is known that the metabolism of cells use these

molecules for physiological processes under normal conditions. However, excess ROS results in oxidative stresses in the cells and abnormal amount of ROS, ultimately, activate cell death mechanisms like apoptosis, necrosis, or autophagy [10].

2.1.1 Mechanisms in PDT

PDT action comprehend three main steps as given in Figure 2.1. Firstly, to eliminate the lesion bearing tissue or cancerous cells, photosensitizers should be administered intravenously or topically. Secondly, cellular accumulation of PS take place after waiting for a period of time. As a final step, light exposure to the tumor site initiates the PDT process. In fact, underlying mechanisms in PDT can be explained via both photochemistry and photophysics concepts [11]. While the two laws of photochemistry states that (First Law) light must be absorbed by a compound (e.g. photosensitizers), and (Second Law) only one molecule can be activated for each absorbed photon of light; photophysics deal with the physical changes during the occurrence of material-photon interactions [11, 12, 13].

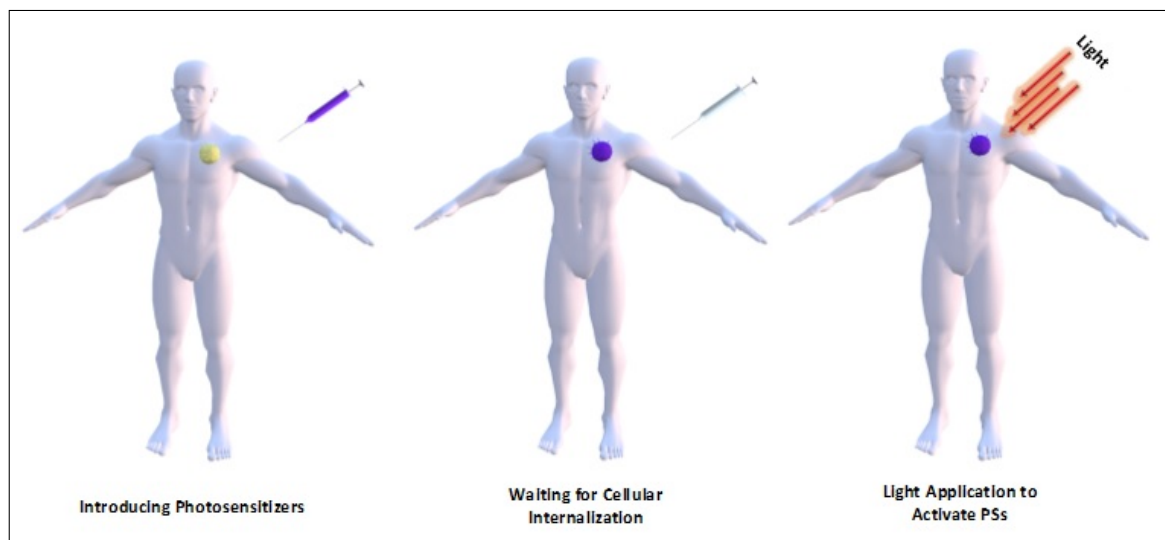


Figure 2.1 Schematic illustration of photodynamic therapy action.

2.1.1.1 Light Absorption. Light absorption for photosensitizers is a mandatory step for PDT action. According to the wave model, an electromagnetic wave can be defined with eq.2.1 [12].

$$c = \lambda \nu \quad (2.1)$$

where c = velocity of light, λ = wavelength of light, ν = frequency of light. The electromagnetic spectrum include a wide range of wavelengths as X-rays (0.1 nm - 10 nm), Ultraviolet (10 nm - 350 nm), Visible (350 nm - 750 nm), Infrared (750 nm - 10^6 nm), Microwaves (10^6 nm - 10^7 nm), and Radiowaves ($> 10^7$ nm) [11]. The energy of light (E) defined in eq.2.2 decreases from X-rays to Radiowaves.

$$E = h(c/\lambda) \quad (2.2)$$

where h is the Planck's constant [12]. To excite molecules in PS, the applied light energy should be high enough and generally VIS range is the best choice to trigger PDT mechanism [14]. However, VIS light penetration depth in tissue is not sufficient for deep-seated cancerous cells.

2.1.1.2 Excited-State Processes of Electrons. Jablonski diagram in Figure 2.2 can be used to have insight about the excitation states and outcome of PDT. Energetically favored state for photosensitizers is their ground state (S_0), where the total spin quantum number (S , defined with paired spins as $+1/2$ and $-1/2$) is zero. The excitation state of PS, on the other hand, can be expressed as excited singlet state (S_1). It is possible to show the excitation reaction for PS with expression 2.3:



where * describes the excited photosensitizers after exposing them with an appropriate light irradiation. Then, relaxation of PS occur and it initiates different chemical reactions or photophysical processes such as luminescence, radiationless decay (i.e. internal crossing (IC), and intersystem crossing (ISC)), electron transfer, bimolecular reactions, or secondary radical formations [2, 13]. These reactions result in the two main pho-

photodynamic mechanisms activation as called Type I and Type II. If Type I mechanism takes place, the excited PS directly interact with molecules in cells and produce radicals such as hydrogen peroxide (H_2O_2), hydroxyl radical ($\cdot OH$), and superoxide anion (O_2^-). Occurrence of Type II mechanism is also possible and it includes the energy transfer of PS to oxygen (O_2), which can generate singlet oxygen (1O_2).

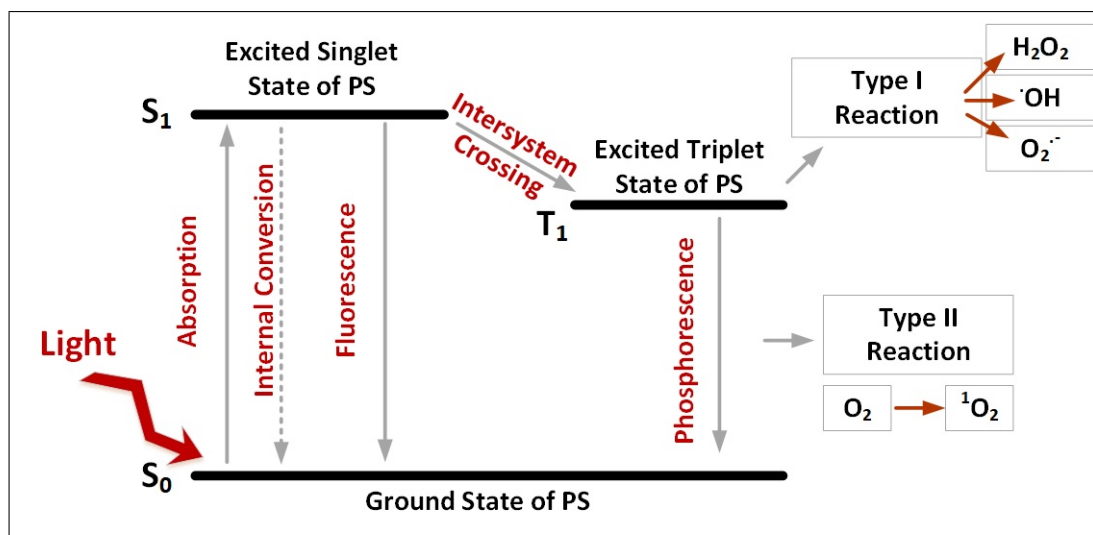


Figure 2.2 Designed Jablonski Diagram for photosensitizers upon light application.

2.1.2 Novel Methodologies in PDT

The three components of PDT, photosensitizers, light and oxygen, must act efficiently when PDT mechanism is considered [15]. At first, PS selection for PDT treatment is a very crucial step because an ideal PS doesn't exist and commercially available ones lead to very different outcomes for *in vitro* and *in vivo* studies [16]. The preferred PS should be nontoxic, selectively captured by cells, excited with higher wavelengths of light in the therapeutic window; and their quantum yield have to be high enough to eliminate cancerous cells [17].

Several group of photosensitizers mostly have tetrapyrrole structure like the first clinically approved porphyrin derivative hematoporphyrin (HpD) and photofrin [18]. Porphyrins, however, cannot fulfill the all requirements as an ideal PS due to their complex chemical structures (long half-life) and their efficient activation band being

around 400 nm (short tissue penetration) [19, 20, 21]. Therefore, second generation PS were produced; chlorins (i.e. Foscan, Verteporfin, Chlorin(e6)) , bacteriochlorins (i.e. TOOKAD, LUZ11), and phthalocyanins (i.e. Zinc Phthalocyanine) [22]. These second generation photosensitizers have better chemical purity, higher penetration depth, and increased ROS production. However, significantly low water solubility is the main drawback during PDT applications with them [23]. Furthermore, the third generation PS are under developmental stage and their production aim depends on the structures possessing higher affinity to the cancerous region [23].

Apart from the PS having tetrapyrrole design, transition metal compounds (i.e. gold, platinum), and natural products (i.e. hypericin, hypocrellin riboflavin, curcumin) can be used for PDT treatment [18]. Besides, other types of PS exist as cationic such as methylene blue or cyanine dyes, and uncharged as merocyanine 540 [22, 24].

The other important PDT element, light, needs to be used with respect to the selected PS. Application of light at higher wavelengths (from 600 to 1000 nm) can enhance PDT because it provides higher penetration depth into the tissues [17]. Besides, illumination can be applied not only via superficial but also interstitial delivery, i.e. fiber [25]. Lastly, the third crucial component, oxygen, during PDT application needs to exist inside or outside of the cancerous cells. However, oxygenation for dense tumor masses is generally not enough for PDT [26]. Hypoxic condition of tumors can be resolved with some oxygen carriers or generators, i.e. hemoglobin, perfluorocarbon, or manganese dioxide [27].

Some of the ongoing investigations to develop PDT are listed as follows:

1. Photochemical Internalization (PCI): It is well known that cells internalize molecules such as drugs, proteins, DNA, RNA, or PS via entrapping them inside the endocytic vesicles, which prevent their full efficiency [28]. PCI, on the other hand, provides a methodology to overcome this problem by using amphiphilic PS (i.e. aluminium phthalocyanine disulfonate, Amphinex) [29]. In fact, these PS have ability to break the endosomes upon light illumination and improve the treatments [30].

2. Theranostics: When diagnostics and therapeutics are combined at once, the term *theranostics* emerge [31]. It allows visualization during treatments and provide real-time monitoring for cancerous region. Fluorescence properties of some PS (i.e. porphyrins) provide this property [32].

3. Photodynamic Immunotherapy: PDT recognizes as a local treatment method and metastasis problem cannot be avoided with this methodology. In fact, cancerous cells/region destruction way (apoptosis, necrosis, or both way) can promote the activation of immune system [33]. However, PDT application alone is mostly not enough to trigger immune response because tumor micro-environment inhibits immunity pathway. Thus, synergistic effects of PDT and immunotherapy can be used to treat tumors [34].

4. Nanotechnology: Nanotechnology means to design precisely engineered materials, mostly named as nanoparticles/nanomaterials in submicron scale [24]. They can be utilized to carry drugs/dyes (i.e. PS), target specific region in body, and provide combinational treatments for novel applications [35]. Although nano-sized carrier systems have numerous benefits like controlled delivery, high drug loading capacity, adjustable chemical property, or multifunctionality; the existence of several disadvantages such as aggregation problems, tuning sizes, or long-term side effects cannot be ignored [36].

The ongoing PDT researches in nanotechnology endeavor to eliminate the problems for nano-carrier systems [18]. The developed nanoparticles have wide range forms: polymeric (i.e. poly-D,L-lactide-co-glycolide (PLGA), polylactic acid (PLA), chitosan, gelatin), metallic (i.e. gold (Au), silver (Ag)), and lipid (i.e. polyethenoglycol (PEG) lipid) [37, 38]. These nano-carrier systems can safely deliver photosensitizers to cancerous region via isolating them from the harsh environment of body. Along side the protection properties, a number of them (i.e. quantum dots, metallic nanoparticles, upconversion nanoparticles) can be activated with light so the treatment/diagnostic properties of PS can be supported.

2.2 Upconversion Nanoparticles

When the nanomaterials interactions with light and photoluminescence properties are considered, there are two classifications as downconversion (DC) and upconversion (UC) fluorescence [39]. While downconversion process (stoke's shift) is named for longer-wavelength photon emission (lower energy), upconversion process (anti-stoke's shift) is the emission of shorter-wavelength photon possessing higher energy. Anti-stokes process is the reverse behavior of most materials and can be succeeded with a few of them like quantum dots, or UCNP [40]. Generally, an upconversion material includes two components: a host lattice, and doping ions. Changing the host matrix or dopants can dramatically differentiate the fluorescence property of the nanomaterials. In this study, we focused on lanthanide-based (rare-earth) upconverters.

Lanthanide ions doped nanomaterials have the ability to convert near-infrared photons to higher energy photons between ultraviolet (UV) and NIR. Near-infrared absorption property make these materials very attractive sources for biomedical applications. It is well known that tissue (i.e. hemoglobin or water) absorbs the NIR (700 nm-1300 nm) light minimally and this region is also called "optical window" [41]. That is, utilizing from NIR light for biological applications provides minimal photo-damage, low auto-fluorescence, and high light penetration depth. Besides, UCNP has sharp and adjustable emission bands, high photostability, long life-time, and minimized toxicity [42].

The mostly known and used rare-earth elements have trivalent ions like Pr^{-3} , Nd^{-3} , Er^{-3} , Tm^{-3} , Yb^{-3} [43]. These ions' upconversion behavior comes from their inner 4f shell because the electrons at 5s and 6p shells (outer shells) are used to bind with surrounding atoms and they are very sensitive to the lattice events [44]. For this reason, when light excites a significant amount of electrons in the 4f shell, they have sufficient lifetimes to form the upconversion process in the excited states [45]. Furthermore, lanthanides include different energy levels, mostly arranged as ladder-like, can initiate sharp and narrow emissions at the same time [41]. The possibility of benefiting from more than one emissions arises with this property.

2.2.1 Energy Mechanisms of UCNP

Luminescent materials mostly follow the rule known as Stoke's law, the emitted photon energy is lower than the absorbed photon energy, and an energy loss occurs. On the other hand, it is possible to observe opposite behavior of materials in some circumstances like upconversion emission. It is actually a nonlinear optical process, discovered by Auzel, Ovsyankin, and Feofilov in 1960s [46, 47]. It was stated that if more than one NIR photons are absorbed by middle energy levels, the wavelength of fluorescence appears shorter than the excited light. Upconversion mechanisms include excited-state absorption (ESA), energy transfer upconversion (ETU), cooperative sensitization upconversion (CSU), cross-relaxation (CR), and photon avalanche (PA).

Excited-State Absorption (ESA): As the simplest activation of upconversion mechanism, initially an ion needs to be excited from ground state to E1 and then another excitation proceeds to E2 thorough additional photon absorption (Figure 2.3 (a)) [48]. Ladder-like energy levels and long lifetimes for excited ions are necessary for this process [44].

Energy Transfer Upconversion (ETU): ETU process includes absorption of two photons and two ions, defined as activator and sensitizer (Figure 2.3 (b)) [48]. When the first absorbed photon excites the sensitizer to metastable level E1, it is possible that sensitizer can transfer its energy to activator being at ground level. Thus, energy transfer and second photon absorption excite the activator to E2 level. Meanwhile, sensitizer (at E1 level) turns back to ground state, and activator (at E2 level) produce upconversion emission. The distance between ions and dopant concentration decide the ETU occurrence.

Cooperative Sensitization Upconversion (CSU): In CSU mechanism, there are three ions that the first and third ions (called as sensitizers) activation transfers energy to the second ion (called as activator) as shown in Figure 2.3 (c) [48]. The relaxation of activator can generate upconversion light. CSU process appearance chance is lower than ESA and ETU.

Cross Relaxation (CR): It is an unwanted process that can occur with ion-ion interaction. The ion in excited state at E2 relaxes back to E1, and subsequently the energy is transferred to the other ion at ground state (Figure 2.3 (d)) [48]. As a result, no upconverted photon can be observed. However, it can trigger the photon avalanche process or cross relaxation can be utilized for arranging upconversion color.

Photon Avalanche (PA): PA is a complicated loop mechanism as demonstrated in Figure 2.4 (e) [48]. Initiating a PA needs a photon threshold value [49]. When the absorbed photon amount is under the threshold, upconverted emission is well below than the expected intensity. On the other hand, photoluminescence increases with respect to absorbed photon increase by orders of magnitude, if the threshold value is exceeded.

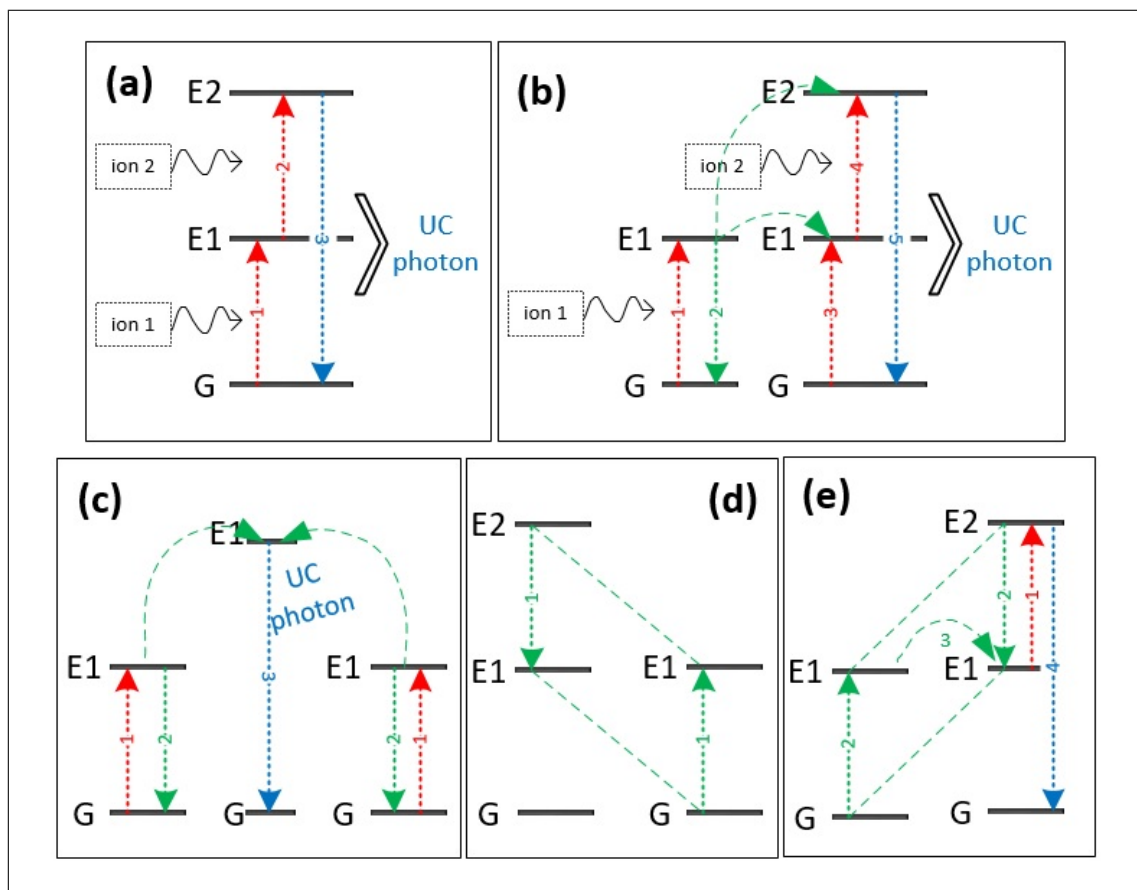


Figure 2.3 Presentation of the mechanisms for the lanthanide doped upconversion nanoparticles: (a) ESA, (b) ETU, (c) CSU, (d) CR, and (e) PA.

2.2.2 Designing Upconversion Nanoparticles for Enhanced Luminescence

The UCNP energy mechanisms efficient existence requires two critical components which are a highly stable host matrix, and two dopant ions named as activator, and sensitizer. While the host material possessing a crystalline structure is used as a protector; sensitizer plays a role during the absorption of energy, and activator provides the emission of light (Figure 2.4) [44]. The importance of the choice of elements/compounds for host matrix, activator and sensitizer cannot be underestimated during the formation of upconversion nanoparticles.

Initially, the host material needs to have great chemical stability, low phonon energy, good transparency between NIR and VIS range, and high durability against optical damage [41]. In fact, its matrix include the dopant ions so the distance between the activator and sensitizer is determined by the used host material. The spatial position of dopant ions has important influence on the efficiency of UCNP [50].

It is well known that Na^+ , Ca^{2+} , Sr^{2+} , Y^{3+} and Ba^{2+} has similar ionic radius and chemical features with the lanthanide ions [50, 51]. Especially, Na^+ and Ca^{2+} fluorides are used to prefer as host materials due to the property of minimized lattice defects and stresses. Besides, the crystal structure of the host material can change the activity of UCNP. Optical property is directly effected with the symmetry of structure. For instance, hexagonal phase $NaYF_4 : Yb/Er$ material has 10 times better efficiency than cubic phase of it [52].

Activators, as a dopant ions, can generate sharp and narrow upconverted light. If the lanthanide ions have completed $5s^2$ and $5p^6$ outer shells, the protected 4f inner shell electrons can stay at the excited states up to 0.1 s [47, 50]. The mostly suitable activators are Er^{3+} , Tm^{3+} , and Ho^{3+} . The other dopant ion to the host matrix is called as sensitizer. Yb^{3+} is extensively used as sensitizer because it has a large absorption cross section close to 980 nm [47, 50]. Its basic structure only include one 4f level excitation ($^2F_{5/2}$). The energy of excited electrons can cross the ions of activators and upconverted emission can appear.

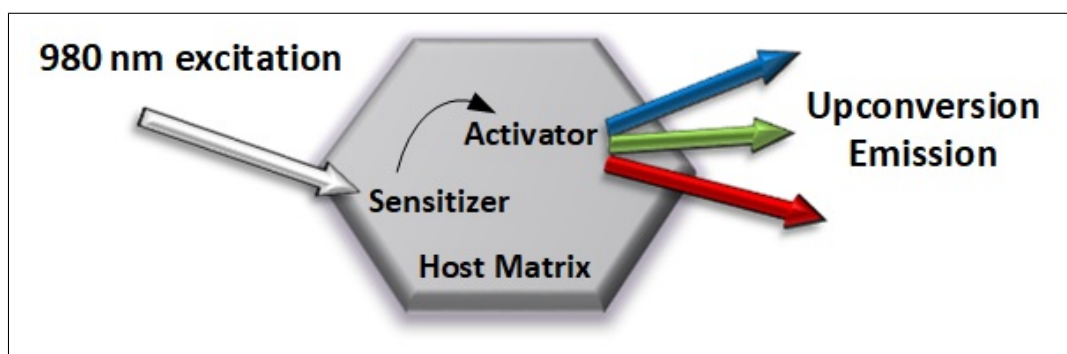


Figure 2.4 The design of upconversion nanoparticles.

2.3 Surface Modification of UCNP for Biological Applications

UCNP can be used for different biomedical applications due to their superior optical properties. However, before utilizing them in bioapplications, some important issues such as biocompatibility, water solubility, or bioconjugation requires to fix [53, 54]. Efficient surface modification of UCNP is the only solution to deal with these inevitable topics. It should also be noted that the possible surface adjustments can enhance the optical features of UCNP, and add drug attaching, or bio-targeting properties.

The concept of surface modification for nanoparticles can be stated that the differentiation of the material surfaces in terms of chemical, physical, or biological pathways [55]. The alterations around the exterior part of UCNP not only arrange their material properties for hydrophilicity, biocompatibility, and surface charge, energy, and reactivity; but also provide a protection from surrounding media. In fact, the stability of nanoparticles during delivery to the desired region in the body is a crucial issue when the hydrophobic nature of UCNP is considered [56].

Although there are different ways to synthesize UCNP, it is mostly preferred to produce them with hydrophobic surfactant ligands (i.e. oleate) to eliminate the aggregation problem of nanoparticles [57]. To add, the oleate ligand can control the growth of nanoparticles with performing as a solvent through the synthesize [58]. Unluckily, UCNP shows a strong hydrophobic behaviour due to its oleate capped surface, which

restrains its dispersal in aqueous media and minimizes biocompatibility [59].

Engineering nanomaterials for biomedical practices require biocompatibility, which can be defined as the capability to accomplish delivering wanted properties (i.e. drugs/PS, light) to the region of body without showing any adverse effects to the other sites [60]. In order to prevent the potential toxicity of nanomaterials for in vitro applications, chemical or physical coatings can be performed around the surface of nanoparticles [53]. Besides, the surface modifications can improve the in vivo studies and increase the biocompatibility for these kind of applications.

In the literature, there are extended methods to make the UCNP applicable for biological studies [59, 61]. They can be divided into four main topics as ligand engineering, ligand attraction, surface silanization, and metal connections. Each approach has its unique characteristics that can be used for different/ similar operations such as drug/PS delivery, targeted therapy/imaging, or biosensing [62, 63].

2.3.1 Ligand Engineering

The ligand functionalization of UCNP is a common method and it can improve the stabilization of nanoparticles [64]. Modification of ligands (i.e. oleic acid or oleylamine) for UCNP is possible with original ligand exchange and direct oxidation of UCNP surface (Figure 2.5) [53]. When the oleic acid (OA) capped UCNP is considered, the carboxyl ends of OA bind strongly to the rare-earth ions due to the two C-O connections [65]. It means the newly connected ligands require stronger bonds than the OA-UCNP linkage; otherwise, they can detach from the surface. Thereby, it brings difficulties, and long duration time synthesis during surface modifications with ligand engineering.

In order to change oleic acid connections with other types of ligands such as $-COOH$, $-NH_2$, or $-SH$ groups; initially OA needs to be removed for ligand exchange studies. Acid treatment, being able to protonates the oleate ligands, is a way to

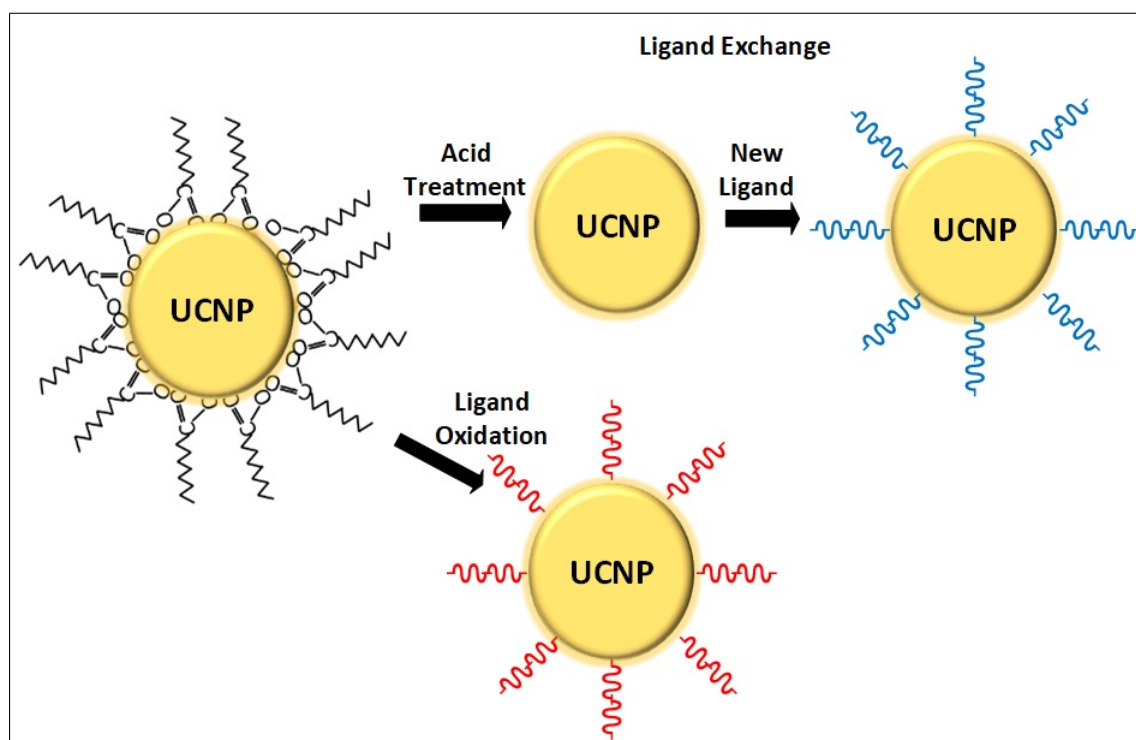


Figure 2.5 Ligand surface engineering for UCNP.

derive bare-UCNP [66]. Then, introducing hydrophilic ligands with citrate, polyethylene glycol (PEG) derivatives, polyacrylic acids (PAA), or phosphate derivatives enables new linkages on UCNP [66, 67]. The functions of each ligand supply different properties to the nanoparticles. For instance, Chen Y. et al. published article in 2020 evaluated carboxyl, poly(monoacryloxyethyl) phosphate (MAEP), amino, and (3-aminopropyl) triethoxysilane (APTES) functionalized UCNP with ligand exchange method [68]. This comparative study showed that while carboxyl-coated UCNP is more stable than the others, MAEP allows the best biocompatibility for UCNP. Another way for ligand exchange method is to alter the surface of UCNP using nitrosonium tetrafluoroborate ($NHBF_4$) or diazonium tetra-fluoroborate compounds [65]. It includes multiple steps but UCNP become soluble inside N,N-dimethyl-formamide (DMF), or dimethylsulfoxide (DMSO) and the nanoparticles become highly stable for a long time. The dissolved nanoparticles small amount in DMSO or DMF can be mixed with an aqueous media for biological applications.

Bifunctional molecules, possessing two different functional groups, usage for

ligand exchange method is also commonly studying in literature. In 2009, Hilderbrand S. A. et al. modified the surface of Y_2O_3 nanoparticles with PAA-PEG for in vivo imaging [69]. As another attractive study, Ge H. et al. recently published poly-cytosine and DNA conjugated UCNP to facilitate them easy cell entrance for possible imaging and therapeutic agents [70].

The direct oxidation of oleic acid or oleylamine is also achievable with Lemieux-Von Rudloff reagents, ozone, or 3-chloroperoxy-benzoic acid [71, 72, 73]. They can lead the hydrophilic carboxylic acid groups formation around UCNP. The generated new ligand include carbon-carbon double bond which restricts capping ligands variety.

2.3.2 Ligand Attraction

Ligand attraction is an approach about connecting amphiphilic polymers to the surface of UCNP [44]. In fact, amphiphilic polymers encompass both hydrophilic, renders water solubility, and lipophilic, enables attaching with fat (like oleic acid) ligands, ends. In this process, the purpose is to link lipophilic ends with UCNP and allow hydrophilic ends to faces outwards (Figure 2.6). Therefore, UCNP can be water soluble and biocompatible with respect to the features of amphiphilic polymer.

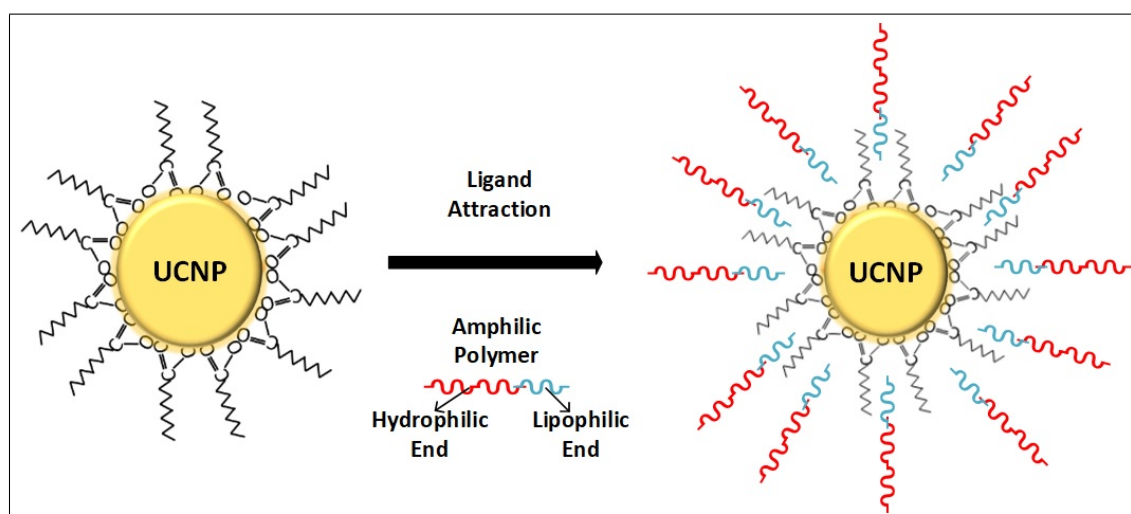


Figure 2.6 Ligand attraction procedure for UCNP.

The amphilic polymers can be poly(acrylic acid)-poly(ethylene glycol), phospholipids with head groups biotin or maleimide, poly (L-lysine), poly(maleic anhydride-alt-1-octadecene) or others [74, 75, 76]. In 2021, Lee S. H. and et al. merged the amphilic polythiophene with UCNP and applied to sense the alprenolol amount, decides the high blood pressure [77]. As an another recent study published in 2020, Guryev E. L. and et al. coated the surface of UCNP with maleic anhydride 1-octadecene (PMAO) and PEG-amine for imaging and treating human adenocarcinoma models [76].

2.3.3 Surface Silanization

Among the surface modification methodologies for UCNP, silica condensation is a highly powerful and advantageous technique [78]. In fact, silica is already considered as "Generally Recognized as Safe" (GRAS) by FDA, proves its high biocompatibility, and easy drug/PS encapsulation within silica moieties [79]. This technique can be performed by two separate functionalization pathways as visualized in Figure 2.7: (I) dense (amorphous) silica formation followed by possible porous silica generation, and (II) direct establishment of mesoporous framework.

As a first way, thin amorphous silica coating around UCNP is generally provided with tetraethoxysilane (TEOS) or similar silica precursors, because the silane reagents is able to react straightly with UCNP face. In 2015, Liu J. N. and et al. was discussed the concept for the UCNP - dense silica conjugation with the UCNP - mesoporous (and hollow) silica junction [80]. In 2016, Han R. and et al. used the interface of amorphous - mesoporous silica (coated around UCNP) to bind Methylene Blue (PS), and utilized from the porous part to load doxorubicin (DOX) [81]. This research showed the possibility of applying these nanoplatforms for both chemotherapy and NIR-triggered PDT.

Encapsulating UCNP with porous silica is a favorable technique because it possess biocompatibility, water-solubility, and drug/PS loading properties without applying any middle-step surface modifications for drug/PS [82]. Indeed, it is well known

that drug/PS have mostly hydrophobic nature, which makes their usage complicated. On the other hand, mesoporous silica can protect and carry drug/PS (especially hydrophobic ones) easily to the biological sites [83].

In 2014, Sun L. and et al. managed the direct production of mesoporous structure on UCNP for imaging human nasopharyngeal epidermal carcinoma cells [84]. They used cetyltrimethylammonium bromide (CTAB) for phase transfer (from hydrophobic to hydrophilic UCNP) and pore formation agent. Then, implemented silica precursor and removed CTAB steps let the mesoporous silica generation around UCNP.

In addition to the notable benefits of silanization UCNP, silica ligands can further functionalized with amino and amine groups, polymers (i.e. PEG, PEI), or biomolecules (i.e. folic acid, biotin, or proteins) [85, 86, 87]. It extensively increases the potential of UCNP usage. For example, Wang Y. and et al. combined mesoporous silica coated UCNP (UCNP@mSiO₂) with (3-aminopropyl)triethoxysilane (APTES) and DOX was loaded inside the porous silica [87]. Charge-reversal APTES added pH-drug delivery feature to the nanoplatforms. Thus, controllable drug release and simultaneous imaging of cancer cells becomes possible.

2.3.4 UCNP-Metal Connections

Metal nanostructures such as gold and silver nanoparticles/shells can mediate surface plasmon resonance (SPR) [88]. Actually, SPR existence within UCNP can enhance optical properties of luminescence and result in heat increase [89]. The synthesize of UCNP with metallic thin layer/nanoparticles can improve the capability of UCNP in different manners if fluorescence of UCNP and absorbance of nano-metals optical absorption are matched. Metallic structures combination with UCNP include extensive engineering designs but in general they used to synthesize metallic/UCNP and UCNP/metallic forms for imaging and treatment applications [44].

When the metallic/UCNP design is considered, the material having upconver-

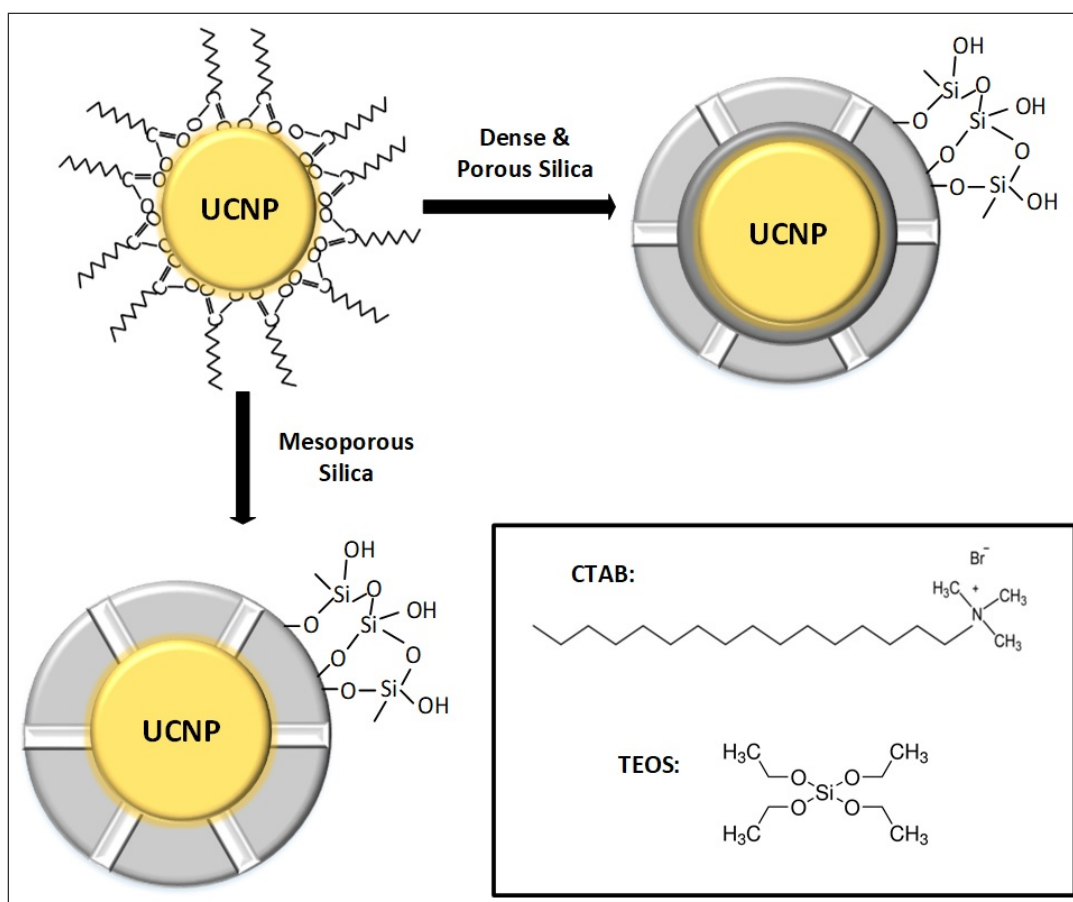


Figure 2.7 Surface silanization of UCNP.

sion property surrounds metallic nanoparticles. For instance, in 2010, Zhang F. et al. designed nanoplatforms include dense silica - $Y_2O_3 : Er$ shell surrounded 50 nm silver (Ag) nanoparticles [90]. The distance between the rare-earth complexes and Ag was evaluated in terms of the possibility for enhanced luminescence or quenching which allow imaging prostate cancer cells. However, the metallic/UCNP design resultant cellular toxicity can be high because the the outer layer include the rare-earth elements.

On the other hand, UCNP-metallic form of union can increase the biocompatibility, especially with the gold nanoparticles. The noble metal, Au, was already used for a clinical trial (Phase I) [91]. Besides, gold np decoration around UCNP can amplify photoluminescence and add photothermal therapy (PTT) feature due to SPR feature of Au [92]. In 2012, Priyam A. et al. produced gold nanoshell coated $NaYF_4$ and their high imaging capability was demonstrated on melanoma cell line [93]. As a recent

study, in 2020 Lin B et al. utilized from gold np coated spindle shape UCNP to kill cancerous cells with PDT [94].

3. MATERIALS AND METHODS

3.1 Upconversion Nanoparticles Synthesis

In this study, we produced Yb^{+3}/Er^{+3} doped $NaYF_4$ nanoparticles by using Ostwald ripening method, depends on the fact that the growth of larger particles is energetically favored compared to smaller nanoparticles [48]. The synthesis protocol was acquired from literature and some modifications were made during the experiments [82].

3.1.1 Materials and Instrumentation

The used reagents; yttrium (III) oxide (Y_2O_3 , 99.99 %), ytterbium (III) oxide (Yb_2O_3 , 99.99 %), and erbium (III) oxide (Er_2O_3 , 99.99 %) were from Alfa Easer. Sulfuric Acid (H_2SO_4 , 95-97 %), hydrochloric acid (HCL, 36%), oleic acid, 1-octadecene, sodium hydroxide ($NaOH$), ammonium fluoride (NH_4F), cyclohexane, ethanol (absolute, reagent, 99.8 %), acetone (ACS reagent, 99.5 %), methanol (anhydrous, 99.8 %), sodium hydroxide (NaOH) were received from Sigma Aldrich.

Three-neck round bottom flask (100 ml), flask adaptors, condenser, thermocouple, glass thermometer, vacuum pump, vortex, ultrasonic bath, centrifuge, centrifuge tube (50 ml), and glass scintillation vial (20 ml) were used equipment for UCNP production.

3.1.2 UCNP Preparation

UCNP synthesis includes the following steps:

- 1) A three-neck bottle and a condenser were initially waited inside a Sulfuric

Acid (H_2SO_4) aqueous solution (30% concentration) for 30 minutes in ultrasonic bath. Then, washing steps were applied with acetone, and ethanol. Teflon band (PTFE, professional Starline) was also wrapped to tips of the connecting glasses to prevent them from high heat and avoid leakage of gas.

2) Y_2O_3 (0.088 g), Yb_2O_3 (0.0395 g), and Er_2O_3 (0.0038 g) were put inside the three-neck-bottle and they were reacted with HCL to obtain YCl_3 , $YbCl_3$, and $ErCl_3$. Initially, sonication was applied and then its heat was increased slowly. When colorless solution was observed, the excess water was evaporated at 110 °C with stirring. White and dry pellet was obtained at the bottom of the flask. The rise in temperature was checked by touching the bottom of the three-neck flask with a glass thermometer.

3) 6 ml oleic acid and 15 ml 1-octadecene were added into the flask having white pellet at the bottom. While oleic acid, as a surface ligand, controlled the size and shape of nanoparticles, 1-octadecene allowed the reaction to reach high temperatures because of its high boiling point.

4) In order to dissolve the pellet, heat was elevated to 150°C while stirring. The solution was kept 1 hour at this condition to get well mixed rare-earth elements. The color of solution was light yellow as shown in Figure 3.1 (a). Afterwards, the temperature was decreased to 50 °C.

5) To initiate precipitation, methanol (5 mL), containing NaOH (0.1 g) and NH_4F (0.148 g), were added into the mixture dropwise. The photograph of solution were given in Figure 3.1 (b) Then, heat of the flask was raised slowly between 110°C and 130°C to evaporate methanol and waited for 1 hour. Some bubbles and color variation were noticed during heat rise (Figure 3.1 (c)).

6) Then, flask was sealed with vacuum and waited for additional 20 minutes to remove moisture and possible remained methanol. Condenser and argon gas (>99.999) cable were also connected to the flask with glass adaptor as demonstrated in Figure 3.1 (d). In order to cool down the condenser, cold water movement was provided

continuously during the synthesis.

7) Argon gas and vacuum were applied in order with 1-minute intervals for three times. Note that, argon gas passage was always under control during the application. The temperature was raised to 300°C with a heating rate 10°C / 2 min. under argon atmosphere. Next, the mixture was maintained at the same temperature for 1 h as presented in Figure 3.1 (e).

8) After 1 hour, the system was cooled down to room temperature without removing argon gas and stopping stirring. Subsequently, the solution poured into 50 mL centrifuge falcon tube. Three necked flask was rinsed with acetone and it was also put inside the same falcon. The added acetone needed to be 40 mL (Figure 3.1 (f) - left photo).

9) The tube was vortexed vigorously for 1 minute for rinsing, and it was centrifuged at 7800 RPM for 10 minutes. After discarding supernatant, pallet was dissolved in 20 mL cyclohexane with vortex. To remove the large particles, it was centrifuged again for 5 minutes and the supernatant poured inside a glass vial (Figure 3.1 (f) - right photo).

3.2 Mesoporous Silica Coating on UCNP Surface

The produced oleate capped UCNP need to be water soluble for PDT. Thus, mesoporous silica, having numerous advantages such as PS loading capacity, high biocompatibility, and further functionalization property, was coated around UCNP through direct formation method [84].

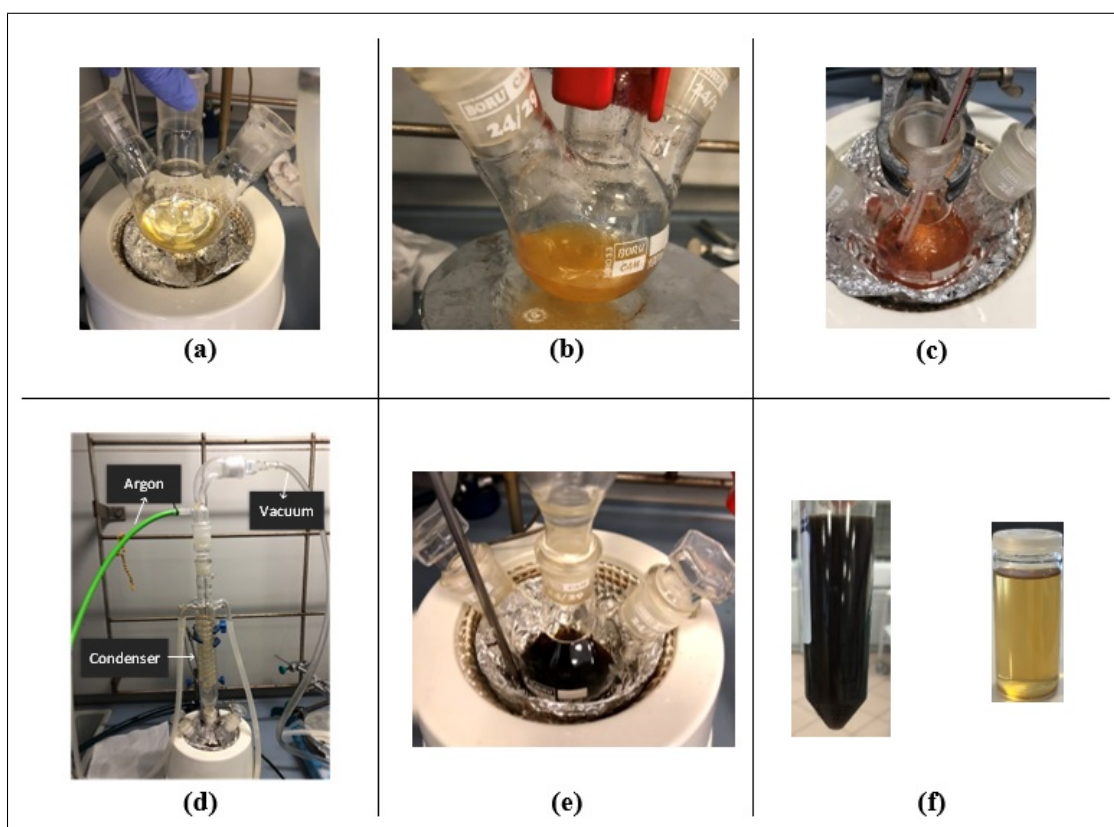


Figure 3.1 Digital photographs at various steps of reactions during Yb/Er doped UCNP synthesis

3.2.1 Materials and Instrumentation

While, Hexadecyl-trimethyl-ammonium bromide (CTAB, Merck), tetraethyl orthosilicate (TEOS, »99%, Merck), ethanol, and sodium hydroxide (NaOH, Sigma Aldrich) were used as chemicals, ultrasonic bath, hotplate magnetic stirrer (Isolab), centrifuge (Beckmen Caulter), ultrasonic probe (Omni-Ruptor 4000), oven, 2 mL centrifuge tubes and 25 mL, 40 mL and 50 mL beaker were utilized as instruments to develop mesoporous silica around UCNP, UCNP@mSiO₂.

3.2.2 UCNP@mSiO₂ Synthesis

In this study, the procedure for coating UCNP with mesoporous silica (UCNP@mSiO₂) is as follows:

Phase transfer from cyclohexane to water: The prepared 20 mL UCNP inside cyclohexane stock solution was waited inside ultrasonic bath for 30 minute. Meanwhile, 100 mg CTAB was dissolved in 10 mL distilled water (DI) with sonication/stirring inside 25 mL beaker. Then, 1 mL of UCNP-stock solution was put slowly into the beaker and vigorous stirring was applied from this point. After 3 hours, heat was increased to 70°C and waited additional 2 hours at this temperature (Figure 3.2 (a)). It is also possible to stir the mixture for 2 day instead of applying heat rise. The main aim at this step was to remove cyclohexane from the solution with evaporating (boiling point of cyclohexane is 80.74°C). Note that, the beaker should be closed with loosed way.

Formation of Silica Surface: Inside a 50 mL beaker 20 mL distilled water, 3 mL ethanol and 150 μ L of 2 Molar NaOH (0.1 g NaOH pellet and 1.2 mL DI) were mixed. Afterwards, phase transferred UCNP solution put into the 50 mL beaker under stirring condition. After its heat was raised to 70°C, 200 μ L TEOS added dropwise and waited 15 minute. In order to remove unbound CTAB and TEOS from the solution, cleaning procedure was employed three times. That is, the solution was placed in 2 mL centrifuge tubes, and then the nanoparticles were precipitated by centrifugation at 13000 RPM for 15 minute. After, the liquid was replaced with ethanol, precipitated nanoparticles were solved with ultrasonic probe. Note that, sonication activity require to be high, otherwise; nanoparticles cannot dissolve properly inside ethanol. The nanoparticles, whose washing process is completed, can be stored in 20 ml of ethanol at room temperature for the following step.

Removing CTAB to Reach Pore Structure: UCNP including ethanol in 20 mL was poured inside a 40 mL beaker and 40 μ L HCL was added while stirring. The temperature of the mix was increased to 60°C. Then, the solution was waited for 3 hours at this condition. Before collecting nanoparticles, denoted as UCNP@mSiO₂; the solution was cleaned with ethanol three times. The nanoparticles were dried in an oven at 80°C overnight and the amount of UCNP@mSiO₂ was determined to be approximately 40 mg (Figure 3.2 (b)).

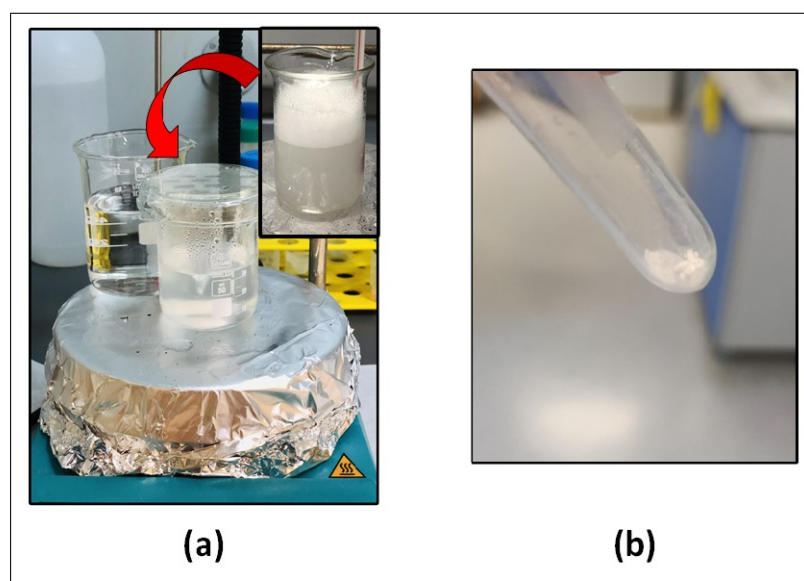


Figure 3.2 (a) During oleate capped UCNP phase transfer to CTAB with heat increase white bubbles formation (inset) and followed by their disappearance, (b) Silica coating protocol completed nanoparticles ($UCNP@mSiO_2$).

3.3 Decorating UCNP with Au Nanoparticles

The silanol groups on the produced $UCNP@mSiO_2$ can be functionalized within the interior of the pores or on the outer surface with various molecules. This modification can provide undesired leakage, or enhanced targeting. If the pores of the mesoporous silica are not sealed by an additional functionalization, the unwanted leakage would occur [95]. Therefore, we coated the surface of mesoporous silica with 3-Aminopropyltriethoxysilane (APTES) to make gate-system for porous [87].

Although amine functionalized nanoparticles can be used to seal the pores of mesoporous silica, it decreases the biocompatibility and the stability of the nanoparticles inside the distilled water. To enhance the properties of nanoparticles for higher upconversion luminescence and additional photodynamic therapy (PDT) activity, gold nanoparticles were bound to the amine ligand [96].

3.3.1 Materials and Instrumentation

The utilized materials were 3-Aminopropyltriethoxysilane (APTES), methanol, gold (III) chloride trihydrate ($HAuCl_4 \cdot 3H_2O$ >99.9% trace metals basis, Sigma-Aldrich), Trisodium citrate dihydrate (Merck), and sodium borohydride ($NaBH_4$, >98.0%, Merck). As the instruments; hotplate magnetic stirrer (Isolab), centrifuge (Beckmen Coulter), ultrasonic probe (Omni-Ruptor 4000), oven, 2 mL centrifuge tubes, and 25 mL beaker were used.

3.3.2 UCNP@Au Production

Amine-functionalization protocol for UCNP-system is as follows:

- 20 mg of UCNP@mSiO₂ was dissolved in 20 ml DI water by using vortex and ultrasonic prob.
- The mixture heat was increased to 45°C and 50 µL APTES was added.
- After 3 hours of stirring, the mixture was separated into 2 mL centrifuge tubes, and then tubes were centrifuged at 13000 RPM for 15 minutes.
- The supernatant was discarded, re-dispersed in methanol, and centrifugation was used again. This step was repeated for three times to remove unbound APTES.
- The nanoparticles, denoted as UCNP@APTES, were dried at 80°C overnight.

Amine ligand - UCNP@mSiO₂ was combined with gold nanoparticles according to the following steps. It should also be noted that synthesise protocol includes initially gold (Au) seeds preparation [97].

- 2.5×10^{-4} Molar $HAuCl_4$ and 2.5×10^{-4} Molar trisodium citrate were mixed in 20 mL DI water for 30 minute.

- Meanwhile, 0.1 Molar $NaBH_4$ were made ready inside cold water ($4^{\circ}C$) and 0.6 mL of $NaBH_4$ were added to the solution while stirring.
- Instantaneously, the color of solution was turned to pink. Thus, following 2 hours stirring, the gold seeds were ready for usage (Figure 3.3 (a)). (They have to be processed in 5 hours, otherwise they may start to aggregate.)
- 20 mg of UCNP@APTES were weighted and dispersed in 10 mL DI water separately. Then, 4 mL of gold seed solution was added.
- After 2 hours stirring, cleaning step was performed with DI water for three times. The nanoparticles, named as UCNP@Au, were kept in 1 mL DI water at room temperature (Figure 3.3 (b)).

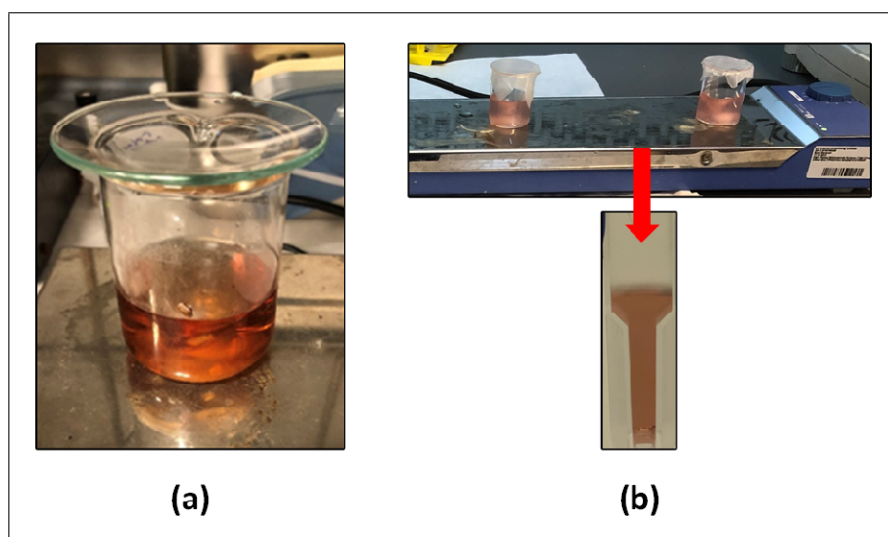


Figure 3.3 (a) The prepared gold seeds, and (b) UCNP@Au formation.

3.4 Loading Photosensitizers into Porous Silica

Mesoporous silica has the ability to load photosensitizers or drugs. In this study, we aimed to activate 540 nm and 660 nm fluorescence intensities under near infrared light (980 nm). Therefore, zinc phthalocyanine (ZnPc) and merocyanine (MC540) photosensitizers were encapsulated with porous silica because both of their absorptions match well with the fluorescence of Yb and Er doped UCNP.

3.4.1 Materials and Instrumentation

Zinc (II) phthalocyanine (ZnPc) and merocyanine 540 (MC540) Dimethyl Sulfoxide (DMSO) were purchased from Sigma-Aldrich. Besides; multi position magnetic stirrer, 5 mL beaker, centrifuge (Beckmen Coulter), absorption spectrophotometer (Thermo Scientific), cuvette (10 mm) were used while loading PS experiments.

3.4.2 MC540 and ZnPc loading into UCNP@Au

Preparation of stock PS solutions: In order to obtain 10 mg/mL MC540 stock solution, 10 mg MC540 were weighted precisely and dispersed in 1 mL DMSO. Additionally, 2 mg ZnPc was also dissolved in 1 mL DMSO to reach the 2 mg/mL concentration for the stock solution of ZnPc. Stock solutions were prepared at dark.

Encapsulating the PS with porous silica: Initially, UCNP@Au was centrifuged, supernatant was removed, and the nanoparticles were dissolved in 1600 μ L DMSO. Next, photosensitizers were loaded in three different ways;

- *Only MC540 Loading:* 400 μ L MC540 (1 mg/mL) and 2000 μ L DMSO were merged with the nanoparticles in 5 mL beaker (Figure 4.4 (a)).
- *Only ZnPc Loading:* 2000 μ L ZnPc (1 mg/mL) and 400 μ L DMSO were merged with the nanoparticles in 5 mL beaker (Figure 4.4 (b)).
- *MC540 and ZnPc Loading:* 400 μ L MC540 and 2000 μ L ZnPc stock solutions (1 mg/mL for each) were merged with the nanoparticles in 5 mL beaker (Figure 4.4 (c)).

They were stirred for 24 hours at dark. The unloaded photosensitizers were removed from the media with centrifuge and the absorption of supernatant was used to determine the loading amount of PS. After completing three times of up-water

cleaning, the nanoplateforms (MC540&ZnPc loaded UCNP@Au) were kept in the dark (-20°C) at a concentration of 10mg/mL.

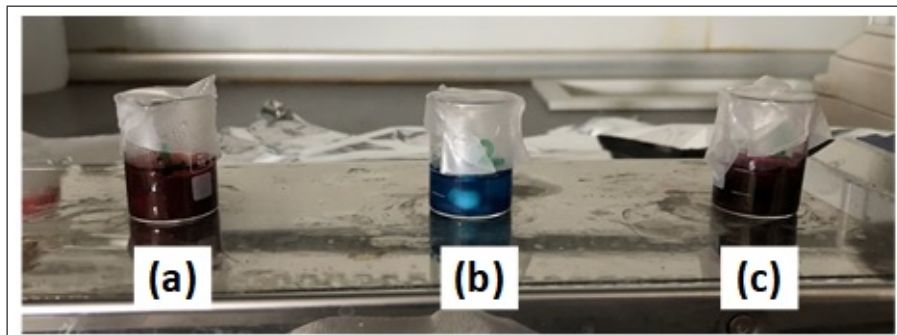


Figure 3.4 The digital photographs of (a) only MC540 loading, and (b) only ZnPc Loading, and (c) both MC540 - ZnPc loading.

Acquiring PS loading and leakage amount: Both MC540 and ZnPc absorption curves were measured with respect to different concentrations by using absorption spectrophotometer. The absorption of the PS solutions were determined using a control prepared with its own solvent in a 10 mm cuvette. Increasing the concentration was also increased the absorption so a straight line was derived as called absorption curves for the PS. A mathematical expression was reached for both MC540 and ZnPc. Therefore, unknown concentrations could be determined with these equations.

In order to find out PS loading amount, absorption measurements of unencapsulated PS solutions were taken. The high concentrations of supernatant was decreased with adding extra DMSO. Then, the obtained absorption measurements were utilized to find the loaded PS amount. It was estimated by using the following expression 3.1:

$$\text{Loading Amount (\%)} = \frac{\text{Mass of Photosensitizers}}{\text{Mass of Nanoparticles}} \times 100 \quad (3.1)$$

In addition, the quantity of leakage during 48 hours was also evaluated with the same method employed to decide the loaded PS amount. The leakage experiment was applied for both photosensitizers loaded UCNP@Au and UCNP@APTES. The

nanoplatfoms having 2 mg/mL concentrations were waited in water for 2 days. Then, the cumulative PS leak (%) was measured from the supernatant of solutions after centrifuge.

3.5 Temperature Measurements

Near-infrared laser and the developed nanoplatfoms can result in high temperature change in cellular environment. The NIR region is considered a therapeutic window due to its minimal absorption in tissue (for hemoglobin and lipid), however, water shows a high absorption coefficient at 980 nm [98, 99]. Besides, nanoplatfoms can trigger temperature rise due to bound gold nanoparticles. It is also well known that gold nanoparticles can initiate photothermal therapy (PTT) by surface plasmon resonance (SPR) generation [100]. Therefore, the produced nanoplatfoms thermal change under laser illumination was evaluated for cellular media.

3.5.1 Materials and Instrumentation

Thermometer (model: Physitemp), T-type needle thermocouple (1 cm diameter), cell medium (RPMI 1640 supplemented with FBS), 980 nm diode laser (Opto Power Corporation, continuous wavelength (CW)), power-meter (Newport 1918-R), cuvette (10 mm) were used for deciding temperature alteration.

3.5.2 Analyzing Temperature Change

At first, cellular medium was prepared with various concentrations of nanoplatfoms (0 mg/mL, 0.025 mg/mL, 0.1 mg/mL, 0.5 mg/mL, and 2 mg/mL). The base nanoplatfom UCNP@Au and MC540&ZnPc loaded UCNP@Au were evaluated in this experiment. Then, the set up was arranged with thermocouple connected thermometer and collimator - optical fiber - 980 nm laser system. T-type needle of thermocouple

was placed into the prepared media at room temperature. Afterwards, cuvette was exposed with 980 nm laser light (1 W/cm^2) for 5 minutes while its temperature change was recording. The measurements were repeated for three times.

3.6 Reactive Oxygen Measurements

Reactive oxygen species (ROS) include one or more unpaired electrons. Generally, healthy cells use ROS to maintain normal metabolism like enzymatic reactions, signal transduction, or gene expression [101]. However, ROS production inside or outside of the cells are in control with the utilized antioxidant enzymes (i.e. superoxide dimutases) and substances (i.e. A, C and E vitamins) [102] Besides, when ROS level elevates in tumor tissue till some level, their cellular activities also increase undesirably [103]. In spite of that cellular processes of ROS, excess amount of it results in cumulative damage to the cell functions and ultimately trigger cell death [104]. In PDT applications, excess ROS production is one of the essential purpose to destroy tumor tissue. Thereby, the designed and synthesized novel nanoplatfoms capability of ROS production was demonstrated in this study with a fluorescent probe, 1,3-Diphenylisobenzofuran (DPBF) [105].

3.6.1 Materials and Instrumentation

1,3-Diphenylisobenzofuran (DPBF, Sigma Aldrich), ethanol (absolute, reagent grade, 99.8 %), cuvette, 980 nm diode laser (Opto Power Corporation, continuous wavelength (CW)), power-meter (Newport 1918-R), ultrasonic probe (Omni-Ruptor 4000), and absorption spectrophotometer (Thermo Scientific) were the supplies in this experiment.

3.6.2 ROS Detection

10 mM DPBF was freshly prepared in 5 mL ethanol. Meanwhile, 10 mg/mL stock solutions of MC540&ZnPc loaded UCNP@Au and base nanoplatfrom (UCNP@Au) were well dispersed with ultrasonic prob (power output:20, pulse:50/100, time:1 min.). 2 mg/mL (200 μ L stock and 800 μ L up-water), 0.5 mg/mL (50 μ L stock and 950 μ L up-water), 0.1 mg/mL (10 μ L stock and 990 μ L up-water), and 0.025 mg/mL (2.5 μ L stock and 997.5 μ L up-water) concentrations were syringed into 1 mL cuvette. 10 μ L from the DPBF solution was also added. Afterwards, they were placed under 980 nm laser at 1 W/cm^2 for 5 minutes. Absorption intensity change was recorded at 420 nm for every 1 minute period via using spectrophotometer.

3.7 *In Vitro* Experiments

Efficiency of the originally designed PS loaded UCNP@Au was evaluated *in vitro* to observe cellular uptake, dark toxicity, and PDT behavior. As a cancer cell model prostate carcinoma was chosen. According to the 2020 World Health Organization (WHO) report, prostate is a third leading cause of death after breast and lung cancer [1]. If the treatment with surgery or radiotherapy manage to be applied in early stage of the illness, approximately 95 % of patients can survive [106]. On the other hand, the known treatment methods to advanced or recurrent prostate carcinoma is not successful because most patients die in five years [107]. At this point, new strategies should be developed and we investigated PDT with MC540&ZnPc uploaded UCNP@Au on prostate cancer cells, PC3.

3.7.1 Materials and Instrumentation

PC-3 (ATCC, CRL-1453), RPMI 1640 (1X, with 2.05 mM L-Glutamine, Biosera), fetal bovine serum (FBS, Biosera), penicillin - streptomycin solution ((100x) antibiotic, Biosera), trypsin (biosera, 0.25 % EDTA), 3-(4,5-dimethylthiazol-2-yl)- 2,5-diphenylte-

trazoliombromide (MTT, sigma-aldrich), cryovial tube (2 mL), cell culture flask (25 mL or 75 mL, sterile), serological pipettes (5 mL, 10 mL, and 25 mL, sterile), pipette tip (10 μ L, 200 μ L, 1000 μ L), 96-well plate (sterile), 24-well plate (sterile), centrifugal tube (15 mL, and 50 mL, sterile) were used materials and disposables.

Laminar flow cabinet (ESCO Class II Type A2), deep freeze(ESCO Lexicon ULT Freezer), CO_2 , incubator (Nuve EC160), microscope (Nicon Eclipse 80i), microplate reader (Bio-Rad iMark), pH meter (Thermo Scientific Orion Star A211), hot water bath (LW Scientific DSB-1000D), autoclave (Nüve OT40L), ultrapure water system (Rephile Direct), centrifuge (HETTICH Rotino 380), 980 nm diode laser (Opto Power Corporation), power meter (Newport 1918-R), and optomechanical devices (Thorlabs) were necessary instrumentation to pursuit the following experiments.

3.7.2 Cell Culturing

PC-3, possessing epithelial morphology in prostate site of human with grade IV adenocarcinoma, were used for culturing. Before opening a stock of PC-3 cells kept in $-80\text{ }^\circ\text{C}$, complete medium was prepared with 10 % FBS and 1 % antibiotic solution supplemented RPMI 1640. Defrosted cells were centrifuged to remove DMSO, and cultured with the complete medium. Then, they were waited in incubator at $37\text{ }^\circ\text{C}$ and 5 % CO_2 atmosphere to accommodate cell proliferation. When the cells reach confluence 80 % in the 25 mL or 75 mL cell culture flask, they were trypsinized and experiments were initiated.

3.7.3 Cellular Uptake of Nanoplatfoms

The regulatory effects and biological activity of nanoplatfoms were examined with the MC540&ZnPc uploaded UCNP@Au. A complex mechanism exist when the interaction of nanoparticles with cells are considered [108]. Although the synthesized nanoparticles can exhibit a profound characteristics in water environment, their physic-

ochemical feature can alter upon touch with the biological elements such as blood, proteins, cells or subcellular organelles [109]. Since physical or chemical properties of nanoparticles can change, it is an inevitable topic to observe biomolecular interaction of produced nanoplatforms.

Therefore, to understand how the designed nanoplatforms act on cells, an imaging experiment was employed as following:

- Microscope cover glasses (25 mm x 75 mm) were cut with diamond scribe in 1 cm x 1 cm scale. (Thus, they could be placed into 24 well plate.)
- Sterilization was implemented to coverslips with acetone, ethanol, and autoclave. Then, they were fitted inside 24 well plates.
- When PC-3 cell reached confluence, they were tyripsinized, and counted. 100 μ L of complete medium involving 10,000 PC-3 cells were carefully put on the coverslips.
- After 3 hours, additional 400 μ L of complete medium was pipetted into the wells and then cells were incubated (24 hours) for cellular adhesion.
- The concentrations of 0.1 and 0.5 mg/mL MC540/ZnPc-UCNP@Au in complete medium was changed with the old media and 24-well plate were placed into incubator for 2 hours.
- Following three times rinsing, new complete media was added and cells were incubated for 24 hours.
- Next day, PC-3 cells were visualized with optical microscope (Nikon, Eclipse 80i).
- Both bright field and fluorescence measurement was measured. Fluorescence detection of nanoplatforms was achieved under 980 nm laser irradiation at 0.5 W/cm² power.

3.7.4 Dark Toxicity Measurements

The toxicity of photosensitizers (MC540 and ZnPc), base UCNP@Au nanoparticles, and MC540&ZnPc loaded UCNP@Au nanoplatfoms were assessed with MTT assay. In fact, MTT has ability to measure metabolic activity of cells by using yellow tetrazolium salt reduction to form purple formazan [110]. The formazan crystals are soluble in DMSO so the colored solution absorbance can be measured between 500 and 600 nm. If the results are compared with control groups, the estimates can be quantified. Each experiment requires to be repeated at least three times.

Photosensitizers cytotoxicity: While MC540 stock solution was including 10 mg/mL, ZnPc stock solution had 2.5 mg/mL in DMSO. Since ZnPc has a hydrophobic surface and cannot be applied in high amounts as MC540, their toxicity has been evaluated at different concentrations. MC540 was applied with 10, 20, 30, 40, and 50 $\mu\text{g}/\text{mL}$ concentrations to the cells. However, while implementing ZnPc, its concentrations were 0.06, 0.3, 0.6, 3, and 6 $\mu\text{g}/\text{mL}$. Meanwhile, confluent PC-3 cells were plated at 8000 cells/well in a 96-well plate and incubated for 24 hours. Next day, old medium was replaced with the new complete medium comprising different concentrations of MC540 or ZnPc. After 2 hours, cells were rinsed with Phosphate-buffered saline (PBS) three times and 96-well were waited in incubator for additional 24 hours. Then, cell viabilities were measured with MTT assay.

Nanoplatfoms cytotoxicity: In order to analyze MC540&ZnPc loaded and unloaded UCNP@Au nanoplatfoms dark toxicity, they were prepared in complete cell medium as; base nanoparticle UCNP@Au: 25, 50, 100, and 200 $\mu\text{g}/\text{mL}$, MC540&ZnPc loaded UCNP@Au nanoplatfoms: 25, 50, 100, 200, 500, 1000, and 2000 $\mu\text{g}/\text{mL}$. Upon culturing cells in 96-well plate, these nanoplatfoms were introduced to cells for 2 hours. Then, the same protocol was applied as following steps that mentioned in photosensitizers cytotoxicity. Briefly, subsequently rinsing cells with PBS and incubating them for following 24 hours, MTT absorption difference was investigated to understand the toxic hazard on the PC-3 cells. During the experiments, cells were studied in dark conditions after resting them with PS-containing nanoplatfoms.

3.7.5 Investigating Photodynamic Therapy

Practising photodynamic therapy requires not only the photosensitizers delivery in profound way but also light transportation to cancerous site efficiently. Indeed, superficial tumor cells can be reached easily with visible light but it is not simple to access the light beam through deep-seated tumor tissue. Herein, near-infrared light is a solution if it can be used to activate photosensitizers with a transducer nanomaterials like upconversion nanoparticles.

In this study, to find out the PDT capacity of nanoplateforms, an optical system was established. The 980 nm diode laser output coupled with a fiber and collimator that accommodated the beam without allowing it to scatter at different angles. Before introducing 980 nm continuous wavelength (CW) to cells, power intensity of light was ascertained at 1 W/cm^2 . Diameter of the beam was also arranged as 1 cm because it was aimed to illuminate 4 wells of 96 well plate at the same time (Figure 3.5). Besides, a black cover was settled to minimize emerging of light beam to other regions of the 96 wells. Since MC540 and ZnPc has absorptions around 540 nm and 660 nm respectively, irradiation was employed in the dark.

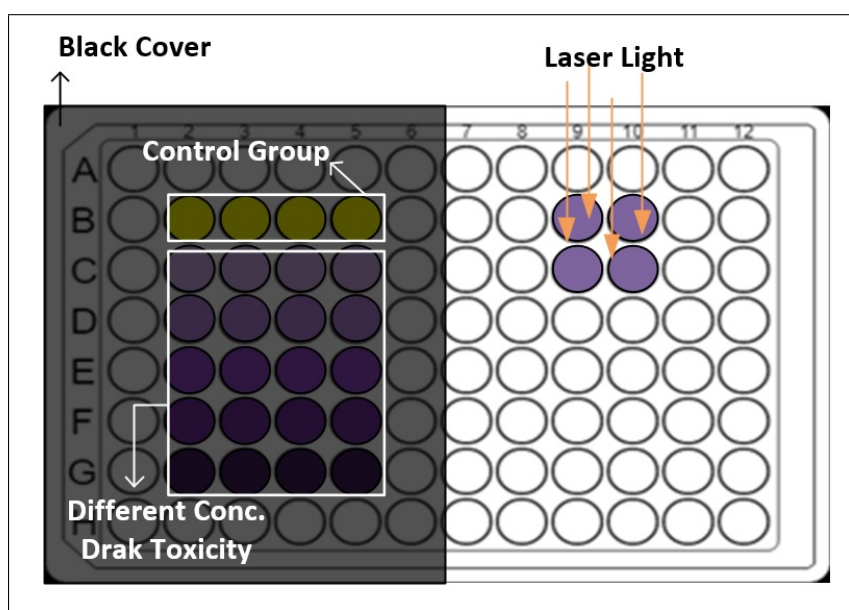


Figure 3.5 Schematic illustration of *in vitro* experiments.

To initiate the experiments, PC-3 cells were seeded into 96 well and they were incubated for 24 hours to settle down them. Different concentrates of nanoplateforms between 25 $\mu\text{g}/\text{mL}$ to 2000 $\mu\text{g}/\text{mL}$ were implemented for two hours. As a next step, the cells were irradiated with 980 nm (CW) by exploiting the established optical system. Then, cells were waited in incubator for additional 24 hours because PDT effect could not be observed as soon as the experiment was performed. Lastly, the percentage of cell viability was quantified via MTT assay and micro-plate reader. Absorption of formazan crystals was evaluated by taking the difference at 570 nm and 760 nm. All results were normalized with respect to the control group.

3.8 Statistical Analysis

It was crucial to determine the obtained results statically. Therefore, IBM SPSS Statistics (Version:25) program interface was used to calculate data groups significance between each other. Firstly, data sets were entered into the program. Then, Shapiro-Wilk test was implemented to decide whether the values were normally distributed or not. Since all the measured data sets were normally distributed in this study, one-way ANOVA (Analysis of Variance) with Tukey's HSD (honestly significant difference) post hoc test was utilized to observe significantly different groups. Both $*P < 0.05$ and $**P < 0.01$ levels were calculated.

4. RESULTS OF MATERIAL CHARACTERIZATION

In this section, it was aimed to present the produced nanoplateforms properties. They were synthesized in multiples steps as given in Figure 4.1. Firstly, upconversion nanoparticles, possessing transducer feature as able to alter near-infrared light to visible light, were developed in uniform and hexagonal form. Secondly, their surface was modified to allow them usable in biological applications. Mesoporous silica coating, amine (NH_2) modulation, and gold nanoparticles conjugation were the main processes during surface modifications. Lastly, two different photosensitizers, MC540 and ZnPc, were loaded to activate PDT mechanisms of nanoplateforms.

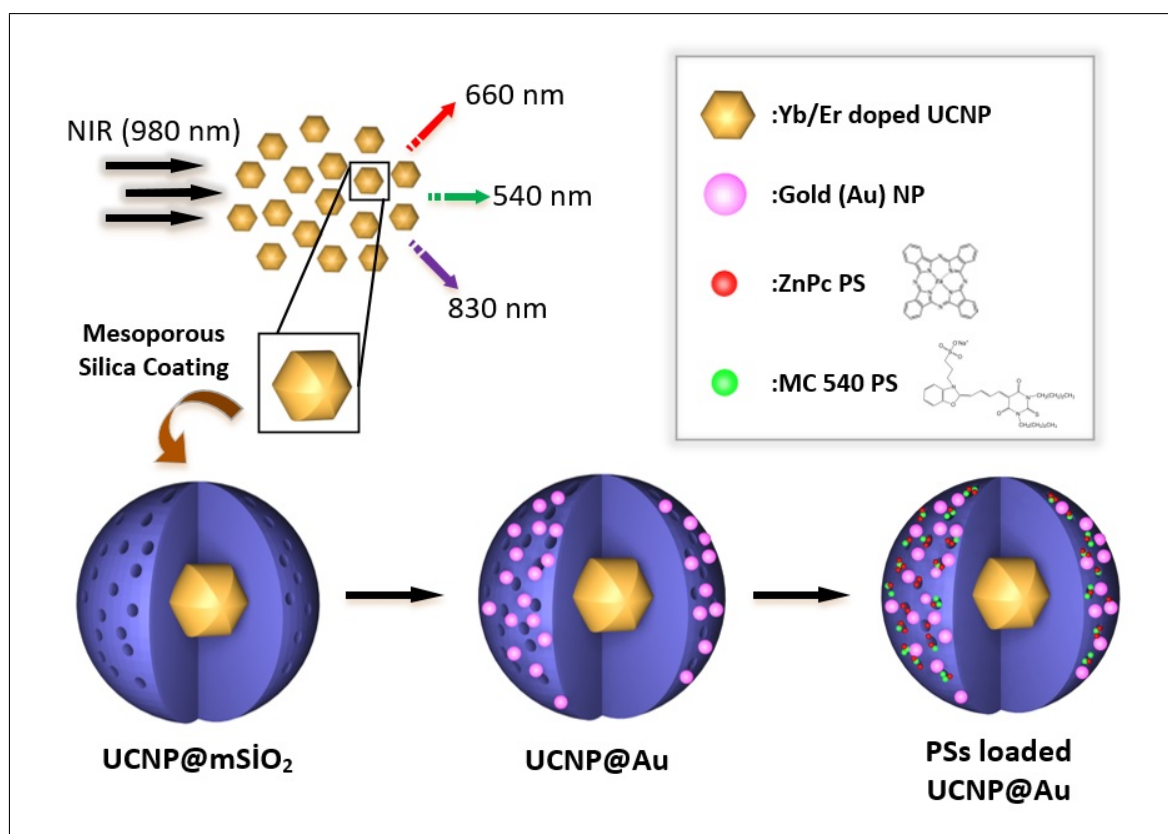


Figure 4.1 Synthesis steps of nanoplateforms.

Characterizations were necessary to fully comprehend the nanoplateforms features while producing, thereby;

- The size, shape, and morphology of nanoparticles were evaluated with dynamic light scattering (DLS), scanning electron microscope (SEM), and thermal electron microscope (TEM).
- To understand the fluorescence of UCNP under 980 nm wavelength, the nanoparticles were examined optically.
- The photosensitizers were physically encapsulated in porous silica, so the mechanism of this process was studied by appealing absorption properties of PS.
- Chemical characteristic of nanoplatforms were also measured in each synthesize step by using fourier transform infrared spectroscopy (FTIR) and energy dispersive spectroscopy (EDS).

4.1 Dynamic Light Scattering (DLS)

It is a technique that is used to determine the nanoparticles sizes in liquid media. The background theory depends on two assumptions: particles has Brownian motion, and Tyndall effect (scattering) [111]. Therefore, an optical set up, including a laser and photomultiplier, can detect the scattered light from 90° angle. Although electron microscopes are applicable to observe the sizes of small nanoparticles, they require dry specimens for imaging that can prone to structural differentiation, aggregation, and growth due to larger surface area against volume [112]. Thus, DLS measurement advantageous because it can give mean estimates of nanoparticles sizes in suspensions with fast data procurement.

DLS measurements were attained with Malvern ZS-Zetasizer which able to obtain the sizes of 0.3 nm-10 μm particles. Both UCNP and UCNP@mSiO₂ nanoparticles DLS results were given in Figure 4.2 and Figure 4.3. Following synthesize protocols of them, 30 μL of UCNP and UCNP@mSiO₂ were added to a glass cuvette with 3 mL cyclohexane and DI water, respectively. The cuvette and dissolvent optical properties entered to DLS device. Afterwards, measurement were acquired.

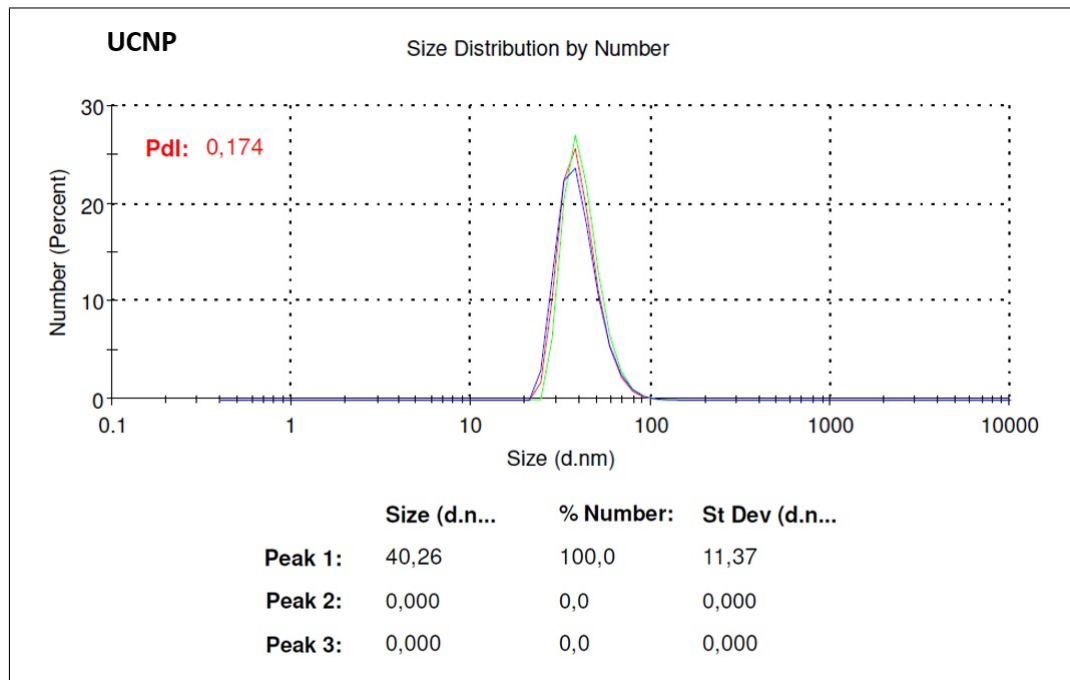


Figure 4.2 DLS measurements for UCNP.

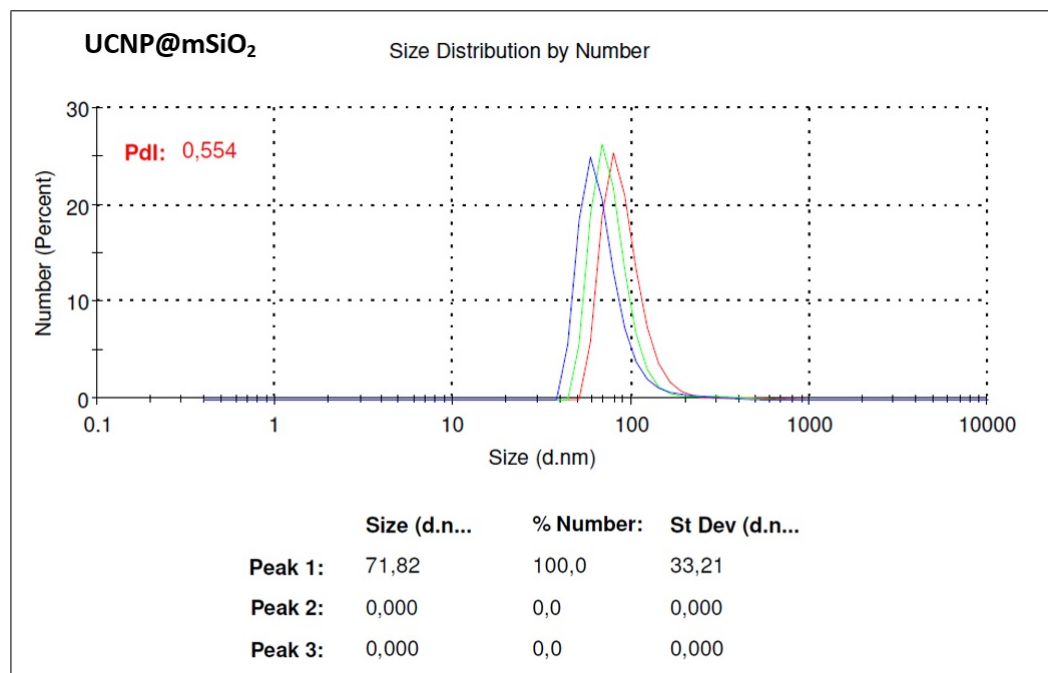


Figure 4.3 DLS measurements for UCNP@mSiO₂.

According to the presented data for UCNP, the hydrodynamic sizes were around 40.26 nm. Besides, they were well distributed because received three different measurements were detected their diameter at the same range. When UCNP@mSiO₂ in water was considered, the nanoparticles diameter increase was found to 71.82 nm. Silica surface provided nanoparticles to be solvable inside water but they were not as well as distributed UCNP. Some aggregation was detected during the acquisition of the three measurements.

Before coating nanoplatforms with gold nanoparticles, produced gold seeds were initially evaluated with DLS measurements. The citrate stabilized gold seeds were actually usable for only three hours after their synthesise as mentioned in literature [97]. Additional applications are necessary because they are too small and start to aggregate very fast. This situation was observed as demonstrated in Figure 4.4. When the first data was obtained in DLS, they were in 3.396 diameter, however; the second and third measurements showed that sizes of gold seeds were changed to 6.76 and 6.941 in a few minutes.

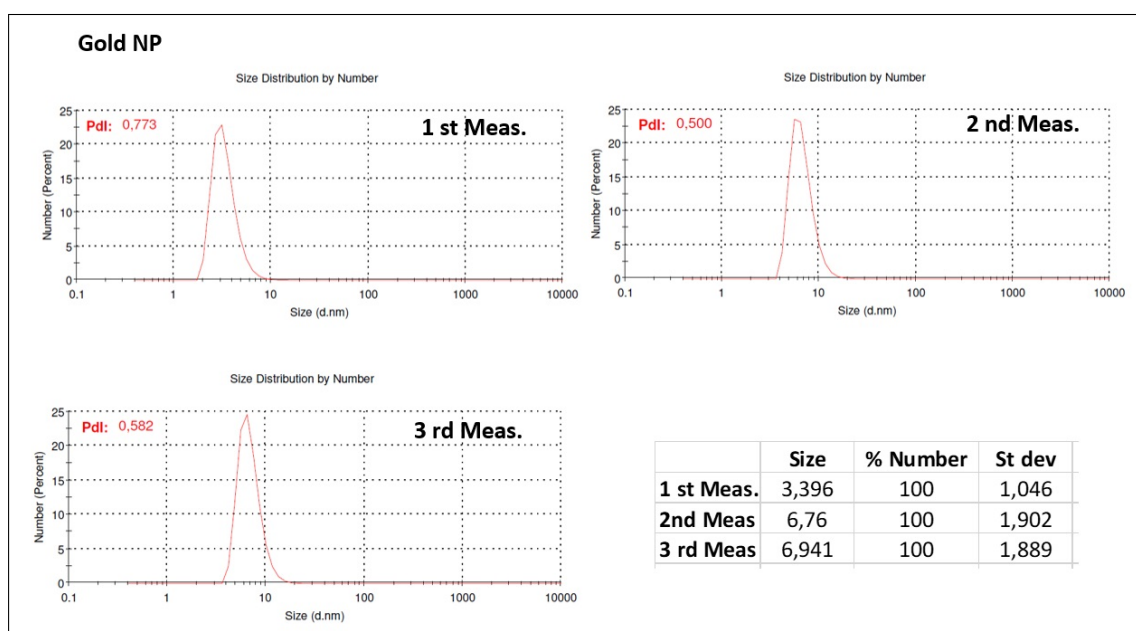


Figure 4.4 DLS measurements of gold (Au) seeds.

4.2 Scanning and Transmission Electron Microscope (SEM and TEM)

SEM and TEM systems can create images for observing the morphology of materials [113]. While SEM is capable of detecting scattered electrons by an electron detector and photomultipliers, TEM capture transmitted electrons passing through an object and provide images with a charged-coupled device (CCD) camera. The major differences are TEM measure smaller particles with higher spatial resolution (SEM resolution: 10-100 nm, TEM resolution: 1 nm-100 nm) but operating SEM is used easier than TEM. The images of nanoparticles were taken with scanning electron microscopy (SEM, thermoscientific and Zeiss Evo LS15), and transmission electron microscopy (TEM, Thermoscientific Talos L120C, 120 kV). The developed nanoparticles 1 μL were firstly dried on a carbon grid (Lacey, 200 mesh), and placed into the electron microscopes. Then, measurements were acquired for nanoparticles as revealed in Figure 4.5.

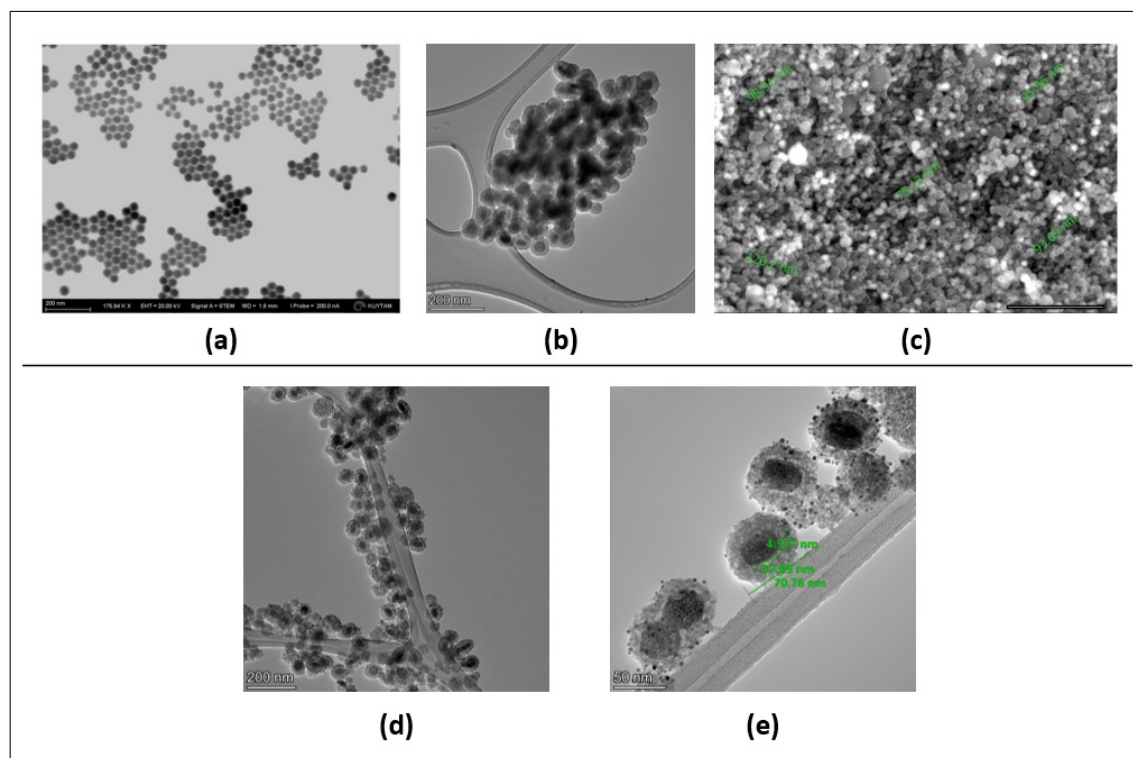


Figure 4.5 SEM and TEM images of (a) Yb/Er doped UCNP in 200 nm scale, (b) mesoporous silica coated UCNP in 200 nm scale, (c) amine conjugated UCNP@mSiO₂ in 1 μm scale, and gold nanoparticle coated UCNP@APTES (d) 200 nm scale, and (e) 50 nm scale.

Upconversion nanoparticles SEM view showed that they were around 40 nm, and in hexagonal shape (Figure 4.5 (a) and 4.6 (a)). The crystal lattice of fringe distances were 0.512 nm, provided inset picture (Figure 4.6 (a)), that can be (100) plane of β -NaYF₄ (hexagonal shape) as discussed before in literature [114]. Porous silica coated UCNP was become approximately 80 nm in diameter. Amine connected nanoparticles were in uniform circular shape as demonstrated in SEM measurements (Figure 4.5 (c)). It was also valid for gold seed coated particles (Figure 4.5 (d-e), and Figure 4.6 (b)). The sizes of gold nanoparticles were determined around 4 nm (Figure 4.5 (e) and Figure 6 (b)). DLS and SEM-TEM results in a manner of size measurements were summarized in Table 4.1.

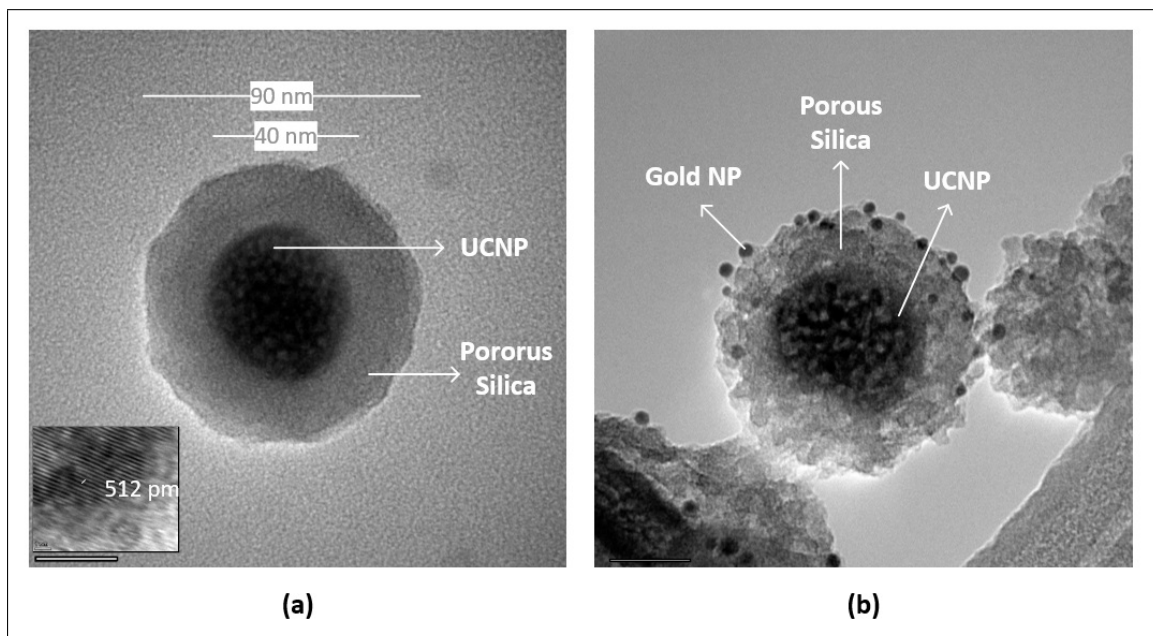


Figure 4.6 Visualization of (a) UCNP@mSiO₂ (inset image: d-spacing of UCNP in 2 nm scale), and (b) UCNP@Au with TEM measurements (20 nm scale)

Table 4.1
Sizes of nanoparticles with DLS and SEM-TEM measurements.

Nanoparticles	DLS (nm)	SEM-TEM (nm)
UCNP	40.26 ±11.37	40.30 ±3.52
UCNP@mSiO ₂	71.82 ±33.21	77.49 ±12.96
UCNP@APTES	not measured	67.33 ±15.94
Au np	3.40 ±1.05	3.88 ±0.85

4.3 Optical Properties of Materials

Light and nanoparticles interactions were studied by performing fluorescence measurements with them. The transducer property of UCNP, which converts 980 nm to higher energy wavelengths in green, red and NIR regions, was recorded with a spectrophotometer (Ocean Optics 4000) at 90 ° degree. When UCNP were faced with 980 nm light illumination, it revealed four sharp emission peaks: in green fluorescence band 532 nm, and 552 nm peaks appeared due to $^2H_{11/2} - ^2I_{15/2}$, and $^4S_{3/2} - ^4I_{15/2}$ transitions; in red emission, 670 nm, emerged because of electrons motion from $^4F_{9/2}$ to $^4I_{15/2}$ excitation bands; and in NIR region 830 nm was observed as a result of $^4I_{9/2}$ to $^4I_{15/2}$. These measurements and related Jablonski energy diagram were demonstrated in Figure 4.7.

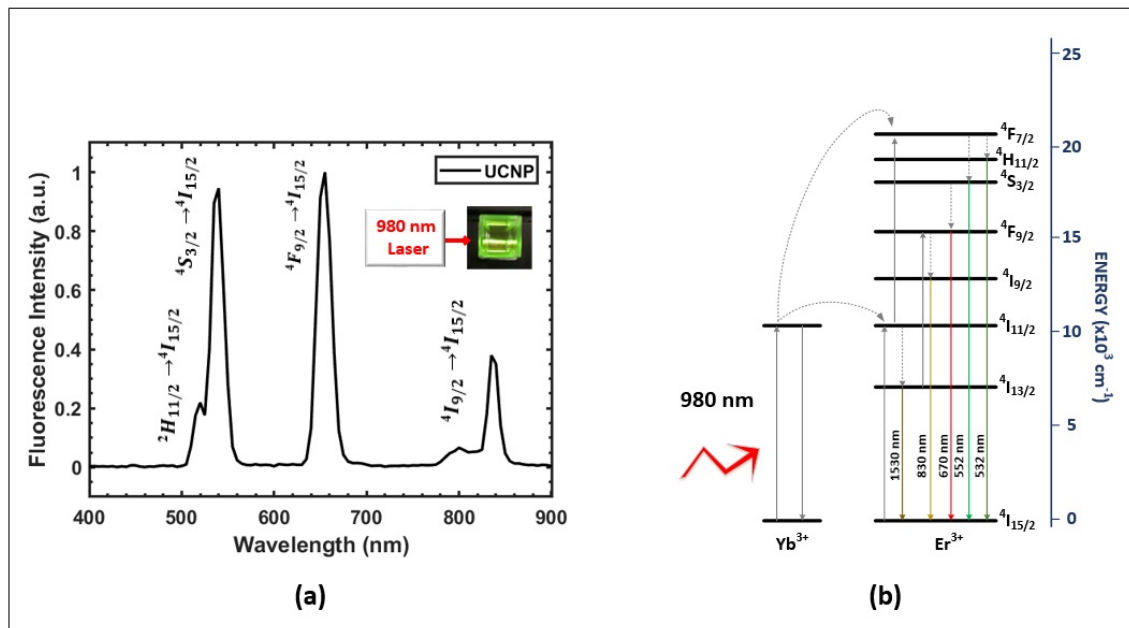


Figure 4.7 (a) Fluorescence of UCNP under 980 nm wavelength, and (b) the Jablonski diagram for this process.

Whereas, mesoporous coated UCNP exhibited less fluorescence intensity as given in Figure 4.8. All emission bands were decreased around 80 %, which was an expected result. The inset digital photographs in Figure 4.8 was taken for both dried and dissolved UCNP@mSiO₂. The fluorescence intensity of nanoparticles visually decreased considering the snapshot of UCNP (in cyclohexane, Figure 4.7 (a-inset)). Furthermore,

MC540 and ZnPC photosensitizers' absorption around green and red region was confirmed with absorption spectrophotometer as provided in Figure 4.9 (a). Additionally, the absorbance of gold seeds (Figure 4.9 (b-inset)) were detected near green spectra (Figure 4.9 (b)). These absorptions matched well with the emission bands of UCNP.

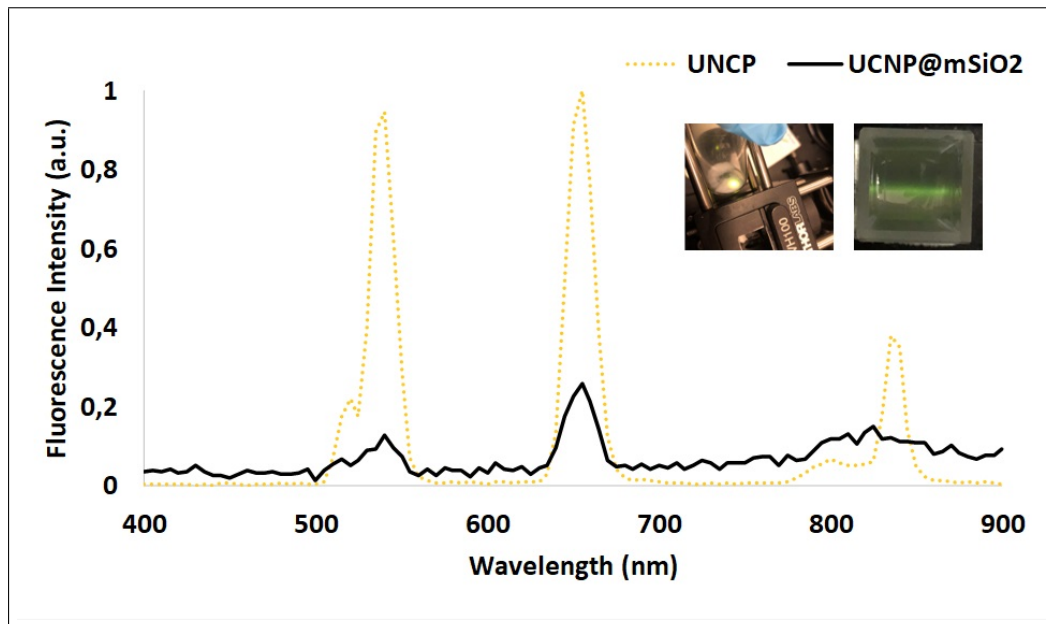


Figure 4.8 UCNP@mSiO₂ behaviour with 980 nm light irradiance.

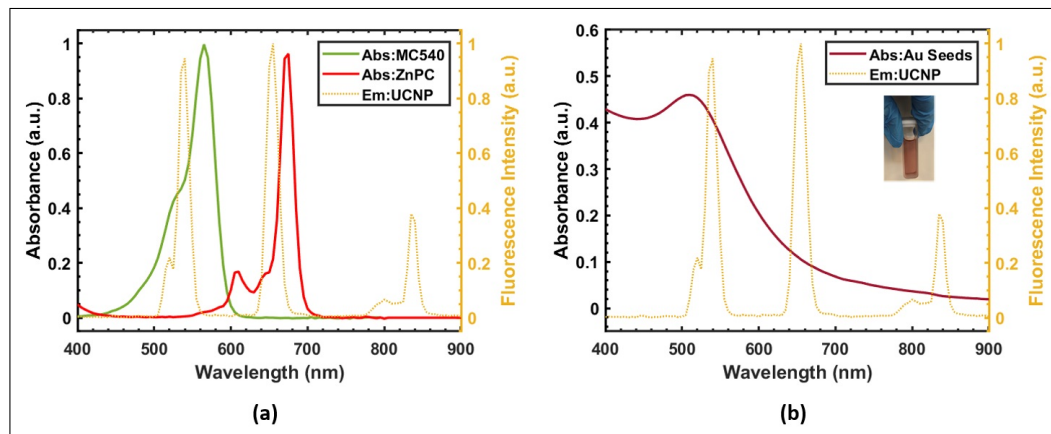


Figure 4.9 Emissions of UCNP and the matching absorption peaks of (a) photosensitizers, and (b) Au nanoparticles.

4.4 Loading Photosensitizers and Leakage

Two photosensitizers, MC540 and ZnPc, were encapsulated into the designed nanoplateforms because both emission peaks in visible range, around 540 and 660 nm, wanted to be utilized. Merocyanine 540 is an anionic lipophilic (affinity for a lipid medium) dye that has been applied for leukemia, colorectal carcinoma, or treatments of virus-infected cells [115, 116]. For instance, in 2014, Wang's group was merged UCNP with only MC540 and evaluated its effect on breast cancer cells [117]. On the other hand, Zinc (II) phthalocyanine (ZnPc) was attracted many researchers attention due to its high quantum yield, being around 0.70 [118]. However, it is not soluble in water so it needs a delivery system such as nanoparticles [119].

The loading amount of both photosensitizers were determined from the supernatant of solutions. Herein, the necessity to measure how PS absorption changes according to the amount has emerged. Thus, concentration against absorption curves were measured for MC540 (Figure 4.10 (a)) and ZnPc (Figure 4.10 (b)). Then, the absorption peaks allowed us to calculate any amount of PS from the absorptions with the reached linear line equations (Figure 4.10 (inset graphs)).

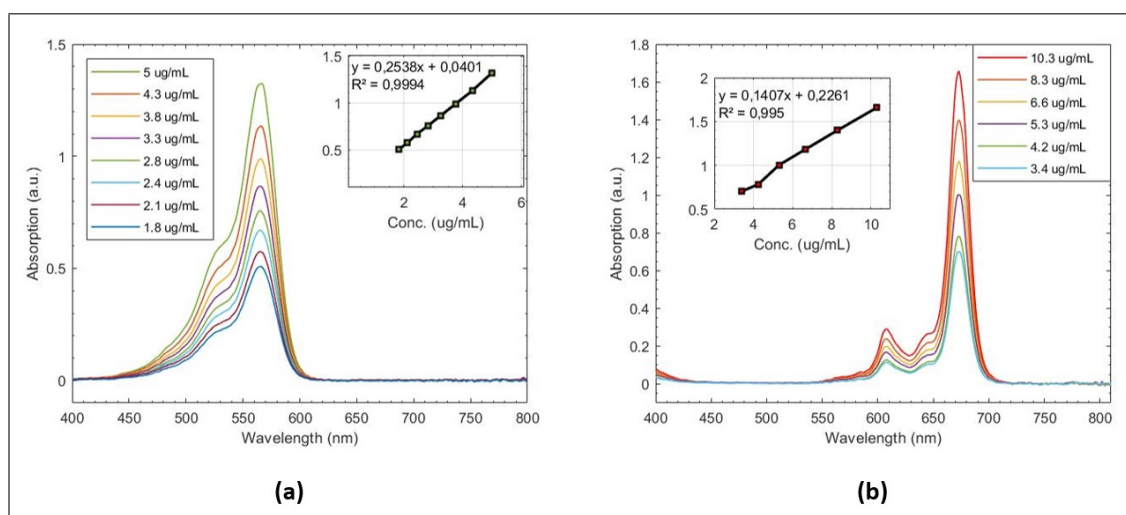


Figure 4.10 Absorptions of (a)MC540, and (b) ZnPc in different concentrations.

In Table 4.2, measured and calculated loading amounts were presented for different situations. When both PS were encapsulated with UCNP@APTES and

UCNP@Au, it was noticed that UCNP@Au was managed to load higher PS. To add, ZnPc encapsulation was greater than MC540. Besides, these photosensitizers combination with UCNP@Au one by one resulted in less PS loading.

The leakage of PS was also examined as demonstrated in Figure 4.11 (a-b). UCNP@APTES and UCNP@Au were investigated for 48 hours after PS loading. For both nanoparticles, ZnPc was not detected in the supernatant, but MC540 was escaped from the pores of silica of particles. That is, 10 % of MC540 for UCNP@APTES, and 5 % of MC540 for UCNP@Au was leaked.

Table 4.2
Loading amount of photosensitizers.

Loading Amount (%)	MC540	ZnPc
ZnPc & MC540 Loaded UCNP@APTES	0.465 ± 0.02	1.540 ± 0.08
ZnPc & MC540 Loaded UCNP@Au	0.550 ± 0.03	2.475 ± 0.31
ZnPc Loaded UCNP@Au	-	2.355 ± 0.25
MC540 Loaded UCNP@Au	0.350 ± 0.02	-

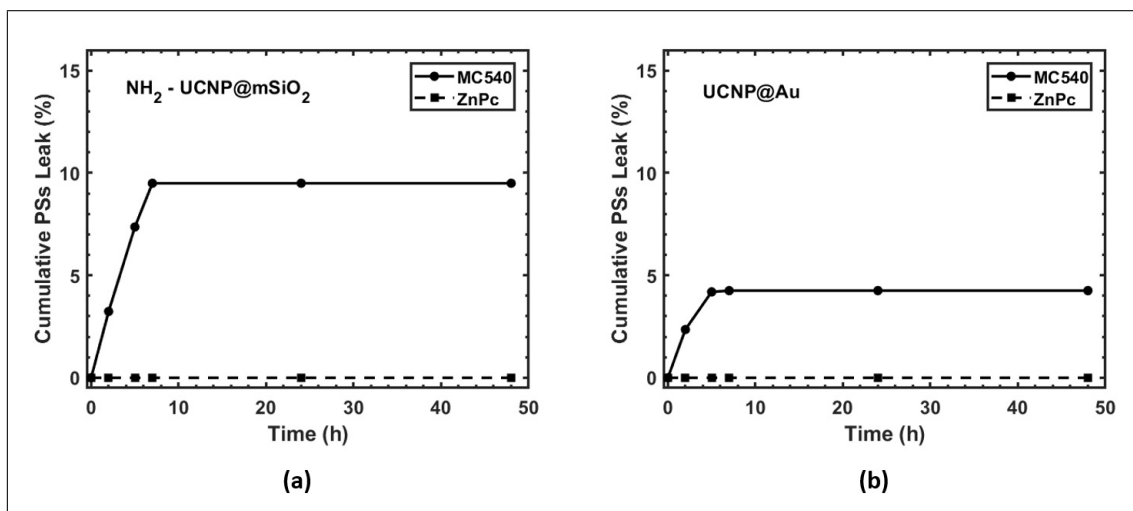


Figure 4.11 Photosensitizers' leakages from (a) UCNP@APTES, and (b) UCNP@Au.

4.5 Fourier Transform Infrared Spectroscopy (FTIR)

Infrared region, including between the 4000 and 400 cm^{-1} portion of electromagnetic spectrum, is very handy to find out mostly unknown organic chemicals of any material [120]. In fact, molecules can absorb and then convert infrared radiation into vibration, rotation, and bending. Thus, an infrared spectrum appear depending on the characteristic of the atom or molecule of materials. In this work, the chemical properties of the newly produced nanomaterials were discussed with FTIR measurements.

In Figure 4.12, the obtained FTIR spectra during synthesis of nanoplateforms were given for UCNP, mesoporous silica coated UCNP, APTES coated UCNP@mSiO₂, and UCNP@Au. UCNP was prepared with oleic acid organic compound so infrared spectrum of UCNP comprise the motions of chemicals in oleate: CH₂ symmetric stretching at 2851 cm^{-1} , CH₂ antisymmetric stretching at 2922 cm^{-1} , C=C stretching at 1653 cm^{-1} , and C-H vibration at 1449 cm^{-1} [120, 121]. When the FTIR spectrum of UCNP@mSiO₂ was assessed, the peaks were appeared because of strong absorption of Si-O bands between 830 and 1110 cm^{-1} , and SiOH group presence at 3312 cm^{-1} (OH absorbance) [120]. Amine (NH₂) functionalized UCNP showed peaks in FTIR were: N-H stretching at 3327 cm^{-1} , N-H bending at 1450 cm^{-1} [120]. When the surface of UCNP merged with Au was finalized, FTIR can successfully detect organic molecules, citrate ($\text{C}_6\text{H}_5\text{O}_7^{-3}$, in Au: O-H stretching vibration at 3300 - 2500 cm^{-1} , O-H bending vibration at 1440 - 1395 cm^{-1} , C=O stretching vibration at 1653 cm^{-1} , and C-O stretching vibration at 1309 cm^{-1} [120]. The cyanine dyes ZnPc and MC540 FTIR spectra was given with both PS loaded UCNP@Au in Figure 4.13. ZnPc and MC540 were displayed similar behavior with application of infrared light. In fact, they contain benzene rings so the spectrum showed the following peaks: a strong C-O stretching at 1042 cm^{-1} (possible to observe between 1260 - 1000 cm^{-1}), O-H bending with C-H wagging vibrations at 1320, 1407, and 1436 cm^{-1} [120]. After these dyes encapsulation, the observed peaks of benzene ring was disappeared. The noticed peak for nanoplateform at 3338 cm^{-1} was because of the solvent, water.

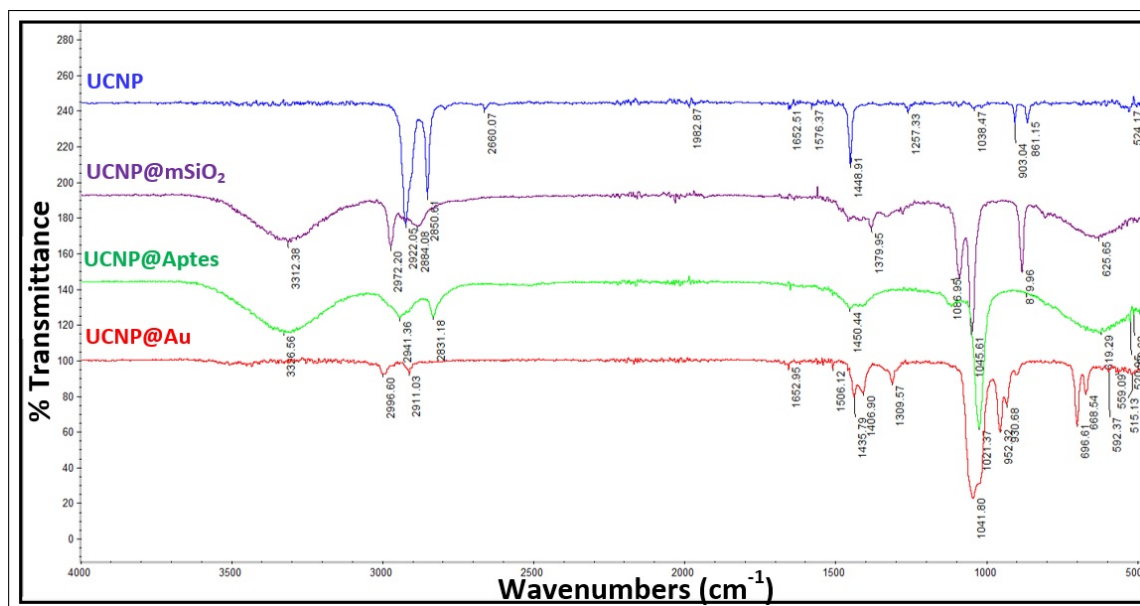


Figure 4.12 FTIR spectra of UCNP, UCNP@mSiO₂, UCNP@APTES, and UCNP@Au.

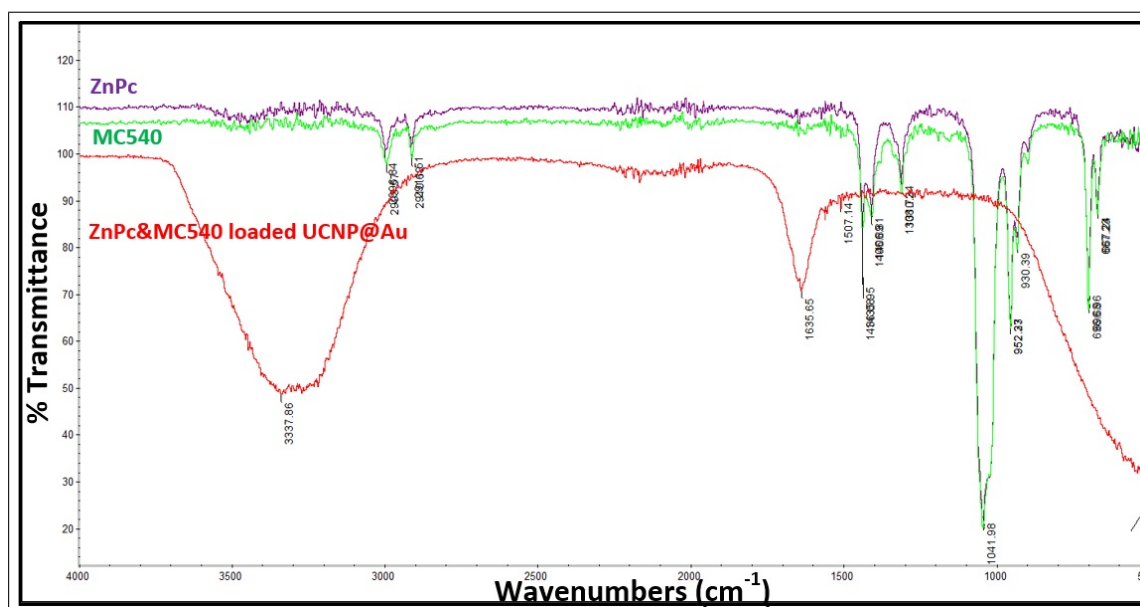


Figure 4.13 FTIR spectra of ZnPc, MC540, and both PS loaded UCNP@Au.

4.6 Energy Dispersive Spectroscopy (EDS)

EDS uses X-rays, highly energetic photons, from the electromagnetic spectrum. Generally, accelerated electrons introduce to a targeted specimen and this causes electron shifts from the shells of materials which regulates a characteristic X-ray emission [122]. These emissions can appear because of K-shell, L-shell, or M-shell. The generated X-rays allow to determine the elements inside an unknown material.

The synthesized nanoparticles were evaluated with SEM-EDS (EDAX METEK) system (Figure 4.14). 10 μL of UCNP@Au (10 mg/mL) was placed on a glass substrate, and dried for 2 hours. Then, measurement was acquired. Elemental mapping demonstrated that N, O, F, Na, Si, Er, Yb, Y, and Au elements were inside the nanoplateforms. The percentages of elements were also presented in Figure 4.14.

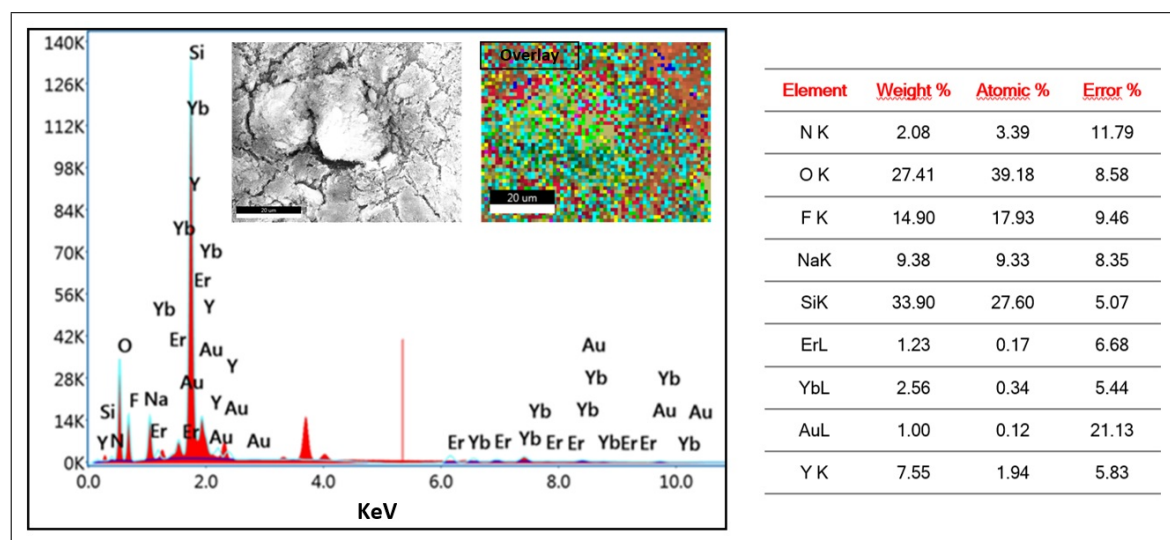


Figure 4.14 Elemental map analyzing of UCNP@Au.

5. RESULTS OF APPLICATIONS

In this part of study, the efficiency of nanoplatforms were examined for biological applications. Firstly, possible thermal differentiation, and reactive oxygen species generation capability of base nanoplatform UCNP@Au, and MC540 & ZnPc loaded UCNP@Au was evaluated. Visible and near-infrared light entrance to a tissue was studied with simulation. Afterwards, *in vitro* results were presented for imaging, dark toxicity and photodynamic therapy.

5.1 Thermal Change

When optical window of tissue, between 600 and 1300 nm, is considered, using 980 nm for PDT is very advantageous due to the less absorption coefficients of tissue constituents like hemoglobin, fat, elastin, and collagen [123]. However, one of the primary element of tissue, water, has higher absorption coefficient at this wavelength. For this reason, it is essential to understand laser thermal effect. In this study, 980 nm laser was used with 1 W/cm^2 power so only light thermal influence was measured on cell complete medium as given in Figure 5.1 (black line). Light resulted in approximately $14 \text{ }^\circ\text{C}$ heat rise.

The nanoplatforms can also have the photothermal (PTT) effect due to the presence of photosensitizers. Especially, ZnPc is able to mediate PTT alongside photodynamic therapy. For instance, Yu's group published recent article indicated that nanocapsulated ZnPc include not only PDT but also PTT behavior on orthotopic hepatocellular carcinoma [124]. They demonstrated $20 \text{ }^\circ\text{C}$ thermal increase and decrease possibility at 10 minutes interval under 730 nm radiance. Therefore, we measured the heat change for different amounts of MC540 & ZnPc loaded UCNP@APTES. The detected temperature rise was around $4\text{-}5 \text{ }^\circ\text{C}$ with the concentrations between 0.025 to 2 mg/mL.

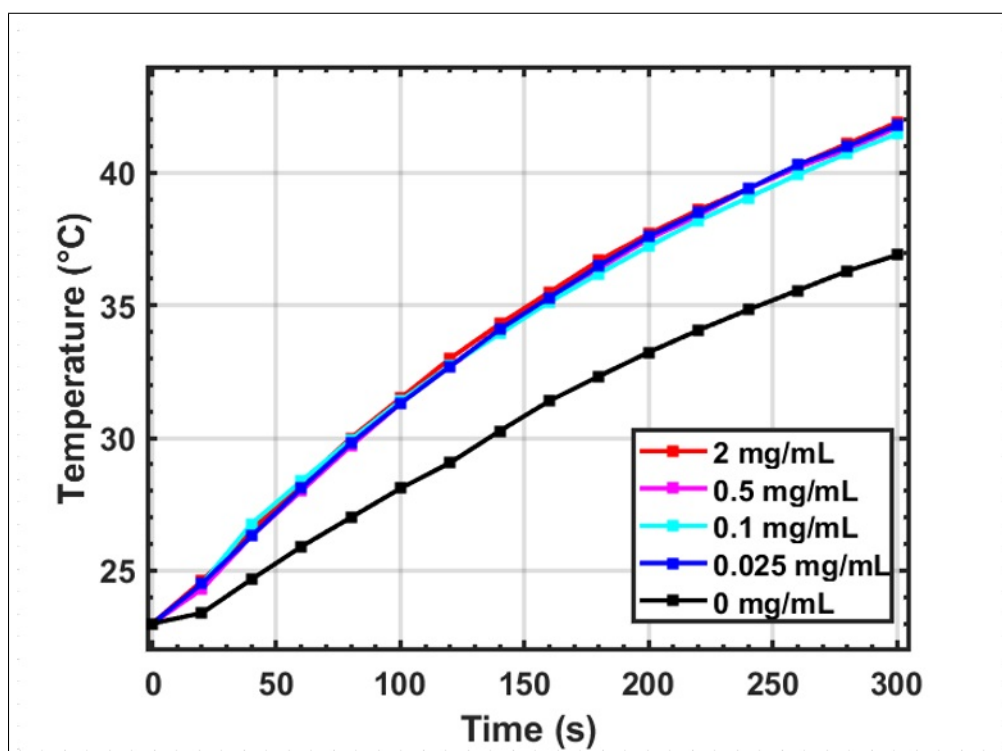


Figure 5.1 Thermal differentiation of MC540 & ZnPc loaded UCNPs@APTES.

Furthermore, MC540 & ZnPc loaded UCNPs@Au nanoplateforms involve 4 nm diameter gold nanoparticles. The gold nanoparticles can actually provide three different mechanisms to the designed system. Firstly, metallic nanoparticles can trigger PTT because of their plasmonic property [125]. However, hot electrons mostly appear with pulsed laser light applications. Previously, Pitsillides' group showed that 10-15 nm gold np can be reached 2000 K with a fluency of 0.5 J/cm^2 (532 nm laser) [126]. Second, there is a non-thermal pathway by which reactive oxygen species can arise with Au np [127]. Lastly, Au can enhance optical property of UCNPs as demonstrated before by Lv's group in 2020 [92].

In order to analyze the gold np thermal effect in the system of MC540 & ZnPc loaded UCNPs@Au, temperature measurements were performed. The concentrations of 0.02, 0.1, 0.5, and 2 mg/mL nanoplateforms were prepared inside cell culture medium. Then, their thermal change was detected three times with an inserted thermocouple into the solution. 4-6 °C heat rise was detected as presented in Figure 5.2.

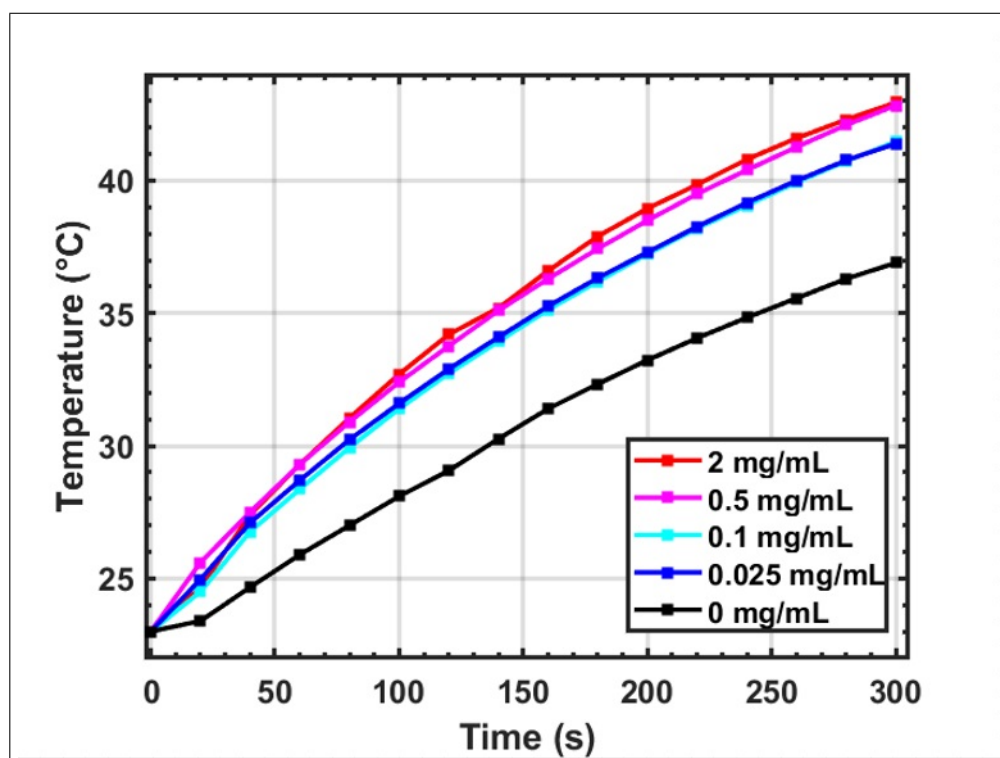


Figure 5.2 Thermal differentiation of ZnPc & MC540 loaded UCNP@Au.

5.2 Reactive Oxygen Species Measurement

The potential of nanoplateforms in PDT is a critical issue before beginning to examine their *in vitro* responses. There are many methodologies to measure reactive oxygen species (ROS) in literature [128]. For example, 1O_2 has an emission band at 1270 nm, thus; it can be detected with expensive equipment and infrared detectors [129]. However, this direct method is not used to prefer. Mostly, chemo-luminescence probes having fluorescence or absorbance properties employ upon reactions of PDT. In this study, the well-known chemical fluorescence probe 1,3-diphenylisobenzofuran (DPBF) was utilized to determine the ability of the nanoplateforms to generate ROS, such as singlet oxygen (1O_2), hydroxyl radical, or hydrogen peroxide (H_2O_2) [130].

The principle of DPBF relies that upon interactions with ROS, endoperoxide appear with $x^2 + x^4$ cycloaddition reaction [128]. The colorless product, endoperoxide, cannot absorb light or contribute fluorescence. Therefore, DPBF bleaching can be monitored around 410 - 430 nm. Although it is an indirect technique to detect ROS,

DPBF used to prefer in many studies due to being an easy method. We also detected ROS formation with DPBF in this study.

As given in Figure 5.3 (a), DPBF incubated with ZnPc & MC540 loaded UCNPs@Au was efficiently produced ROS. While the bleaching of DPBF without nanoplateforms (0 mg/mL) was negligible, the other groups consumed DPBF efficiently. While the concentrations 0.025 mg/mL and 0.1 mg/mL were resulted in 25 % of DPBF absorption decrease, 0.5 mg/mL and 2 mg/mL were diminished the absorbance approximately 40 % and 50 %, respectively. The significant differences were not detected between 0.025 and 0.1 mg/mL but the other concentration groups showed significant difference ($p < 0.05$).

The degradation of DPBF was also examined for the base nanoplateform UCNP@Au (without PS loading) as demonstrated in Figure 5.3 (b). Combination of citrate stabilized gold nanoparticles well matched absorbance with the fluorescence of UCNP around 530 nm was resulted in significant ROS generation. In fact, the concentrations between 0.025 and 2 mg/mL induced about 20 % absorbance reduction. On the other hand, the absorbance of DPBF did not change significantly when the concentration of UCNP@Au was raised.

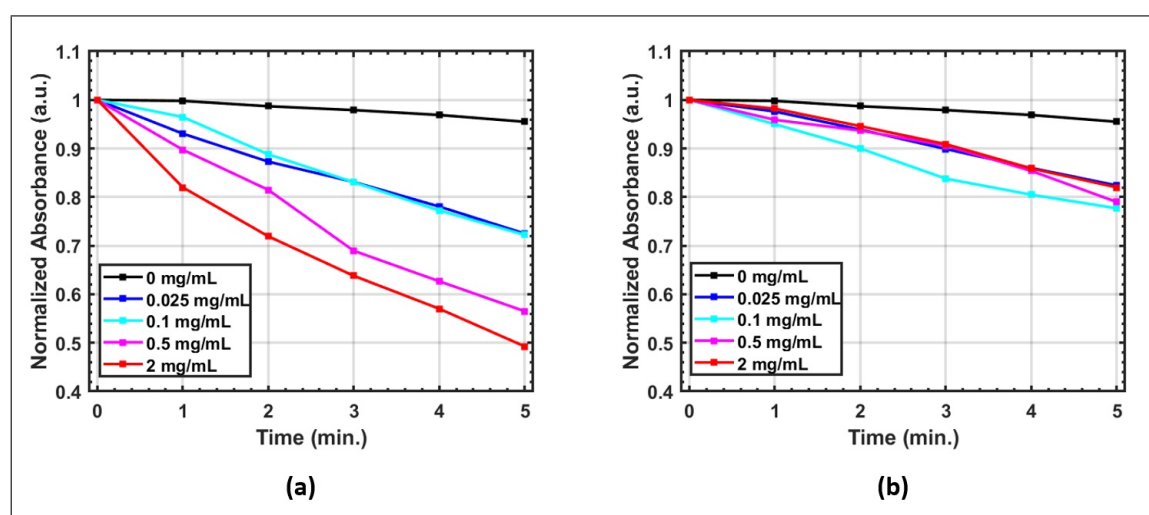


Figure 5.3 Photobleaching of DPBF under 980 nm laser irradiation (1 W/cm^2) in the presence of UCNPs@Au nanoplateforms (a) with PS and (b) without PS.

5.3 Light - Tissue Interaction: Simulation

Most photosensitizers, especially those with high quantum efficiency, can be activated by visible light, and this is the most bottleneck issue of photodynamic therapy. Penetration depth of visible light is actually restricted within a few millimeter to tissue. Increasing wavelength of light increases the tendency of beam entrance due to the decreased absorbance coefficients biological constituents except water [131].

Utilizing near-infrared region at 980 nm to activate PS was one of the main purpose of this study, which can allow PDT occurrence in deeper tissue region. In fact, the commercially available ZnPc and MC540 photosensitizers can be activated with 660 and 540 nm, respectively. In order to examine the light penetration depth with 980 nm, 660 nm, and 540 nm, a simulation was performed with Monte Carlo method. Indeed, Monte Carlo, a stochastic model, depends on the fact that expected value of combinational several random variables is equivalent to the value of a physical quantity wanted to be determined. Thus, expected values can be estimated with the average of multiple random variables [132]. This approach has been carrying out for modelling light behavior in biological environment since the development of the C code for photon transport in turbid tissues by Wang in 1992 [133].

In order to calculate fluence rate of 980 nm wavelength light with respect to distance from the source the optical parameters of biological tissue (dermis) is determined from the literature (Figure 5(a)) [134]. Monte Carlo simulation begins by inserting photons above the tissue at a location defined by x, y, z coordinates and then the photons interact with the tissue according to the selection of a random number [0,1] distance. The weight of the photon reduces by absorption with each photon steps. The non-absorbed photons travel based on a scattering function. The calculated results for penetration depth of 540 nm, 660 nm, and 980 nm was given in Figure 5 (b). It showed that while 540 nm and 660 nm wavelengths can penetrate 0.6 and 0.8 cm into tissue, 980 nm entrance depth is around 1.5 cm.

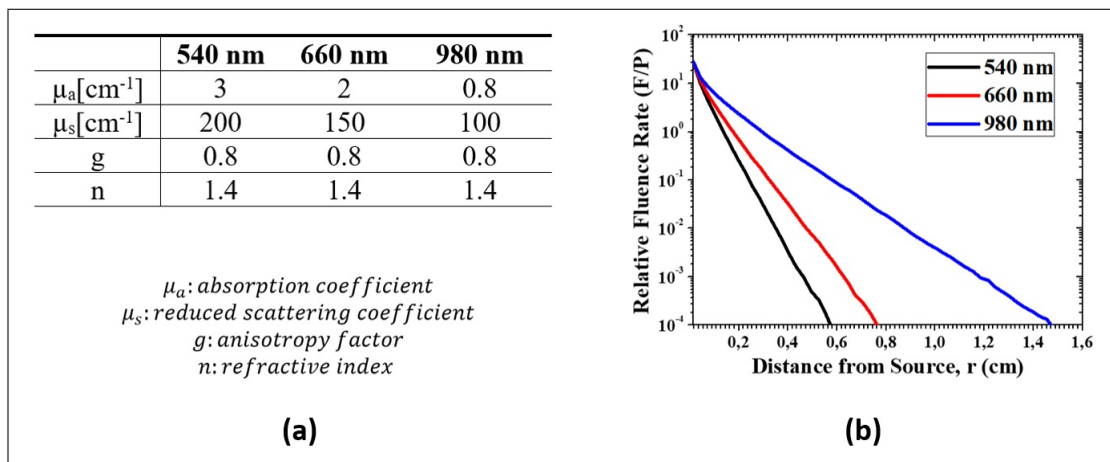


Figure 5.4 (a) Optical parameters of biological tissue (dermis) and (b) Relative fluence rate of penetrated light into dermis tissue for different wavelengths.

5.4 Imaging Cells

Although photosensitizers delivery with nanoparticles is very advantageous because of especially the additional features of np, cellular interaction of NP include various mechanisms. The physicochemical properties of nanoparticles such as size, morphology (shape), charge (negative, or positive), hydrophobicity / hydrophilicity or surface functionality effect their behavior with respect to cell type [135]. It is possible that nanoparticles can contact with cells through the inner internalization (endocytic pathways) or outer cell membrane (exocytic pathways) [136].

In this study, the produced nanoparticles' surface was decorated with gold nanoparticles which had the greatest influence on cells when the other elements, rare-earth elements, silica, amine (NH₂) were thought. Gold np have been searched in biological studies extensively in literature and their low toxicity as drug delivery component was demonstrated before [137]. Regarding these researches, 40-50 nm gold spheres uptake to cells was higher if they are compared with other diameters [138]. Besides, negative surface functionalization generally gives better internalization to Au for prostate cancer cell line, PC-3 [137].

PC3 cells were visualized with optical microscope under bright field mode and

980 nm laser illumination to understand placements of nanoplateforms upon cellular interactions. In Figure 5.5 (a-c), images of control group was given. 980 nm (500 mW/cm²) did not cause any fluorescence from the cells or other regions of culture medium. On the other hand, nanoplateforms applied at different concentrations presented the Figure 5.5 (d-i) results. Firstly, cells were waited inside 0.1 mg/mL and 0.5 mg/mL MC540 & ZnPc loaded UCNP@Au concentrations for 2 hours, and then incubated in complete medium for additional 24 hours. For both concentrations, nanoplateforms emitted visible lights with 980 nm radiation. The merged images exhibited that nanoplateforms were internalized or adsorbed by PC3 cells.

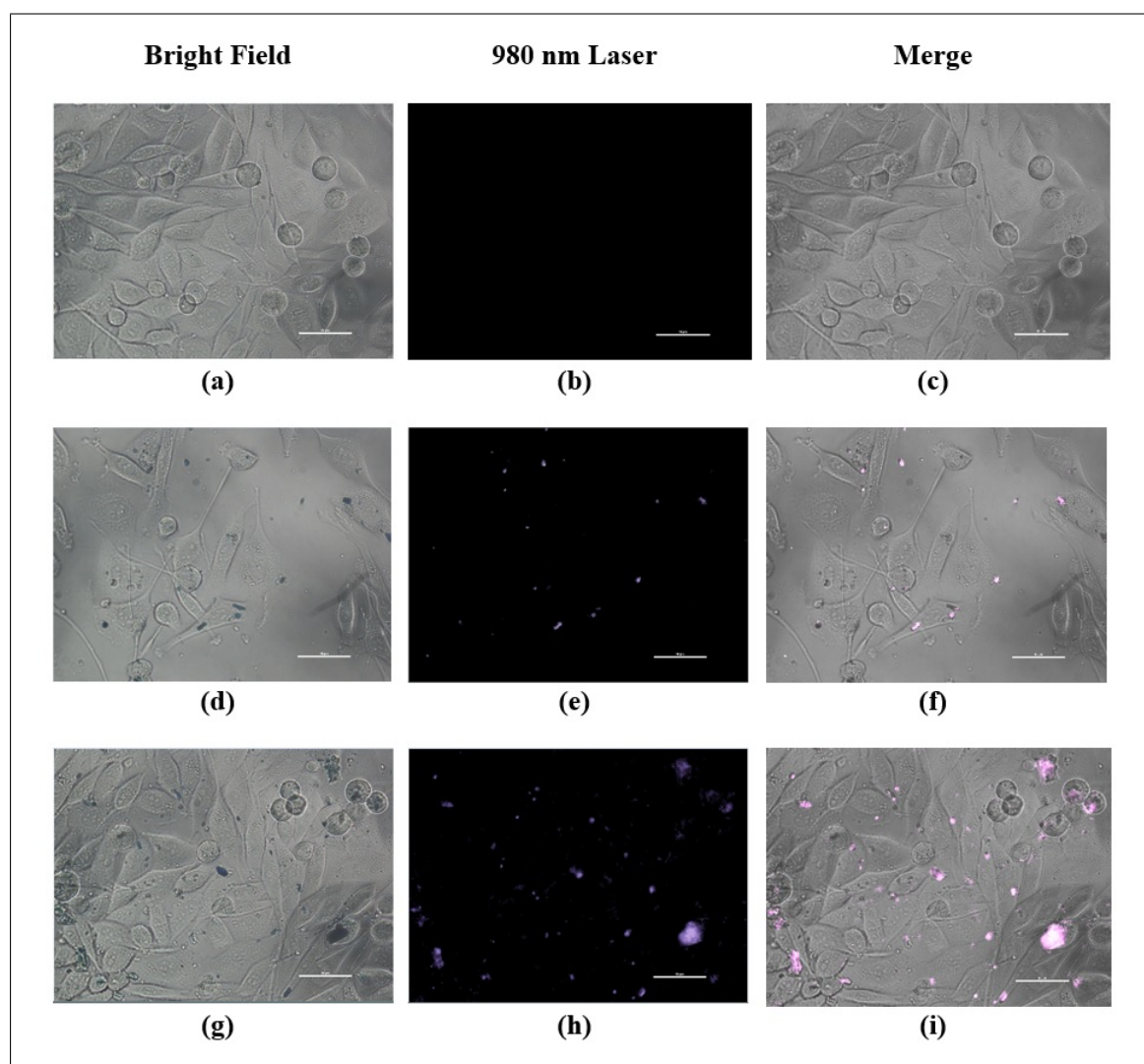


Figure 5.5 Images of PC-3 cells with optical microscope: (a-c) control group, (d-f) 0.1 mg/mL loaded nanoplateforms group, and (g-i) 0.5 mg/mL loaded nanoplateforms group.

5.5 Photodynamic Therapy Results

5.5.1 Cytotoxicity of Photosensitizers

Both MC540 and ZnPc toxicity were evaluated for their various amounts in cellular medium. The photosensitizers were introduced to PC-3 cells for 2 hours, and 24 hours later MTT assay was exerted to find out the survived cells. Cells viability (%) were calculated by considering the control group and all measurements were repeated at least three times.

The dark toxicity of MC540 was measured between 10 and 50 $\mu\text{g}/\text{mL}$ as displayed results in Figure 5.6 (green bars). No significant data were reached with these concentrations. Thus, it can be stated that they are highly biocompatible for *in vitro* PC-3 applications. However, the MC540 has a very low quantum efficiency for singlet oxygen formation, which is between 0.002 and 0.06 according to the literature [115]. In 2014, Wang's group connected UCNP with MC540 for cell imaging and PDT under 980 nm laser exposure (2 W/cm², 30 minutes) [117]. The developed novel nano-system was unfortunately required very high power and long time illumination due to insufficient singlet oxygen property of MC540.

Furthermore, the assessed ZnPc photosensitizers' results were demonstrated different behaviour, as given in Figure 5.6 (red bars). Although the concentrations 0.06 and 0.3 $\mu\text{g}/\text{mL}$ were drawn from the same population with control group; 0.6 $\mu\text{g}/\text{mL}$ ($p < 0.05$) and between 3 - 6 $\mu\text{g}/\text{mL}$ ($p < 0.01$) groups were significantly different from the control group. Indeed, ZnPc toxicity is high in biological environment for even with very small amounts but they have high quantum yields under 660 nm light. In order to ascertain PDT efficiency of ZnPc, PC-3 cells were additionally radiated with 660 nm laser (400 mW, 5 minutes) following incubation with ZnPc for 2 hours (Figure 5.7). Since 0.6 $\mu\text{g}/\text{mL}$ concentration was significantly toxic, the used highest concentration was 0.5 $\mu\text{g}/\text{mL}$ in this experiment. According to the measurements, about 40 % of cells could not survive due to PDT with 660 nm laser light for 0.25 and 0.5 $\mu\text{g}/\text{mL}$. Other groups did not lead to PDT significantly.

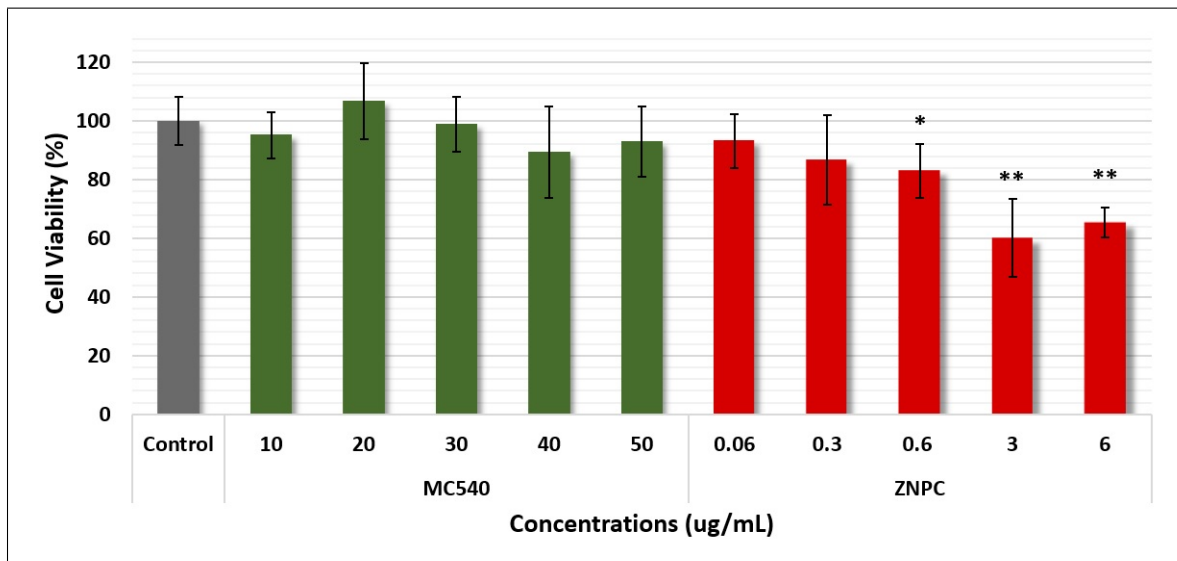


Figure 5.6 Dark toxicity results for MC540 and ZnPc photosensitizers on PC-3 cells. P values: *P<0.05, and **P<0.01.

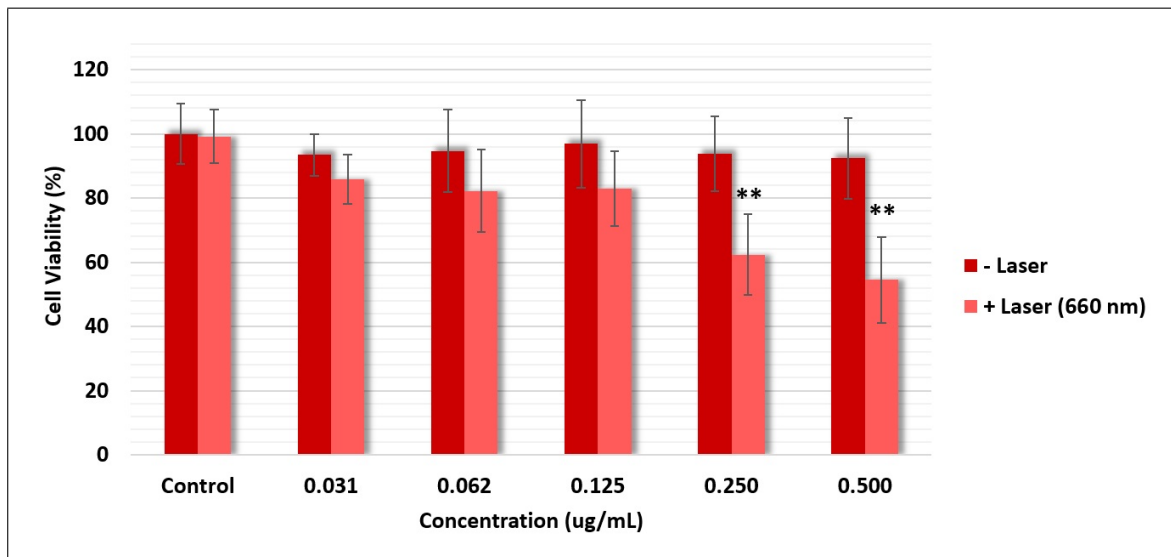


Figure 5.7 PDT for various concentrations of ZnPc via 660 nm laser (400 mW/cm², 5 minutes). P values: *P<0.05, and **P<0.01.

5.5.2 Only 980 nm Laser Application

It was already mentioned that near-infrared region can result in heat rise because water has increased absorption in this range. Besides, measurements in 'thermal change' part of this study proved this possibility. Indeed, two critical things should be considered at the same time: (I) the highest PDT efficiency needs to be reached, and (II) the unwanted temperature increase require to be prevented. Therefore, appropriate power and duration of laser were determined via 980 nm light exposure to PC-3 cells.

Confluence cells in flask were tyripsinized, and counted for experiments. 8000 cells/well were settled into 96-wells with 100 μ L complete medium and then they were waited inside incubator for 24 hours. To add, the design of seeding was important because light should not effect other groups on the 96-well. Since light output was aligned as 1 cm, four wells was irradiated at the same time. Meanwhile, 980 nm laser exposure intensities were arranged as 0.4, 0.6, 0.8, 1, and 1.2 W/cm² by power-meter. Cells were illuminated with these powers for two particular duration times, 5 and 10 minutes. After waiting cells for 24 hours in incubator, alive/death percentage was measured and calculated as depicted in Figure 5.8 ((a) 5 minutes, and (b) 10 minutes laser exposure).

The laser output power can cause an undesirable temperature increase around the cells, and it is known that heat increases with the laser light intensity rise. High heat decreased cell viability as obtained in this experiment for both 5 and 10 minutes light irradiance at 1.2 W/cm². When cells were exposed light for 5 minutes, cells viability were decreased below 80 % with 1.2 W/cm² power but the intensities between 0.4 to 1 W/cm² did not change the number of cells. The similar result was also acquired for 10 minutes light radiance. As a further note, 10 min. time duration was decreased cells viability to 90 % but its data were not significantly different from the control group.

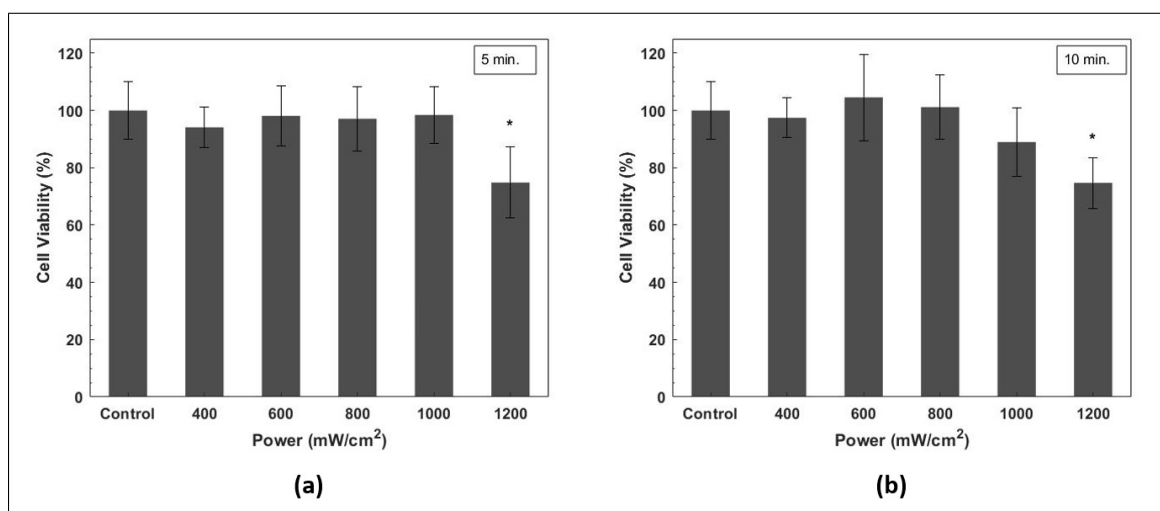


Figure 5.8 PC-3 cells viability upon 980 nm light exposure with different powers and duration; (a) 5 minutes, and (b) 10 minutes. P value: *P<0.05.

5.5.3 Base Nanoplatfrom: UCNP@Au

The designed base nanoplatfrom, UCNP@Au, include rare-earth elements, possessing ability to transform 980 nm to 660 and 540 nm lights, and gold nanoparticles, owning absorption feature around 530 nm to generate SPR. Note that gold np were too small in diameter and ROS formation feature was not detected before. Besides, dark toxicity of nanoplatfroms expected to be minimal for even their high amounts usage against to cells. Thus, an experiment was done with these foreseen facts.

UCNP@Au, between 0.025 and 0.2 mg/mL concentrations, were employed to cells with and without light exposure as displayed in Figure 5.9. There was no significant data group with these concentrations in dark, means that they are biocompatible against to cells. When laser sustained results were measured and calculated, it was detected that 0.2 mg/mL group was capable to initiate PDT. In fact, gold nanoparticles were very small to generate ROS but they managed to kill approximately 20 % of cells. All experiments were repeated for three times and 5 minutes applied light had 980 nm wavelength with 1 W/cm² intensity.

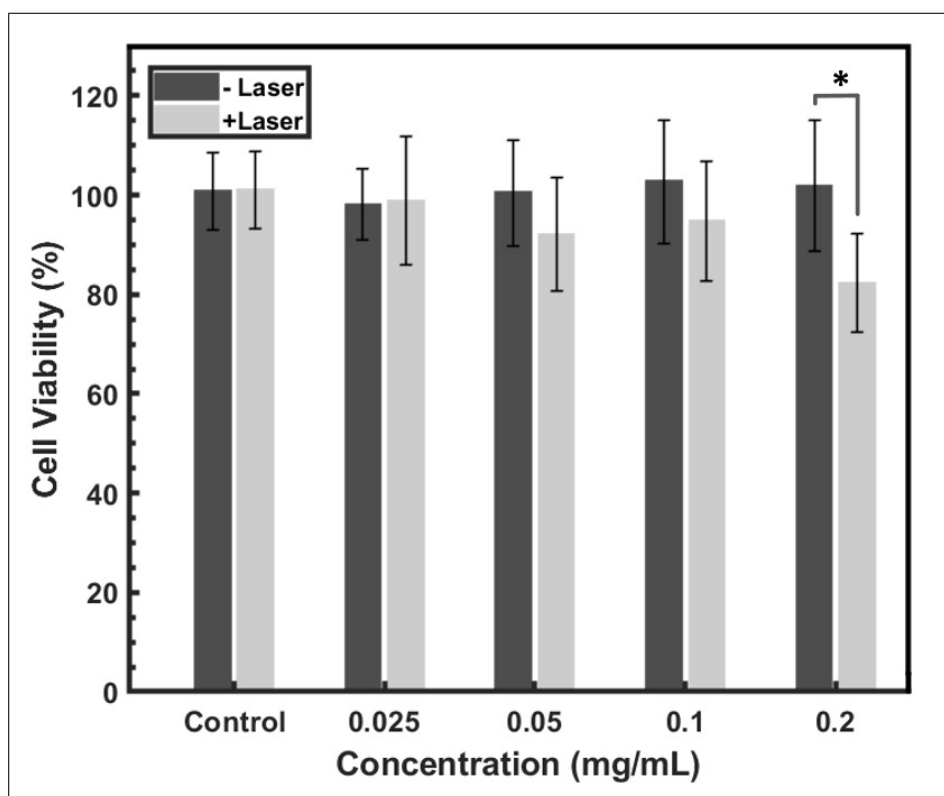


Figure 5.9 UCNP@Au (without PS loading) dark toxicity and PDT property under 980 nm laser (1 W/cm², 5 minutes). P value: *P<0.05.

5.5.4 MC540 & ZnPc Loaded UCNP@Au

As final experiments both MC540 and ZnPc encapsulated UCNP@Au was carried out for not only dark cytotoxicity but also photodynamic therapy. Prostate cancer cell line, PC-3, was cultured into 96 well plate, firstly. Afterwards, they were incubated with nanoplateforms in 0.025, 0.05, 0.1, 0.5, 1, and 2 mg/mL concentrations for two hours in dark. In Figure 5.10, (- laser) data were attributed to the dark toxicity experiments. It was seen that 0.025 and 0.05 mg/mL groups did not demonstrate any toxicity, on the other hand, 0.1, 0.2, 0.5, 1, and 2 mg/mL concentrations were significantly different from the control group. However, between 0.1 and 2 mg/mL groups were drawn from the same population, that they were not killed cells more than 20%. Besides, concentrations of ZnPc and MC540 photosensitizers were also calculated inside these amounts of nanoplateforms (Table 5.1). The given corresponding amounts helped to determine bare PS and loaded PS dark toxicity on PC-3 cells.

Photodynamic therapy action of the same amounts of nanoplateforms with light application revealed the outcomes in Figure 5.10 (+ Laser). Although light transported to the control group (0 mg/mL np) at a wavelength of 980 nm (1 W/cm² intensity, 5 min) did not kill any cells, it significantly reduced cell viability in the other groups. That is, the presence of photodynamic therapy was demonstrated with the whole concentrations. Cell viability was around between 60 % and 70 % for the concentrations 0.025 - 0.5 mg/mL, 50 % for 1 mg/mL, and 30 % for 2 mg/mL. All measurements were repeated three times.

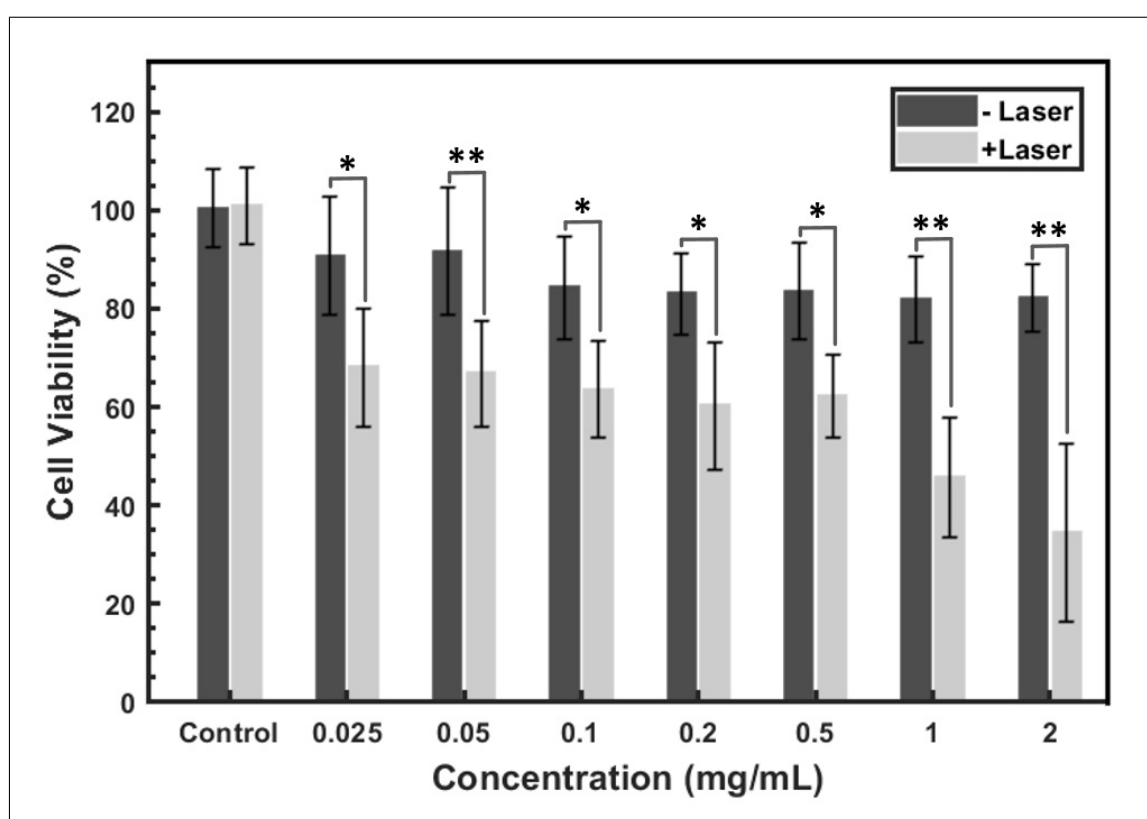


Figure 5.10 Dark toxicity and PDT (980 nm laser with 1 W/cm² and 5 minutes application) measurements for various concentrations of ZnPc and MC540 loaded UCNP@Au. P values: *P<0.05, and **P<0.01.

Table 5.1
Corresponding concentrations of photosensitizers inside UCNP@Au.

Concentrations of Nanoplatfoms	Concentrations of MC540	Concentrations of ZnPc
0.025 mg/mL	0.15 $\mu\text{g/mL}$	0.5 $\mu\text{g/mL}$
0.05 mg/mL	0.3 $\mu\text{g/mL}$	1 $\mu\text{g/mL}$
0.1 mg/mL	0.6 $\mu\text{g/mL}$	2 $\mu\text{g/mL}$
0.2 mg/mL	1.2 $\mu\text{g/mL}$	4 $\mu\text{g/mL}$
0.5 mg/mL	3 $\mu\text{g/mL}$	10 $\mu\text{g/mL}$
1 mg/mL	6 $\mu\text{g/mL}$	20 $\mu\text{g/mL}$
2 mg/mL	12 $\mu\text{g/mL}$	40 $\mu\text{g/mL}$

6. DISCUSSION

Photodynamic therapy is a light, and photosensitizer mediated technique (with the presence of oxygen) to remove unwanted region or tissue in a body. Although light, photosensitizer, or oxygen have no / minimal effect to a biological environment one by one, their combination is lethal for lesions like tumors. In fact, connecting light and PS results in reactive oxygen species generation which trigger cell death mechanisms, i e. apoptosis, necrosis, or autophagy activation. When PDT treatment is compared with the conventional methods such as chemotherapy, radiotherapy, or surgical dissection; the followings are the main advantages:

- PDT treatment offers selective photosensitizers accumulation and localized light application so that the systemic side effects of chemotherapy can be avoided.
- It does not damage the surrounding healthy tissue, such as radiotherapy or surgical dissection.
- PDT can deal with especially resistance cancer cells to chemotherapeutic drug or radiotherapy.

Nevertheless, PDT did not still take a place among standard modalities because it still requires some improvements. The existing some drawbacks of PDT can be shortly ordered as followings:

- Most photosensitizers are not appropriate for direct biological usage because of their chemical formulations.
- Photosensitizers activation depends on the energy of light and visible wavelength range is the best region for the commercially available PS. Unfortunately, visible wavelength penetration to tissue is superficial.

- Cancer tissues are usually less oxygenated and oxygen is one of the important component of PDT.
- Metastatic cancer lesions cannot be treatable with the current PDT technology.

In this study, it is aimed to develop photodynamic therapy treatment by utilizing nanoparticle technology. A nano-deliver system was designed and synthesized to allow deep-penetration treatment with near-infrared light activated PDT. Besides, photosensitizers were combined with the highly biocompatible nanoplatforms to protect not only PS but also biological environment. Then, their activity was discussed for PC-3 prostate cancer cell lines.

Since most conventional photosensitizers activation is in visible wavelength range, and visible light penetration is superficial; nanoparticles possessing transducer property were produced in the first place. The transducers, was also used to named as upconversion nanoparticles in this study, have the ability to convert near-infrared light to visible lights. During synthesise, Ostwald ripening method allowed growing smaller particles to larger particles with heat and appropriate conditions.

Ytterbium (30 %) and Erbium (3 %) were doped into NaYF_4 matrix to fabricate UCNP with rare earth elements. The size measurements with SEM showed that they had approximately 40 nm diameter (Figure 4.2 and Figure 4.5(a)). Besides, UCNP was well distributed in cyclohexane with respect to DLS results because three different measurements gave the similar size peaks in minutes. The hexagonal shapes (Figure 4.5 (a)) and lattice fringe (512 pm, Figure 4.6 (a-inset)) of UCNP indicated that they were in crystalline beta-phases and thus, high emission peaks in visible range could be detected.

980 nm laser irradiation to UCNP was resulted in naked-eye observable fluorescence as presented in Figure 4.7 (a-inset). As an efficient transducer, UCNP was transformed lower energy NIR light (980 nm) to higher energy emissions in red, green, and near-infrared regions. UCNP was monitored with fluorescence spectroscopy and

the resultant sharp-intensities were at 532 nm - 552 nm (green), 670 nm (red), and 830 nm (NIR). In fact, a protocol similar to that in the literature was used with small alterations to synthesize UCNP [82]. According to the fluorescence measurement results obtained by Gnanasammandhan M. K. and et al., UCNP can generate emissions at blue, green and red regions. On the other hand, blue emission was not detected in this study but instead NIR (830 nm) intensity was monitored. At this point, it can be concluded that very small changes in synthesize can differentiate the transducer properties of UCNP.

UCNP was actually stabilized with oleic acid, as evidenced by its FTIR spectra (Figure 4.12), which inhibited water solubility of the nanoparticles. Therefore, surface modifications were proceeded to make UCNP hydrophilic, and more biocompatible. In addition, it was also crucial that the photosensitizers and UCNP must be linked in order to receive the visible light emitted by UCNP. The preferred and applied design for surface modification have three main stages in this research: (i) mesoporous silica coating (UCNP@mSiO₂), (ii) amine functionalization (UCNP@APTES), and (iii) gold np conjugation (UCNP@Au);

- UCNP@mSiO₂: Porous silica was coated around UCNP with silica precursor TEOS. While hydrodynamic size measurements with DLS displayed the new PS sizes become 71.82 ± 33.21 nm (Figure 4.3), TEM results showed they were around 90 nm in diameter (Figure 4.6 (a)). Both measurements were supported each other. According to the TEM images UCNP@mSiO₂, no UCNP was observed as uncoated but a few only mesoporous silica nanoparticles formation was detected. Since silica has better biocompatibility than rare-earth elements, it would not cause significant problems in biological applications. Moreover, hydrodynamic distribution of UCNP@mSiO₂ was not as well as oleic stabilized UCNP because zeta potential of porous silica is very close to zero with respect to literature [139]. It means higher coagulation can occur for UCNP@mSiO₂ when compared with UCNP distribution. Furthermore, after mesoporous silica coating around UCNP was caused fluorescence of UCNP decrease because most part of

emissions were trapped inside nanoparticles. FTIR analysis were also demonstrated surface of UCNP@mSiO₂ have SiOH groups presence. That is, porous silica was efficiently combined with UCNP.

- UCNP@APTES: Since photosensitizers was aimed to load into porous of silica without chemical linkage, they could escape outside during biological implementation if a gate system was not used. Thus, APTES was conjugated around the silica with direct mixing under heat. It is known that APTES molecule has two general groups as Si-O and NH₂. While Si-O heads can easily be connected with silica, NH₂ groups stay outside of nanoparticles. In fact, APTES can inhibit PS efflux and conversely allow the movement of generated ROS into the biological environment. In this study, amine conjugation was evaluated with SEM and FTIR measurements. SEM demonstrated that nanoparticles were not aggregated and were still in 90 nm diameter (Figure 4.5 (c)). On the other hand, FTIR spectra of UCNP@APTES showed that the successful junction with the detected N-H bending and stretching under infrared light (Figure 4.12).
- UCNP@Au: Plasmonic metal nanoparticles were combined with NH₂ head groups in order to improve UCNP optical efficiency in PDT practice. Before starting conjugation with UCNP, citrate stabilized gold seeds were synthesized. DLS analyse of Au np as given in Figure 4.4 showed that their hydrodynamic differentiation was too fast to detect them in similar sizes. Indeed, Au seeds tend to coagulate immediately due to the high surface energy. However, no aggregation was observed as soon as they were combined with UCNP (Figure 4.6 (b)). Besides, UCNP@Au FTIR spectra provided additional measurement with the detected citrate molecules on the surface means that Au was successfully attached to the UCNP@APTES (Figure 4.12). Moreover, UCNP emission spectrum at green region matched well with gold np absorption as demonstrated in Figure 4.9 (b), thus plasmonic activity of Au can be achieved under 980 nm irradiation.

In order to finalize nanoplatform synthesise, both ZnPc and MC540 were encapsulated into porous part of nanoparticles. UCNP@Au and PS were mixed for 24 hours to load ZnPc & MC540. Loading amount was determined by measuring supernatant

part of the np-including solution. According to the presented results in Figure 4.11 (a), uploading ZnPc & MC540 into UCNP@Au is higher than UCNP@APTES. The hydrophobicity of UCNP@APTES may be the main reason why both PSs do not allow to penetrate the pores as in UCNP@Au. Besides, loading both PS at the same time elevated the encapsulation quantity because interactions between ZnPc and MC540 possibly not let their departures from the pores of silica after entrance. Furthermore, ZnPc encapsulation was highly different than MC540 and it can be evaluated as; ZnPc chemical structure is much more compact than the complex element ordering of MC540, so ZnPc entrance to pores was probably easier than MC540. To add, higher amount of ZnPc could be preferred due to their higher quantum yield if compared with MC540. However, MC540 photosensitizers high biocompatibility cannot be underestimated and MC540 might also prevent quenching of ZnPc. When the leakage of PS was examined additional surface functionalization with Au to nanoparticles was lessen escape of PS from the pores (Figure 4.11(b-c)). Therefore, Au was not only increased the amount of loading but also prevented leakage of them.

The designed novel nanoplatfroms, ZnPc & MC540 loaded UCNP@Au, were examined generally in a manner of temperature change, ROS generation, and *in vitro* PDT applications. 980 nm laser (Continuous wave, CW) was determined for possible overheating issue, high penetration depth property, and potential *in vitro* light damage. Thereby, PDT features of both nanoplatfroms and light were managed to discuss in different view points.

In this study, it was worrying that overheating can be a problem because of the preferred intensity of laser, 1 W/cm^2 , which is higher than the maximum permissible exposure for skin according to American National Standard [140]. Thus, an experiment was performed to observe heat change of cellular medium under 980 nm (continuous wave, CW) laser for 5 minutes (Figure 5.1 and 5.2). As an expected and unlucky result, light was caused $14 \text{ }^\circ\text{C}$ temperature differentiation. However, no cellular damage was monitored when laser light was applied to PC-3 cells at the same intensity for 5 minutes (Figure 5.8). If the laser power was 1.2 W/cm^2 , viable cell amount would have been decrease significantly as demonstrated in Figure 5.8. Hence, it was considered that

exposing cells with 1 W/cm^2 laser intensity for 5 minutes is safe.

As an another view of point, the achieved results in cellular experiment with both nanoplatfrom and light might not be attributed only to PDT. Photosensitizers and gold nanoparticles might have triggered photothermal therapy. In order to understand the underlying mechanism, possible thermal change of base nanoplatforms (UCNP@Au) and PS encapsulated UCNP@Au were evaluated with experiments (Figure 5.1 and Figure 5.2). The observed heat rise due the presence of both nanoplatforms was around $5 \text{ }^\circ\text{C}$ (when only laser illumination heat rise was excluded) and it was discussed that heat transfer property of the small nanoparticles was responsible from this. Similar conclusion was also observed in literature [141].

Additionally, under light radiation gold nanoparticles might behave in two separate ways: (i) they can initiate PTT or (ii) ROS can be generated via non-thermal route. It is well known that when gold nanoparticles are irradiated with pulsed laser light hot electrons may appear and trigger ROS photogeneration. On the other hand, continuous wave (CW) light cannot yield hot electrons (except primary hot electrons) as a result of the rapid electronic relaxation but CW light can interestingly produce ROS and induce cell death. In 2016, Chadwick's group showed that citrate stabilized 15 nm spherical gold nanoparticles' temperature is only 80 mK higher than the surrounding (produced hot electrons cause 10 K rise but energy lose occur in a few picoseconds due to the electron-phonon scattering) under light illumination and able to produce ROS [127]. In this study, we did not detect significant thermal change with UCNP@Au nanoparticles. Nevertheless, UCNP@Au revealed reactive oxygen species (Figure 5.3 (b) and these nanoplatforms were even activated the cell death mechanism (Figure 5.9).

Although it has been mentioned in the literature that light penetration depth of visible range cannot be as well as NIR light, 980 nm wavelength was compared with 660 nm and 540 nm by utilizing a general simulation for light-tissue interaction. The calculated results with Monte-Carlo proved that 980 nm light entrance to tissue is almost twice of red and green wavelength (Figure 5.4). Therefore, PDT would affect

deeper cancerous cells with the help of UCNP.

Once 980 nm were absorbed by UCNP, they can generate visible wavelengths of light. Thus, as another feature of the nanoplatfrom-light system, cells can be visualized if ZnPc & MC540-UCNP@Au internalization/adsorption to cells is provided. Experiment with this point of view was successful as shown in Figure 5.5. This suggests that visualization and photodynamic therapy can be applied simultaneously.

In this research, the used conventional photosensitizers are merocyanine-540 and zinc phthalocyanine because their absorption fit appropriately UCNP emissions at 540 and 660 nm (Figure 4.9 (a) and Figure 4.10). When their dark cytotoxicity examined on PC-3 cells, MC540 can employed with higher concentrations than ZnPc (Figure 5.6). That is, 50 $\mu\text{g}/\text{mL}$ concentration of hydrophilic MC540 did not result any significant cell death but 0.6 $\mu\text{g}/\text{mL}$ of hydrophobic ZnPc was toxic to cells. On the other hand, ZnPc has better quantum yield than MC540 and PDT property of ZnPc were detected for even 0.25 $\mu\text{g}/\text{mL}$ concentration. Upon both PS were loaded into UCNP@Au, dark toxicity of nanoplatforms were measured between 25 and 2000 $\mu\text{g}/\text{mL}$ concentrations. In this experiment, no significant cell death was observed up to a concentration of 100 $\mu\text{g}/\text{mL}$, meaning that the 50 $\mu\text{g}/\text{mL}$ nanoplatforms were actually non-toxic to cells. 50 $\mu\text{g}/\text{mL}$ nanoplatforms were actually including 0.3 $\mu\text{g}/\text{mL}$ MC540 and 1 $\mu\text{g}/\text{mL}$ ZnPc concentrations. Therefore, it can be concluded that encapsulating PS allow us to use them in higher concentrations because encapsulated 1 $\mu\text{g}/\text{mL}$ ZnPc did not show any toxicity but bare 0.6 $\mu\text{g}/\text{mL}$ ZnPc significantly caused cell death. Furthermore, nanoplatforms possessing 100 and 2000 $\mu\text{g}/\text{mL}$ concentrations were not developed any significant data between them and cell viability were still above 80 % (Figure 5.10). If the nanoplatforms having 2 mg/mL concentration is discussed, 12 $\mu\text{g}/\text{mL}$ MC540 and 40 $\mu\text{g}/\text{mL}$ ZnPc were implemented to cells. ZnPc amount was extremely higher than its possible bare-application (0.6 $\mu\text{g}/\text{mL}$) to cells.

Photodynamic therapy was evaluated with the base nanoplatfrom UCNP@Au and ZnPc & MC540-UCNP@Au as presented in Figure 5.9 and 5.10. UCNP@Au did not demonstrate any dark toxicity between 0.025 and 0.2 mg/mL concentrations but

significant PC-3 cells viability decrease was detected at 0.2 mg/mL. Au nanoparticles around UCNP@APTES probably triggered ROS generation by the non-thermal pathway previously measured with the DPBF probe (Figure 5.3 (b)). It should be noted that PDT with Au having 3-4 nm sizes was not measured before on cells as far as we know. Lastly, ZnPc & MC540-UCNP@Au of PDT efficiency was evaluated. All concentrations between 0.025 and 2 mg/mL reduced cancerous prostate cells significantly. While 0.05 mg/mL concentration, possessing no dark toxicity, killed around 40 % of cells; 2 mg/mL concentration, having slight dark toxicity, decreased viable cells amount to approximately 35 %. It can be said that the newly developed ZnPc & MC540-UCNP@Au nanoplatfroms that can be activated by NIR light show very effective photodynamic therapy on PC-3 cells.

7. CONCLUSION

Advances in photodynamic therapy, like the published study from this thesis, may allow a less invasive treatment method to become conventional [142]. Although traditional techniques such as chemotherapy, radiotherapy, or surgical dissections are serving people well today regarding the cancer type/degree, it is clear that these approaches are not sufficient and require replacement or development (e.g. combined therapy) with fresh/less harmful methodologies. Fortunately, the progresses on nanotechnology and lasers give a hope that PDT's most critical limitations (i.e. photosensitizers delivery and light penetrations) may be resolved over time.

Since different properties can be added to nanoparticles thanks to nanotechnology, a successfully designed system for necessary biomedical application can provide efficient outcomes. In the light of recent improvements on PDT, near-infrared light can be used to activate traditionally available photosensitizers if a transducer-like nanoparticle can be merged with PS. For this study, a nanoparticle system was engineered to improve PDT treatment on cancerous cells.

The nano-design shortly included four main elements; upconversion nanoparticles, porous silica region, gold nanoparticles, and two different photosensitizers (MC540 and ZnPc). While upconversion nanoparticles was converting 980 nm wavelength light to visible ranges at around 540, 660 and 830 nm due to anti-stokes property of UCNP, the coated porous silica around UCNP supplied an opportunity for PS merging with nanoparticles. Thus, emitted light by UCNP can be collected with MC540 and ZnPc. Moreover, gold nanoparticles in 4 nm size were bound to the surface of porous silica following amine functionalization. The amine molecules contributed in forming a gate system in the open portions of the silica to prevent PS leakage. Au np added three important features to nano-system; (i) biocompatibility, (ii) enhanced UCNP luminescence, and (iii) ROS generation with non-thermal pathway.

Afterwards, MC540 & ZnPc - UCNP@Au, possessing strong features, were evaluated for PDT applications. Thermal change, reactive oxygen species production, bare photosensitizers (MC540 and ZnPc) cytotoxicity, and PDT efficiencies were examined. As a conclusion, the experiments exhibited that the designed and successfully synthesized nanoplatforms showed impressive PDT results on PC-3 cells.

As future works, MC540 & ZnPc - UCNP@Au nanoplatforms can be employed *in vivo* experiments. However, before starting these experiments, further development of nanoplatforms would be better. The synthesized NaYF₄: Yb, Er (UCNP) can be converted to the core-shell type so that less light intensity will be sufficient to trigger them. Thus, generated heat due to the high laser intensity can be avoided. Moreover, different types of drugs, i e. curcumin, chemotherapeutic/immunotherapeutic drugs, might be loaded into the pores of silica. Cell targeting properties, such as ph-targeting, folic acid, can also be added to these nanoplatforms. On the other hand, it would be very interesting to understand cellular death mechanisms with these nanoplatforms because it might help to decide which types of features should be added to nanoparticles.

7.1 List of publications produced from the thesis

1. Near infrared light activated upconversion nanoparticles (UCNP) based photodynamic therapy of prostate cancers: An in vitro study B. Güleriyüz, U. Ünal, M. Gülsoy, *Photodiagnosis Photodyn Ther.*, Vol. 36, 102616, 2021.

REFERENCES

1. Sung, H., J. Ferlay, R. L. Siegel, and et al., "Global cancer statistics 2020: Globocan estimates of incidence and mortality worldwide for 36 cancers in 185 countries," *CA: a cancer journal for clinicians*, Vol. 71, no. 3, pp. 209–249, 2021.
2. Hamblin, M. R., and P. Mroz, *Advances in Photodynamic Therapy Basic, Translational, and Clinical*, United States: Artech House, 1st ed., 2008.
3. Peng, Q., A. Juzeniene, J. Chen, and et al., "Lasers in medicine," *Reports on Progress in Physics*, Vol. 71, no. 056701, 2008.
4. Zhang, P., W. Steelant, M. Kumar, and et al., "Versatile photosensitizers for photodynamic therapy at infrared excitation," *Journal of the American Chemical Society*, Vol. 129, no. 15, pp. 4526–4527, 2007.
5. Lan, M., S. Zhao, W. Lee, and et al., "Photosensitizers for photodynamic therapy," *Advanced healthcare materials*, Vol. 8, no. 1900132, 2019.
6. Patra, J. K., D. G. Das, L. F. Fraceto, and et al., "Nano based drug delivery systems: recent developments and future prospects," *Journal of nanobiotechnology*, Vol. 16, no. 1, pp. 1–33, 2018.
7. Reynolds, T., "Photodynamic therapy expands its horizons," *J Natl Cancer Inst.*, Vol. 89, pp. 112–114, 1997.
8. Baumler, W., *Photodynamic Therapy and Fluorescence Diagnosis in Dermatology*, Vol. 898 of *Comprehensive Series in Photosciences 2*, pp. 83–98. Elsevier, 2001.
9. Agostinis, P., K. Berg, K. A. Cengel, and et al., "Photodynamic therapy of cancer: An update," *CA CANCER J CLIN*, Vol. 61, pp. 250–281, 2011.
10. Robertson, C. A., D. Hawkins, and H. Abrahamse, "Photodynamic therapy (pdt): A short review on cellular mechanisms and cancer research applications for pdt," *Journal of Photochemistry and Photobiology B: Biology*, Vol. 96, pp. 1–8, 2009.
11. Balzani, V., P. Ceroni, and A. Juris, *Photochemistry and Photophysics Concepts Research Application*, Germany: Wiley-VCH, 1st ed., 2014.
12. Beiser, A., *Concepts of Modern Physics*, New York: Mc Graw Hill, 6th ed., 2003.
13. Persico, M., and G. Granucci, *Photochemistry A Modern Theoretical Perspective*, Switzerland: Springer, 1st ed., 2018.
14. Juarranz, A., P. Jaen, F. Sanz-Rodriguez, and et al., "Photodynamic therapy of cancer. basic principles and applications," *Clin Transl Oncol*, Vol. 10, pp. 148–154, 2008.
15. Calixto, G. M. F., J. Bernegossi, L. M. D. Freitas, and et al., "Nanotechnology-based drug delivery systems for photodynamic therapy of cancer: A review," *Molecules*, Vol. 21, no. 342, pp. 3–18, 2016.
16. Allison, R. R., and K. Moghissi, "Oncologic photodynamic therapy: Clinical strategies that modulate mechanisms of action," *Photodiagn. Photodyn. Ther.*, Vol. 10, pp. 331–341, 2013.

17. Yoon, I., J. Z. Li, Y. K. Shim, and et al., "Advance in photosensitizers and light delivery for photodynamic therapy," *Clin. Endosc.*, Vol. 46, pp. 7–23, 2013.
18. Abrahamse, H., and R. K. Hamblin, "New photosensitizers for photodynamic therapy," *Biochem J.*, Vol. 15, no. 4, pp. 347–364, 2016.
19. Battersby, A. R., "Tetrapyrroles: the pigments of life," *Nat Prod Rep.*, Vol. 17, pp. 507–526, 2000.
20. Krammer, B., and K. Plaetzer, "Ala and its clinical impact, from bench to bedside," *Photochem Photobiol Sci.*, Vol. 7, pp. 283–289, 2008.
21. Dennis, E. J., G. C. Dolmans, D. Fukumura, and et al., "Photodynamic therapy for cancer," *Med. Phys.*, Vol. 3, pp. 380–387, 2003.
22. Detty, M. R., S. L. Gibson, and S. J. Wagner, "Current clinical and preclinical photosensitizers for use in photodynamic therapy," *American Chemical Society*, Vol. 47, no. 6, 2004.
23. Kwiatkowski, S., R. Knap, D. Przystupski, and et al., "Photodynamic therapy â mechanisms, photosensitizers and combinations," *Biomedicine Pharmacotherapy*, Vol. 106, pp. 1098–1107, 2018.
24. Paszko, E., C. Ehrhardt, M. O. Senge, and et al., "Nanodrug applications in photodynamic therapy," *American Chemical Society*, Vol. 8, pp. 14–29, 2011.
25. Baran, T. M., and T. H. Foster, "Comparison of flat cleaved and cylindrical diffusing fibers as treatment sources for interstitial photodynamic therapy," *Med. Phys.*, Vol. 41, 2014.
26. Huo, M., L. Wang, L. Zhang, and et al., "Photosynthetic tumor oxygenation by photosensitizer-containing cyanobacteria for enhanced photodynamic therapy," *Angew. Chem.*, Vol. 132, pp. 1922–1929, 2020.
27. He, H., L. Liu, R. Liang, and et al., "Tumor-targeted nanoplatfrom for in situ oxygenation-boosted immunogenic phototherapy of colorectal cancer," *Acta Biomaterialia*, Vol. 104, pp. 188–197, 2020.
28. Norum, O. J., J. V. Gaustad, E. Angell-Petersen, and et al., "Photochemical internalization of bleomycin is superior to photodynamic therapy due to the therapeutic effect in the tumor periphery," *Photochem Photobiol.*, Vol. 85, pp. 740–749, 2009.
29. Nguyen, L., S. J. Madsen, K. Berg, and et al., "Nanodrug applications in photodynamic therapy," *American Chemical Society*, Vol. 8, pp. 14–29, 2011.
30. Jerjes, W., T. Upile, H. Radhi, and et al., "Photodynamic therapy vs. photochemical internalization: the surgical margin," *Head Neck Oncol.*, Vol. 3, no. 53, 2011.
31. Vatansever, F., R. Chandran, M. Sadasivam, and et al., "Multi-functionality in theranostic nanoparticles: is more always better?," *HJ Nanomed Nanotechnol.*, Vol. 3, no. 120, 2012.
32. Charron, D. M., J. Chen, G. Zheng, and et al., "Theranostic lipid nanoparticles for cancer medicine," *Cancer Treat Res.*, Vol. 166, pp. 103–127, 2015.

33. Liu, Z., Z. Xie, W. Li, and et al., "Photodynamic immunotherapy of cancers based on nanotechnology: recent advances and future challenges," *J Nanobiotechnol*, Vol. 19, no. 160, 2021.
34. Yang, Y., Y. Hu, and H. Wang, "Targeting antitumor immune response for enhancing the efficacy of photodynamic therapy of cancer: Recent advances and future perspectives," *Oxidative Medicine and Cellular Longevity*, Vol. 2016, pp. 103–127, 2016.
35. Calixto, G. M. F., J. Bernegossi, L. M. D. Freitas, and et al., "Nanotechnology-based drug delivery systems for photodynamic therapy of cancer: A review," *Molecules*, Vol. 21, no. 342, 2016.
36. Prasad, R., N. K. Jain, J. Conde, and et al., "Localized nanotheranostics: recent developments in cancer nanomedicine," *Materials Today Advances*, Vol. 8, no. 100087, 2020.
37. Silva, C. O., J. O. Pinho, J. M. Lopes, and et al., "Current trends in cancer nanotheranostics: Metallic, polymeric, and lipid-based systems," *Pharmaceutics*, Vol. 11, no. 22, 2019.
38. Hussain, Z., M. Arooj, A. Malik, and et al., "Nanomedicines as emerging platform for simultaneous delivery of cancer therapeutics: new developments in overcoming drug resistance and optimizing anticancer efficacy," *ARTIFICIAL CELLS, NANOMEDICINE, AND BIOTECHNOLOGY*, Vol. 46, pp. 1015–1024, 2018.
39. Dong, J., W. Han, Y. Wang, and et al., "Plasmon-enhanced upconversion photoluminescence: Mechanism and application," *Reviews in Physics 4*, Vol. 4, no. 100026, 2019.
40. Nguyen, P. D., S. J. Son, and J. Min, "Upconversion nanoparticles in bioassays, optical imaging and therapy," *J. Nanosci. Nanotechnol.*, Vol. 14, no. 1, pp. 157–174, 2014.
41. Altavilla, C., *Upconverting Nanomaterials Perspectives, Synthesis, and Applications*, US: CRC Press, 1st ed., 2016.
42. Yang, Y., "Upconversion nanoparticles in bioassays, optical imaging and therapy," *Microchim Acta*, Vol. 181, pp. 263–294, 2014.
43. Wang, R., and F. Zhang, "Nir luminescent nanomaterials for biomedical imaging," *J. Mater. Chem. B*, Vol. 2, pp. 2422–2443, 2014.
44. Zhang, F., *Photon Upconversion Nanomaterials*, Berlin: Springer, 1st ed., 2015.
45. Li, X. M., F. Zhang, and D. Y. Zhao, "Highly efficient lanthanide upconverting nanomaterials: progresses and challenges," *Nano Today*, Vol. 8, pp. 643–676, 2013.
46. Ovsyanki, V. V., and P. P. Feofilov, "Mechanism of summation of electronic excitations in activated crystals," *Sov. J. Exp. Theor. Phys. Lett.*, Vol. 3, pp. 322–325, 1966.
47. Auzel, F., "Upconversion and anti-stokes processes with f and d ions in solids," *Chem. Rev.*, Vol. 104, pp. 139–173, 2004.
48. Chen, G. Y., H. L. Qju, P. N. Prasad, and X. Y. Chen, "Upconversion nanoparticles: design, nanochemistry, and applications in theranostics," *Chem. Rev.*, Vol. 114, pp. 5161–5214, 2014.
49. Joubert, M. F., "Photon avalanche upconversion in rare earth laser materials," *Opt. Mater.*, Vol. 11, pp. 181–203, 1999.

50. Wang, F., and X. G. Liu, "Recent advances in the chemistry of lanthanide-doped upconversion nanocrystals," *Chem. Soc. Rev.*, Vol. 38, pp. 976–989, 2009.
51. Haase, M., and H. Schafer, "Upconverting nanoparticles," *Angew. Chem. Int. Ed.*, Vol. 50, pp. 5808–5829, 2009.
52. Heer, S., K. Kompe, H. U. Gudel, and M. Haase, "Highly efficient multicolour upconversion emission in transparent colloids of lanthanide-doped NaYF_4 nanocrystals," *Adv. Mater.*, Vol. 16, pp. 2102–2105, 2004.
53. Muhr, V., S. Wilhelm, T. Hirsch, and O. S. Wolfbeis, "Upconversion nanoparticles: From hydrophobic to hydrophilic surfaces," *Acc. Chem. Res.*, Vol. 47, pp. 3481–3493, 2014.
54. Gu, Z., L. Yan, G. Tian, Z. Chai, and et al., "Recent advances in design and fabrication of upconversion nanoparticles and their safe theranostic applications," *Adv. Mater.*, Vol. 23, pp. 3758–3779, 2013.
55. Biju, V., "Chemical modifications and bioconjugate reactions of nanomaterials for sensing, imaging, drug delivery and therapy," *Acc. Chem. Res.*, Vol. 43, pp. 744–764, 2014.
56. Treccani, L., T. Y. Klein, F. Meder, and et al., "Functionalized ceramics for biomedical, biotechnological and environmental applications," *Acta Biomater.*, Vol. 9, pp. 7115–7150, 2013.
57. Hong, E., Y. Wang, L. Liu, and et al., "Controlled synthesis of gadolinium fluoride upconversion nanoparticles capped with oleic acid or polyethylene glycol molecules via one-step hydrothermal method and their toxicity to cancer cells," *J Nanopart Res*, Vol. 22, no. 343, pp. 1–27, 2020.
58. Reddy, K. L., R. Balaji, A. Kumar, and et al., "Lanthanide doped near infrared active upconversion nanophosphors: Fundamental concepts, synthesis strategies, and technological applications," *Small*, Vol. 14, no. 1801304, 2018.
59. Guller, A. E., A. N. Generalova, E. V. Petersen, and et al., "Cytotoxicity and non-specific cellular uptake of bare and surface-modified upconversion nanoparticles in human skin cells," *Nano Research*, Vol. 8, no. 5, pp. 1546–1562, 2015.
60. Zor, F., F. N. Selek, G. Orlando, and D. F. Williams, "Biocompatibility in regenerative nanomedicine," *Nanomedicine*, Vol. 14, pp. 2763–2775, 2019.
61. Saleh, M. I., B. R. Hle, S. Wang, and et al., "Assessing the protective effects of different surface coatings on $\text{NaYF}_4:\text{Yb}^{3+}, \text{Er}^{3+}$ upconverting nanoparticles in bufer and dmem," *Sci. Rep.*, Vol. 10, no. 19318, 2020.
62. Mader, H. S., P. Kele, S. M. Saleh, and O. S. Wolfbeis, "Upconverting luminescent nanoparticles for use in bioconjugation and bioimaging," *Current Opinion in Chemical Biology*, Vol. 14, pp. 582–596, 2010.
63. Arai, M. S., S. S. D. Camargo, G. Orlando, and D. F. Williams, "Exploring the use of upconversion nanoparticles in chemical and biological sensors: from surface modifications to point-of-care devices," *Nanoscale Adv.*, Vol. 3, pp. 5135–5165, 2021.
64. Sperling, R. A., and W. J. Parak, "Surface modification, functionalization and bioconjugation of colloidal inorganic nanoparticles," *Philos. Trans. Math. Phys. Eng. Sci.*, Vol. 368, pp. 1333–1383, 2010.

65. Duong, H. T. T., Y. Chen, A. A. Tawfik, and et al., "Systematic investigation of functional ligands for colloidal stable upconversion nanoparticles," *RSC Adv.*, Vol. 8, pp. 4842–4849, 2018.
66. Gee, A., and X. Xu, "Surface functionalisation of upconversion nanoparticles with different moieties for biomedical applications," *Surfaces*, Vol. 1, pp. 96–121, 2018.
67. Himmelstob, S. F., and T. Hirsch, "Long-term colloidal and chemical stability in aqueous media of nayf4-type upconversion nanoparticles," *Part. Part. Syst. Charact.*, Vol. 36, no. 1900235, pp. 1–11, 2019.
68. Chen, Y., C. DâAmario, A. Gee, and et al., "Dispersion stability and biocompatibility of four d nayf4: Yb, er upconversion nanoparticles," *Acta Biomaterialia*, Vol. 102, pp. 384–393, 2020.
69. Hilderbrand, S. A., F. Shao, F. Salthouse, and et al., "Upconverting luminescent nanomaterials: application to in vivo bioimaging," *Chem. Commun.*, pp. 4188–4190, 2009.
70. Ge, H., D. Wang, Y. Pan, and et al., "Sequence-dependent dna functionalization of upconversion nanoparticles and their programmable assemblies," *Angew. Chem. Int. Ed.*, Vol. 59, pp. 8133–8137, 2020.
71. Hu, H., M. Yu, F. Li, and et al., "Facile epoxidation strategy for producing amphiphilic up-converting rare-earth nanophosphors as biological labels," *Chem. Mater.*, Vol. 20, pp. 7003–8713, 2008.
72. Zhou, H. P., C. H. Xu, W. Sun, and et al., "Clean and flexible modification strategy for carboxyl/aldehyde-functionalized upconversion nanoparticles and their optical applications," *Adv. Funct. Mater.*, Vol. 19, pp. 3892–3900, 2009.
73. Chen, Z., H. Chen, H. Hu, and et al., "Versatile synthesis strategy for carboxylic acid-functionalized upconverting nanophosphors as biological labels," *J. Am. Chem. Soc.*, Vol. 130, pp. 3023–3029, 2008.
74. Nichkova, M., G. Dosev, S. J. Gee, and et al., "Microarray immunoassay for phenoxybenzoic acid using polymer encapsulated eu:gd2o3 nanoparticles as fluorescent labels," *Anal. Chem.*, Vol. 77, pp. 6854–6057, 2005.
75. Liras, M., M. G. Bejar, E. Peinado, and et al., "Thin amphiphilic polymer-capped up-conversion nanoparticles: Enhanced emission and thermoresponsive properties," *Chem. Mater.*, Vol. 26, no. 13, pp. 4014–4022, 2014.
76. Guryev, E. L., A. S. Smyshlyaeva, N. Y. Shilyagina, and et al., "Ucnp-based photoluminescent nanomedicines for targeted imaging and theranostics of cancer," *Molecules*, Vol. 25, no. 18, 2020.
77. Lee, S. H., S. M. Tawfik, D. T. Thangadurai, and et al., "Highly sensitive and selective detection of alprenolol using upconversion nanoparticles functionalized with amphiphilic conjugated polythiophene," *Microchemical Journal*, Vol. 164, no. 106010, 2021.
78. Cheng, Y. J., J. J. Hu, A. Y. Quin, and et al., "Recent advances in functional mesoporous silica-based nanoplatforms for combinational photo-chemotherapy of cancer," *Biomaterials*, Vol. 232, no. 119738, 2020.

79. Gerzaran, M. G., and M. V. Regi, "Influence of the surface functionalization on the fate and performance of mesoporous silica nanoparticles," *Nanomaterials*, Vol. 10, no. 916, pp. 1–49, 2020.
80. Liu, J. N., W. B. Bu, and J. L. Shi, "Silica coated upconversion nanoparticles: A versatile platform for the development of efficient theranostics," *Acc. Chem. Res.*, Vol. 48, pp. 1797–1805, 2015.
81. Han, R., H. Yi, J. Shi, and et al., "ph-responsive drug release and nir-triggered singlet oxygen generation based on a multifunctional core-shell structure," *Phys. Chem. Chem. Phys.*, Vol. 18, pp. 25497–25503, 2016.
82. Gnanasammandhan, M. K., N. M. Idris, A. Bansal, and et al., "Near-ir photoactivation using mesoporous silica-coated $\text{NaYF}_4:\text{Yb,Er/Tm}$ upconversion nanoparticles," *Nature Protocols*, Vol. 11, no. 4, pp. 688–713, 2016.
83. Watermann, A., and J. Brieger, "Mesoporous silica nanoparticles as drug delivery vehicles in cancer," *Nanomaterials*, Vol. 7, no. 189, pp. 1–17, 2017.
84. Sun, L., T. Liu, Y. Qiu, and et al., "Direct formation of mesoporous upconverting core-shell nanoparticles for bioimaging of living cells," *Microchim Acta*, Vol. 181, pp. 775–781, 2014.
85. Lv, R., D. Wang, L. Xiao, and et al., "Stable icg-loaded upconversion nanoparticles: silica core/shell theranostic nanoplatform for dual-modal upconversion and photoacoustic imaging together with photothermal therapy," *Scientific Reports*, Vol. 7, no. 15753, 2017.
86. Sivakumar, S., P. R. Diamente, F. C. J. M. V. Veggel, and et al., "Silica-coated In^{3+} -doped LaF_3 nanoparticles as robust down- and upconverting biolabels," *Chem. A Eur. J.*, Vol. 12, pp. 5878–5884, 2006.
87. Wang, Y., J. Sun, J. Wang, and et al., "Charge-reversal aptes-modified mesoporous silica nanoparticles with high drug loading and release controllability," *ACS Appl. Mater. Interfaces*, Vol. 8, no. 27, pp. 17166–17175, 2016.
88. Jain, P. K., X. Huang, I. H. E. Sayed, and et al., "Review of some interesting surface plasmon resonance-enhanced properties of noble metal nanoparticles and their applications to biosystems," *Plasmonics*, Vol. 2, no. 3, pp. 107–118, 2007.
89. Mendez-Gonzalez, D., S. Melle, O. G. Laurenti, and et al., "Control of upconversion luminescence by gold nanoparticle size: from quenching to enhancement," *Nanoscale*, Vol. 11, no. 29, pp. 13832–13844, 2019.
90. Zhang, F., G. B. Braun, Y. Shi, and et al., "Fabrication of $\text{Ag}@ \text{SiO}_2 @ \text{Y}_2\text{O}_3:\text{Er}$ nanostructures for bioimaging: Tuning of the upconversion fluorescence with silver nanoparticles," *J. Am. Chem. Soc.*, Vol. 132, pp. 2850–2851, 2010.
91. Libutti, S. K., G. F. Paciotti, A. A. Byrnes, and et al., "Phase I and pharmacokinetic studies of cyt-6091, a novel pegylated colloidal gold-rhtnf nanomedicine," *Clin Cancer Res.*, Vol. 16, no. 24, pp. 6139–6149, 2010.
92. Lv, R., F. Yang, X. Jiang, and et al., "Plasmonic modulated upconversion fluorescence by adjustable distributed gold nanoparticles," *Journal of Luminescence*, Vol. 220, no. 116974, pp. 1–10, 2020.

93. Priyam, A., N. M. Idris, and Y. Zhang, "Gold nanoshell coated nayf4 nanoparticles for simultaneously enhanced upconversion fluorescence and darkfield imaging," *J. Mater. Chem.*, Vol. 22, pp. 960–965, 2012.
94. Lin, B., J. Liu, Y. Wang, and et al., "Enhanced upconversion luminescence-guided synergistic antitumor therapy based on photodynamic therapy and immune checkpoint blockade," *Chemistry of Materials*, Vol. 32, pp. 4627–4640, 2020.
95. Li, B., H. Liu, C. Sun, and et al., "Core-shell strtio3:yb3+,er3+@msio2 nanoparticles for controlled and monitored doxorubicin delivery," *RSC Adv.*, Vol. 6, pp. 26280–26287, 2016.
96. Lv, R., M. Feng, W. J. Warang, and et al., "Up-conversion luminescence properties of lanthanide-gold hybrid nanoparticles as analyzed with discrete dipole approximation," *Nanomaterials*, Vol. 8, no. 12, 2018.
97. Jana, N. R., L. Gearheart, and C. J. Murphy, "Seeding growth for size control of 5â40 nm diameter gold nanoparticles," *Langmuir*, Vol. 17, pp. 6782–6786, 2001.
98. Gulsoy, M., Z. Derehi, and H. O. Tabakoglu, "Closure of skin incisions by 980-nm diode laser welding," *Lasers Med Sci*, Vol. 21, pp. 5–10, 2006.
99. Hale, G. M., and M. R. Querry, "Optical constants of water in the 200-nm to 200-Î¼m wavelength region," *Appl. Opt.*, Vol. 12, pp. 555–563, 1973.
100. Yang, Y., H. Liang, and S. Ma, "Gold nanoparticle based photothermal therapy: Development and application for effective cancer treatment," *Sustainable Materials and Technologies*, Vol. 22, no. e00109, 2019.
101. Byar, H., "Reactive oxygen species," *Critical Care Medicine*, Vol. 33, no. 12, pp. 498–501, 2005.
102. Thannickal, V. J., and B. L. Fanburg, "Reactive oxygen species in cell signaling," *American Journal of Physiology-Lung Cellular and Molecular Physiology*, Vol. 279, no. 6, pp. 1005–1028, 2000.
103. Liou, G. Y., and P. Storz, "Reactive oxygen species in cancer," *Free radical research*, Vol. 44, no. 5, pp. 479–496, 2010.
104. Ryter, S. W., H. P. Kim, A. Hoetzel, and et al., "Mechanisms of cell death in oxidative stress," *Antioxidants and Redox Signaling*, Vol. 9, no. 1, pp. 49–89, 2007.
105. Gomes, A., E. Fernandes, and J. L. Lima, "Fluorescence probes used for detection of reactive oxygen species," *Journal of biochemical and biophysical methods*, Vol. 65, no. 2-3, pp. 45–80, 2005.
106. Park, J. C., and M. A. Eisenberger, "Advances in the treatment of metastatic prostate cancer," *In Mayo Clinic Proceedings*, Vol. 90, no. 12, pp. 1719–1773, 2015.
107. Bulmahn, J. C., H. L. Kutscher, K. Cwiklinski, and et al., "A multimodal theranostic nanoformulation that dramatically enhances docetaxel efficacy against castration resistant prostate cancer," *Journal of Pharmaceutical Sciences*, Vol. 109, no. 9, pp. 2874–2883, 2020.
108. Huhn, J., C. Carrillo-Carrion, and M. G. Soliman, "Selected standard protocols for the synthesis, phase transfer, and characterization of inorganic colloidal nanoparticles," *Chemistry of Materials*, Vol. 29, no. 1, pp. 399–461, 2017.

109. Donahue, N. D., H. Acar, and S. Wilhelm, "Concepts of nanoparticle cellular uptake, intracellular trafficking, and kinetics in nanomedicine," *Advanced Drug Delivery Reviews*, Vol. 143, pp. 68–69, 2019.
110. Berridge, M., and A. Tan, "Characterization of the cellular reduction of 3-(4,5-dimethylthiazol-2-yl)-2,5-diphenyltetrazolium bromide (mtt): Subcellular localization, substrate dependence, and involvement of mitochondrial electron transport in mtt reduction," *Archives of Biochemistry and Biophysics*, Vol. 303, no. 2, pp. 474–482, 1993.
111. Pecora, R., "Dynamic light scattering measurement of nanometer particles in liquids," *Journal of nanoparticle research*, Vol. 2, no. 2, pp. 123–131, 2000.
112. Hassan, P. A., S. Rana, and G. Verma, "Making sense of brownian motion: Colloid characterization by dynamic light scattering," *Langmuir*, Vol. 31, no. 1, pp. 3–12, 2015.
113. Jones, R. F., *Physical principles of electron microscopy, An introduction to TEM, SEM, and AFM, 2nd ed.*, New York: Springer, 2005.
114. Feng, A. L., M. L. You, and L. Tian, "Distance-dependent plasmon-enhanced fluorescence of upconversion nanoparticles using polyelectrolyte multilayers as tunable spacers," *Scientific reports*, Vol. 5, no. 1, pp. 1–10, 2015.
115. Nowak-Sliwinska, P., A. Karocki, L. Elas, and et al., "Verteporfin, photofrin ii, and merocyanine 540 as pdt photosensitizers against melanoma cells," *Biochemical and biophysical research communications*, Vol. 349, no. 2, pp. 549–555, 2006.
116. Pervaiz, S., J. L. Hirpara, M. V. Clement, and et al., "Caspase proteases mediate apoptosis induced by anticancer agent preactivated mc540 in human tumor cell lines," *Cancer letters*, Vol. 128, no. 1, pp. 11–22, 1998.
117. Wang, H., Z. Liu, S. Wang, and et al., "Mc540 and upconverting nanocrystal coloaded polymeric liposome for near-infrared light-triggered photodynamic therapy and cell fluorescent imaging," *ACS applied materials and interfaces*, Vol. 6, no. 5, pp. 3219–3225, 2014.
118. Acedo, P., J. C. Stockert, J. C. Canete, and et al., "Two combined photosensitizers: a goal for more effective photodynamic therapy of cancer," *Cell death and disease*, Vol. 5, no. 3, pp. e1122–e1122, 2014.
119. Ricci-Junior, E., and J. M. Marchetti, "Zinc (ii) phthalocyanine loaded plga nanoparticles for photodynamic therapy use," *International journal of pharmaceuticals*, Vol. 310, no. 1-2, pp. 187–195, 2006.
120. Silverstein, R. M., X. F. Webster, and J. D. Kiemle, *Spectrometric identification of organic compounds, 7th edition*, New York: Jhon Wiley and Sons, 2005.
121. Lee, D. H., R. A. Condrate, and W. C. Lacourse, "Ftir spectral characterization of thin film coatings of oleic acid on glasses: part ii. coatings on glass from different media such as water, alcohol, benzene and air," *J. Mater. Sci.*, Vol. 35, pp. 4961–4970, 2000.
122. Avula, A., A. Galor, P. Blackwelder, and et al., "Application of scanning electron microscopy with energy-dispersive x-ray spectroscopy for analyzing ocular surface particles on schirmer strips," *Cornea*, Vol. 36, no. 6, 2017.
123. Algorri, J. F., M. Ochoa, P. Roldan-Varona, and et al., "Light technology for efficient and effective photodynamic therapy: A critical review," *Cancers*, Vol. 13, no. 3484, 2021.

124. Yu, X. N., Y. Zhang, G. C. Liu, and et al., "Sorafenib-conjugated zinc phthalocyanine based nanocapsule for trimodal therapy in an orthotopic hepatocellular carcinoma xenograft mouse model," *ACS applied materials interfaces*, Vol. 12, no. 15, pp. 17193–17206, 2020.
125. Huang, X., M. A. E. Sayed, G. C. Liu, and et al., "Gold nanoparticles: Optical properties and implementations in cancer diagnosis and photothermal therapy," *Journal of advanced research*, Vol. 1, no. 1, pp. 13–28, 2010.
126. Pitsillides, C. M., C. M. Joe, X. Wei, and et al., "Selective cell targeting with light-absorbing microparticles and nanoparticles," *Biophysical journal*, Vol. 84, no. 6, pp. 4023–4032, 2003.
127. Chadwick, S. J., D. Salah, P. M. Livesey, and et al., "Singlet oxygen generation by laser irradiation of gold nanoparticles," *Journal of Physical Chemistry C*, Vol. 120, pp. 10647–10657, 2016.
128. Ogilby, P. R., "Singlet oxygen: there is indeed something new under the sun," *Chemical Society Reviews*, Vol. 39, no. 8, pp. 3181–3209, 2010.
129. Schmidt, R., and E. Afshari, "Collisional deactivation of 1O_2 ($^1\hat{1}g$) by solvent molecules. comparative experiments with $^{16}O_2$ and $^{18}O_2$," *Berichte der Bunsengesellschaft für physikalische Chemie*, Vol. 96, no. 6, pp. 788–794, 1992.
130. Entradas, T., S. Waldron, and M. Volk, "The detection sensitivity of commonly used singlet oxygen probes in aqueous environments," *Journal of Photochemistry and Photobiology B: Biology*, Vol. 204, no. 111787, 2020.
131. Ash, C., M. Dubec, K. Donne, and et al., "Effect of wavelength and beam width on penetration in light-tissue interaction using computational methods," *Lasers in medical science*, Vol. 32, no. 8, pp. 1909–1918, 2017.
132. Lux, I., and L. Koblinger, *Monte Carlo particle transport methods: neutron and photon calculations*, Boston: CRC, 1991.
133. Wang, L., *Monte Carlo Modeling of Light Transport in Multi-layered Tissues in Standard C*. PhD thesis, University of Texas, Anderson Cancer Center, 1992.
134. Salomatina, E. V., V. Jiang, B. Novak, and et al., "Optical properties of normal and cancerous human skin in the visible and near-infrared spectral range," *Journal of biomedical optics*, Vol. 11, no. 6, 2006.
135. Behzadi, S., V. Serpooshan, W. Tao, and et al., "Cellular uptake of nanoparticles: journey inside the cell," *Chemical Society Reviews*, Vol. 16, no. 14, pp. 4218–4244, 2017.
136. Salatin, S., M. D. Solmaz, and A. Y. Khosroushahi, "Effect of the surface modification, size, and shape on cellular uptake of nanoparticles," *Cell biology international*, Vol. 39, no. 8, pp. 801–890, 2015.
137. Yang, J. A., H. T. Phan, S. Vaidya, and et al., "Nanovacuum: Nanoparticle uptake and differential cellular migration on a carpet of nanoparticles," *Nano letters*, Vol. 13, no. 5, pp. 2295–2302, 2013.
138. Jiang, W., B. Y. S. Kim, J. T. Rutka, and et al., "Nanoparticle-mediated cellular response is size-dependent," *Nat. Nanotechnol.*, Vol. 3, pp. 145–150, 2008.

139. Yakin, F. E., M. Barisik, and T. Sen, "Pore size and porosity dependent zeta potentials of mesoporous silica nanoparticles," *The Journal of Physical Chemistry C*, Vol. 124, no. 36, pp. 19579–19587, 2020.
140. Han, R., Y. Tang, Y. Hou, and et al., "Ultralow-intensity near infrared light synchronously activated collaborative chemo/photothermal/photodynamic therapy," *Biomaterials Science*, Vol. 8, pp. 607–618, 2020.
141. Zhang, D., L. Wen, R. Huang, and et al., "Mitochondrial specific photodynamic therapy by rare-earth nanoparticles mediated near-infrared graphene quantum dots," *Biomaterials*, Vol. 153, pp. 14–26, 2018.
142. Güteryüz, B., U. Ünal, and M. Gülsoy, "Near infrared light activated upconversion nanoparticles (ucnp) based photodynamic therapy of prostate cancers: An in vitro study," *Photodiagnosis Photodynamic Therapy*, Vol. 36, no. 102616, 2021.